Collision Risk Model for "rufa" Red Knots (*Calidris canutus rufa*) Interacting with a Proposed Offshore Wind Energy Facility in Nantucket Sound, Massachusetts

US Department of the Interior
Bureau of Ocean Energy Management
Office of Renewable Energy Programs

BOEM
BUREAU OF OCEAN ENERGY MANAGEMENT

Collision Risk Model for "*rufa*" Red Knots (*Calidris canutus rufa*) Interacting With a Proposed Offshore Wind Energy Facility in Nantucket Sound, Massachusetts

Principal Authors

Caleb Gordon and Chris Nations

US Department of the Interior
Bureau of Ocean Energy Management
Office of Renewable Energy Programs

BOEM
BUREAU OF OCEAN ENERGY MANAGEMENT

DISCLAIMER

Study concept, oversight, and funding were provided by the US Department of the Interior, Bureau of Ocean Energy Management, Office of Renewable Energy Programs, Washington, DC, under Contract Number GS-10F-072BA Order Number M14PD00050. This report has been technically reviewed by BOEM and it has been approved for publication. The views and conclusions contained in this document are those of the authors and should not be interpreted as representing the opinions or policies of the US Government, nor does mention of trade names or commercial products constitute endorsement or recommendation for use.

REPORT AVAILABILITY

To download a PDF file of this Office of Renewable Energy Programs report, go to the US Department of the Interior, Bureau of Ocean Energy Management, website at: www.boem.gov/Renewable-Energy-Completed-Studies

This report can be obtained from the National Technical Information Service; the contact information is below.

> US Department of Commerce
> National Technical Information Service
> 5301 Shawnee Rd.
> Springfield, VA 22312
> Phone: (703) 605-6000, 1(800)553-6847
> Fax: (703) 605-6900
> Website: http://www.ntis.gov/

CITATION

Preface

This report details the objectives, structure, scope, results, and conclusions of the United States (US) Department of the Interior, Bureau of Safety and Environmental Enforcement (BSEE) and Bureau of Ocean Energy Management (BOEM) order #M14PD00050, issued under Government Services Administration contract # GS-10F-072BA, titled "Risk of an Offshore Wind Project to a Migrant Shorebird." This project was awarded to Western EcoSystems Technology, Inc. (WEST) on September 25, 2014, before the U.S. Fish and Wildlife Service designating the Red Knot (*Calidris canutus rufa*) as threatened under the Endangered Species Act. The objective of this study, as stated in the contract, was as follows:

To quantitatively estimate the mortality of Red Knots due to collision with operating wind turbines at a yet-to-be-constructed offshore wind energy facility in federal waters of Nantucket Sound, Massachusetts (the "Facility")[1]. This study serves as a test case of a modeling approach that could be applied to other offshore wind projects on the outer continental shelf.

The contract outlined a set of three tasks intended to accomplish this objectives, as follows:

- Task 1: Develop a method to estimate mortality
- Task 2: Conduct a peer-review of the method
- Task 3: Implement the revised method

In the remainder of this preface, we describe the approach that WEST took to these tasks, detailing the composition and roles of the members of the Project team, as well as the general processes undertaken by the team to perform the work of this Project.

Task 1 Develop a method to estimate mortality. This task comprised the bulk of the technical work of the Project, and can be conceptually divided into five distinct phases. These phases were, to a large extent, necessarily sequential, as each built upon the products of the previous phases. However, we note that there was also some overlap between phases, particularly during model development, testing, and results interpretation, as these processes were more intertwined, entailing iterative processes of simulation, refinement, and results-based feedback. The five phases of Task 1 are listed and described below.

1. Develop a modeling approach based on review of existing methods
2. Develop the biological and meteorological basis for model inputs and assumptions
3. Construct the model
4. Run simulations to generate interim collision predictions and explore sources of variation

---

[1] BOEM issued a suspension order pursuant to 30 CFR 585.418; no construction or installation activities related to commercial lease OCS-A 0478 may occur during the lease suspension period (http://www.boem.gov/Lease-Suspension-Order/).

5. Interpret and write up the interim results

Phase 1: Develop a modeling approach based on review of existing methods

During the first phase of Task 1, the Project team completed a review of existing methodologies and approaches for modeling bird collision risk at offshore wind energy facilities and developed a consensus approach for the original modeling effort to be undertaken for the current Project. This phase took place from late September through early November, 2014. The effort to review existing bird collision risk methodologies was led by Mark Collier of Bureau Waardenburg, with input from the technical team (see personnel table below), and is presented within this report in Chapter 2. On the basis of this information, along with a series of discussions involving the Project's technical contributors, a consensus was formed for a general modeling approach to be used for the Project. This approach is described in detail in Chapter 3. In summary, the decision was made to develop an original simulation model to generate quantitative estimates of Red Knot fatalities resulting from the movement of birds through a spatially-explicit representation of the approved Facility in Nantucket Sound, Massachusetts. This model was to incorporate the Band model (Band 2012) to represent certain specific dynamics of collision geometry, as this model was determined to be the best available tool for representing certain parts of birds' interactions with a wind energy facility, and it is currently the most widespread and accepted model for application to bird collision risk at offshore wind facilities. However, the concept for the original model to be developed for the current Project was that it would also incorporate additional dynamics that are not included within the Band model to enable the fatality rates of Red Knots at the subject wind energy Facility to be estimated with a higher degree of biological and meteorological realism, in hopes of generating more realistic and precise fatality estimates for the specific case study of interest than could be generated using the Band model alone.

Phase 2: Develop the biological and meteorological basis for model inputs and assumptions

The second phase of Task 1 consisted of an intensive series of teleconferences held by the 4-person technical team (C. Gordon, C. Nations, J. L. Niles, and M. Collier; see personnel table below) during fall 2014. The objective of this phase was to fully develop the phenomenological underpinning for the structure, inputs, and assumptions of the original model that was to be developed. The primary phenomena of interest were biological characteristics of "rufa" Red Knots (*C. c. rufa*) and meteorological characteristics of the approved Facility, as these two sets of characteristics interact to govern the risk of Red Knots colliding with structures associated with the approved Facility. The outcomes of these meetings are presented within Chapter 3: *Methods*, Section 3.3: *Input Assumptions and Data* of this report, which describes the technical team's consensus decisions about the different quantitative structures, inputs, and assumptions to incorporate within the model, as well as the justification for each choice based on best available scientific information.

Phase 3: Construct the model

With the phenomenological basis for the model established, an original model was then developed by lead modeler, C. Nations, with some assistance from D. Russo (see personnel table below), between January and April, 2015. The technical composition of this model is described in Chapter 3: *Methods*, Section 3.4: *Model Description* of this report. Once completed, WEST biometrician P. Rabie performed an independent review of the model's structure and underlying

programming code, to ensure that the model was robust, and consistent with the conceptual basis for the model generated by the Project's technical team (see personnel table).

Phase 4: Run simulations to generate interim collision predictions and explore sources of variation

With the model's programming and QA/QC review complete, WEST performed a series of initial simulation tests with the model in April and May, 2015. The goals of these simulations were to generate initial quantitative fatality predictions of Red Knot fatality rates due to collisions with the approved Facility, and also to explore sources of variation in the model, to characterize the sensitivity of the model's outputs to variation in different model input values, structures, and assumptions. The plan for the simulation tests that were conducted during this phase was developed through a series of discussions between the scientific director C. Gordon and lead modeler C. Nations (see personnel table). The basic simulation process is described in Chapter 3: *Methods*, Section 3.5: *Simulation Protocol* of this report. This phase included several iterations of simulation modeling in order to generate a refined and comprehensive set of simulation results for the Project's interim report that incorporated feedback from the entire technical team in response to their interpretation of the results of the initial simulation iterations.

Phase 5: Interpret and write up the interim results

The final phase of Task 1, conducted in June and July, 2015, consisted of interpretation of the simulation modeling results, and packaging all of the information generated by Task 1 into the interim report, which was submitted to BSEE and BOEM in August, 2015. This report was also distributed to the peer-review team (see Task 2) for review, as a precursor to finalization and publication of the results.

Task 2 Conduct a peer-review of the method. Between August 2015 and March 2016, WEST conducted a formal peer review of the interim report, including the essence of the model and the simulation testing that had been performed, for the purpose of improving the model and the report. The review process was directed by Steven Courtney, and included reviews by four technical experts in relevant subject areas, listed below:

- Mark Desholm, Head of conservation and science, Birdlife Denmark
- Marc Mangel, Distinguished research professor of applied mathematics and statistics, University of California, Santa Cruz
- Barry Noon, Professor of Fish, Wildlife, and Conservation Biology, Colorado State University
- Michael Runge, United States Geological Survey, Patuxent Wildlife Research Center

The review process was fully described, and the comments of the four reviewers fully reproduced in the peer review report, submitted by WEST to BSEE and BOEM in March, 2016. As a step in the integration of the reviewers' comments into the revision process, the peer review director classified 22 of the individual comments as "substantive," requiring response from the Project's technical team. Appendix A lists these comments, and describes the technical team's response to each.

<u>Task 3 Implement the revised method.</u> Based on the reviewers' comments, it was determined that no alterations to the model or the simulation testing were required, hence no additional simulations were performed. Revision of the interim report to produce the draft final report consisted of incorporating a number of the reviewers' comments into text, tables, and figures of the report.

Project personnel with institutional affiliation and Project role

Person	Institution	Project Role(s)
Sang Han	BSEE	Contract Officer
David Bigger	BOEM	Contract Officer's Representative
Caleb Gordon	WEST	Project Manager, Scientific Director, Lead Author
Steven Courtney	WEST	Peer-Review Director
Chris Nations	WEST	Lead Programmer/Modeler, Co-Author
David Russo	WEST	Programmer
Paul Rabie	WEST	Programming Reviewer
Greg Johnson	WEST	Report Review
Andrea Palochak	WEST	Technical Editor
Mark Collier	Bureau Waardenburg	Technical Contributor
Karen Krijgsveld	Bureau Waardenburg	Technical Contributor
Martin Poot	Bureau Waardenburg	Technical Contributor
J. Lawrence Niles	Niles and Associates	Technical Contributor
Marc Mangel	University of California, Santa Cruz	Peer-Reviewer
Barry Noon	Colorado State University	Peer-Reviewer
Mark Desholm	Birdlife Denmark	Peer-Reviewer
Michael Runge	US Geological Survey	Peer-Reviewer

Acknowledgment

Summary

The objective of the present study was to produce a robust, quantitative prediction of fatality rates of "rufa" Red Knots (*Calidris canutus rufa*) resulting from collisions with the physical structures of a yet-to-be-constructed offshore wind energy facility (the "Facility") that has been approved for construction in federal waters of Nantucket Sound, Massachusetts. To accomplish this objective, we assembled a technical team consisting of field leading experts in offshore wind bird collision risk assessment, collision risk modeling, and Red Knot biology to synthesize existing technical information on this subject, and to use this synthesis as the basis for developing an original quantitative collision risk modeling effort.

A comprehensive review of technical literature related to bird collision risk modeling at offshore wind energy facilities was performed as an initial step in this process. On the basis of this review, we adopted a modeling approach that included the Band (2012) model to represent a subset of collision dynamics, with various additional elements incorporated to represent the most important biological and meteorological dynamics of the system of interest, as hypothesized and conceived by the Project's technical team on the basis of best available scientific information. We developed an original simulation model to represent this system, and conducted a series of simulations with the model in order to produce quantitative predictions of Red Knot fatality rates resulting from collisions with the structures of the approved Facility. These simulations included variation in several of the model's inputs in order to characterize the sensitivity of the model's fatality rate predictions to changes in these inputs.

The overall average collision fatality rate for rufa Red Knots at the approved Facility predicted by our model was 0.16 Red Knots per year equivalent to one fatality every 6.25 years, composed of 0.10 predicted fatalities per fall migration season and 0.060 predicted fatalities per spring migration season, under baseline, or default model inputs. Predicted fatalities scaled linearly with population size, such that under the assumption of a "recovered" population three times the size of the current population, the predicted fatality rates were exactly three times higher.

Collision fatality rates were largely driven by collisions of Red Knots with stationary structures, and particularly turbine towers, in our modeled results, with turbine towers accounting for roughly 90% of all collision fatalities in most simulations. The influence of collisions with turbine towers was also evidenced by the result that for all model iterations in which at least one collision occurred, the average number of collisions was approximately eight, corresponding to the number of Red Knot wingspan lengths in the tower's diameter. Red Knots were represented flying in chevron-shaped flocks, aligned wingtip to wingtip in our model, hence when the path of a flock intercepted a turbine tower, seven or eight collisions typically resulted, depending on the elevation at which the flock encountered the tapered, cylindrical towers.

Biologically realistic representations of the influence of variations in wind speed and direction, precipitation, and visibility were incorporated into the model in the form of behavioral switches between high and low elevation migratory flight altitude distributions (effective headwind speed, heavy precipitation), fall migratory flight departure delay decisions (effective headwind speed), and avoidance rate parameters (heavy precipitation, visibility, and effective headwind speed).

Simulation results indicated that of these, only effective headwind speed exerted a strong influence on the fatality rates. The relative insensitivity of fatality rates to variation in precipitation was explained by the relative rarity of heavy precipitation events during the migratory seasons of interest, as characterized by an empirical summary of hourly precipitation data from regional meteorological data. Low visibility events occurred more frequently than heavy precipitation events within the Facility region during the seasons of interest. Nonetheless, low visibility conditions were still far less common than high visibility conditions, resulting in an overall weak influence of variation in visibility on modeled fatality rates. By contrast to heavy precipitation and low visibility, the effective headwind conditions that were hypothesized to trigger behavioral switches in migrating Red Knots occurred more commonly, and consequently exerted a more important influence on modeled fatality rates. Specifically, fatality rates were significantly higher when the effective headwind speed threshold for fall migratory flight departure was below the effective headwind speed threshold for switching from the high-altitude to the low-altitude flight distribution. Under such conditions, fall migrating birds would commonly decide to fly under conditions that would cause them to fly at a lower altitude. In all other conditions, fall migrating birds would either tend to fly at a higher altitude, or not fly at all.

Relaxing the Band model's assumption of perpendicular approach angle had a marginally significant influence on fatality rates for approach angles close to perpendicular to the rotor (head on) and a negligible influence for approach angles close to parallel to the rotor. Altering the mean flight altitudes had a slight influence on modeled fatality rates for the high-altitude flight distribution, which was elected by migrating birds in our model under favorable weather conditions, and a moderate influence on fatality rates for the low-altitude flight distribution, which was elected by migrating birds in our model under poor weather conditions.

Avoidance behaviors were incorporated in our model at two distinct spatial scales. Macro-avoidance was defined as the avoidance of the entire modeled wind farm by a flock of birds that sees the Facility from a distance. Our model included the assumption that macro-avoidance ability was diminished to near zero (0.01) under low visibility conditions or heavy precipitation. Micro-avoidance was defined as the avoidance of a wind energy Facility structure by a flock that was present within the Facility, and approaching the structure. In our model, micro-avoidance capacity was reduced by the presence of heavy precipitation, strong headwinds, and low visibility, and separate micro-avoidance rates were included for stationary versus (vs.) moving structures. Modeled fatality results generally exerted a moderate level of sensitivity to variation in macro-avoidance rates and a high level of sensitivity to variation in micro-avoidance rates. These patterns are consistent with a general trend reported in previous studies of bird collision risk with offshore wind energy facility structures, and highlight the importance of characterizing birds' behavioral responses to wind energy facilities for understanding collision risk.

Contents

List of Figures

List of Tables

Abbreviations and Acronyms

°	degree
BOEM	Bureau of Ocean Energy Management
BSEE	Bureau of Safety and Environmental Enforcement
COP	Construction and Operation Plan
CCDF	complementary cumulative distribution function
DECC	Department of Energy & Climate Change
ECDF	empirical cumulative distribution function
Eq.	Equation
ESA	Endangered Species Act
ESP	electrical service platform
EST	Eastern Standard Time
Facility	the approved Cape Wind Offshore Wind Energy Facility
ft	foot
ft/s	feet/second
hr	hour
km	kilometer
m	meter
m/s	meters per second
mm	millimeter
MNWR	Monomoy National Wildlife Refuge
NCDC	National Climatic Data Center
Neg Bin	Negative Binomial
pers. comm.	personal communication
Project	The current research project undertaken by WEST, Inc.
QA/QC	quality assurance/quality control
rpm	revolutions per minute
US	United States
USFWS	US Fish and Wildlife Service
UTC	Coordinated Universal Time
vs.	versus
WEST	Western EcoSystems Technology, Inc.

1.   Introduction

The Bureau of Ocean Energy Management (BOEM) contracted Western EcoSystems Technology, Inc. (WEST) to perform the current study to undertake a biological synthesis, research, and modeling effort to produce a scientifically sound, quantitative estimate of the mortality of "rufa" Red Knots (*Calidris canuta rufa*) from an off-shore wind energy facility that has been approved in federal waters of Nantucket Sound, Massachusetts. As stated in the contract, the purpose of this study is, "to quantitatively estimate the mortality of Red Knots due to collision with operating wind turbines at a yet-to-be-constructed offshore wind energy facility in federal waters of Nantucket Sound, Massachusetts." The "rufa" subspecies of the Red Knot was formally listed as a threatened species under the United States (US) Endangered Species Act (ESA) on December 11, 2014 (US Fish and Wildlife Service [USFWS] 2014a), primarily due to loss of food and habitat in the breeding and migration ranges (USFWS 2014b). Because of this listing, the USFWS is required to evaluate and regulate all actions harmful to rufa Red Knots, including any mortality due to anthropogenic causes. Rufa Red Knots are known to migrate through the general region in which the yet-to-be-constructed offshore wind energy facility (the "Facility") has been approved in Nantucket Sound, and it was determined by BOEM that individual Red Knots could potentially be killed in collisions with the Facility's wind turbines. Because BOEM is the action agency responsible for issuing a lease to construct and operate the Facility in federal waters, BOEM anticipates engaging in Section 7 ESA consultation with the USFWS regarding potential take of rufa Red Knots by the Facility. Although BOEM has completed several previous studies addressing risks posed to birds by offshore wind development on the Atlantic Outer Continental Shelf (Gordon et al. 2011, Robinson Willmott et al. 2013), these studies have not addressed quantitative estimates of Red Knot collision mortality at the project level. Therefore, one of the objectives of the current Project is to develop a scientifically credible risk analysis to form the basis for Section 7 ESA consultation with the USFWS regarding potential take of rufa Red Knots by the Facility.

The generation of a robust, quantitative estimate of collision mortality for Red Knots at the approved Facility is challenging because of several key gaps in scientific knowledge regarding the phenomena of interest. At a general level, because of the inherent difficulties in measuring bird collisions with wind turbines at offshore wind turbines, it has proven much more difficult to produce accurate and reliable quantitative bird fatality rate estimates for offshore wind facilities than for land-based wind facilities (Krijgsveld et al. 2011). This difficulty is compounded by the larger gaps in our knowledge of bird biology in marine environments relative to terrestrial environments. As a result, fatality rate estimates for birds at offshore wind energy facilities have tended to rely on modeling approaches that make various assumptions in order to fill knowledge gaps. At a specific level, in the case of the rufa Red Knot, while some biological information germane to offshore wind collision rate estimation is available, such as spatiotemporal patterning of coastal migratory stopover locations (Gordon et al. 2011), many specific knowledge gaps remain, including typical migratory flight altitudes, specific trans-oceanic migratory flight paths, turbine avoidance behaviors under different environmental conditions (Gordon et al. 2011, Burger et al. 2011).

In light of the objectives and the inherent challenges of this Project, WEST assembled a technical team and developed a technical approach predicated on a strategy of incorporating the best available scientific information on the natural phenomena of interest into an original

1

collision modeling effort based on current state-of-the-art methodologies. In this report, we present a complete description of the team, approach, methods, and results that have been generated by this effort.

2. Review of Existing Models

2.1 Introduction

As an initial step of the Project, the technical team conducted a comprehensive review of existing collision risk modeling approaches and methodologies, as they have been applied to model the risk of bird collisions with wind turbines at offshore wind energy facilities. The objective of this review was to identify a modeling approach that was optimally suited to the task of obtaining quantitative predictions of rufa Red Knot fatalities resulting from interactions with the Facility that has been approved in federal waters of Nantucket Sound, Massachusetts.

Our review included both peer-reviewed and non-peer-reviewed literature, as well as appropriate publications and websites. Furthermore, material presented at relevant conferences was also used (e.g., Conference on Wind Energy and Wildlife Impacts, Trondheim, Norway, 2011; Conference on Marine Renewables and Birds British Ornithologists Union, Peterborough, United Kingdom, 2012; Conference on Wind Energy and Wildlife Impacts, Stockholm, Sweden, 2013; International Marine Conservation Congress, United Kingdom, 2014). Where appropriate, contact was also made with the authors of collision rate models to request details of their models.

Several of the models described in the review are partly based on other models or present an alternative approach to a similar model. In some such cases, we have grouped different models as we deemed appropriate, in order to represent the true variation in structural and conceptual elements of different bird-wind collision risk models within our review. For example, a number of studies are available that focus on a specific site and/or species, and which use case-specific information to inform certain aspects of the model, such as the numbers of birds at risk. These studies have used existing models for calculating collision probability and encounter rate and as such are not classified separately in our review in all cases. Some of these studies however, provide useful case studies for the inclusion of site- and species-specific information for informing certain aspects of the models and are described where relevant.

In total, our review included a total of 13 distinct bird – wind turbine collision models. An overview of these models is given in Table 2.1. For two of these models, the model equations, or other structural elements of the models were not publicly available, and these models were excluded from further consideration. Several others were combined, as they essentially consisted of minor variations of each other, resulting in more detailed evaluation of nine models.

Table 2.1 Overview of bird – wind turbine collision models described in publicly available literature.

For models for which not all calculations are available, some details could not be provided. '+' indicates that the model covers this aspect, thus providing a means for the aspect to be calculated; '-' indicates that it model does not cover the aspect; '?' indicates that details are unavailable and aspect cannot be assessed.

Model and Reference	Calculations Available	Collision Probability	Encounter Probability	Exposure Rate	Avoidance Rate	Model/ Case Study	Description of Model
Tucker 1996	+	+	-	-	-	General model	The first general mathematical model to calculate collision probability. Includes changing probabilities in relation to birds' point of passage and multi-directional passage through rotor.
Band 2000	+	+	+	-	-	General model	Similar to Tucker (1996). Uses average collision probability and perpendicular flights. Spreadsheets of calculations available. Further described in Band et al. (2007), which describes approaches for encounter probability.
Bolker et al. 2006, 2014	+	-	+	-	-	General model	Main focus on encounter probability, based on flight and wind direction. Spreadsheets of calculations available. Uses a fixed collision probability but gives little indication of how this was derived.
Podolsky 2008	-	+	+	-	?	General model	Similar to Tucker (1996) and perhaps Troost (2008). Described in Podolsky (2005), few further details available.
Troost 2008	+	+	+	+	+	General model	Three approaches for estimating collision rate based on comparisons with existing wind farms (routes 1 and 2), or on theoretical collision probability models (route 3) using Band (2000). Spreadsheets of calculations available. Generalized approach described for offshore situation. No predefined way to calculate exposure rate.
Holmstrom et al. 2011	-	+	+	+	+	General model	Based on Tucker (1996), although includes multi-directional passage through rotor.

Folkerts, *in* Department of Energy & Climate Change (DECC) 2012	-	+	+	+	?	General model	First described in 2006 (M. Perrow, personal communication [pers. comm.] 2014), this model seems to take a similar approach to that later described in Band (2012), basing collision risk on Tucker (1996). The component for encounter probability seemingly follows Bolker et al. (2006, 2014). Unlike Band (2012), allows multi-directional passage through rotor. Also in Green and Perrow (2012).
Band 2012	+	+	+	+	+	General model	Similar to Tucker (1996), Band (2000) and Folkerts (*in* DECC 2012) and expanded for use with seabird data collected at offshore wind farms. Option to include adjusted encounter probability and collision probability based on birds' flight height distribution. Spreadsheets of calculations available.
Smales et al. 2013	-	+	+	+	+	General model	Similar to Band (2000), but includes multi-directional passage through rotor area and static structures of turbine. Also known as Biosis model.
Hatch and Brault 2007	Not applicable					Case study	Case study for Roseate Tern and Piping Plover using Bolker et al. (2006).
Nations and Erickson 2010	Not applicable					Case study	Case study for Marbled Murrelet. Uses Tucker (1996) for collision probability. Focused on obtaining situation-specific rates for exposure and avoidance rates.
Gordon et al. 2011	Not applicable					Case study	Case study for Roseate Tern and Piping Plover. Encounter probability using Bolker et al. (2006) and collision probability from Hatch and Brault (2007). Focused on obtaining situation-specific exposure rates and multi-scale avoidance rates.
Eichhorn et al. 2012	Not applicable					Case study	Case study for Red Kites. Uses collision probability from Band et al. (2007) and empirical data on avoidance rates along with landscape model.

In the remainder of this section, we first present definitions of certain key terms in order to create a standard language for the review. We then describe how certain key modeling aspects are handled in each of the nine distinct models we reviewed in-depth, with a focus on five "general" models that could potentially be adapted or applied to the current study. We conclude with a recommendation for a modeling approach to be applied to the current study. The recommendation was generated through consideration of six specific model evaluation criteria, as well as the specific objectives and characteristics of the current Project.

2.2   Key Terms of Collision Models

In this section, we define four key terms that comprise core elements of most models of bird collisions with wind energy facilities. We then discuss the ways in which these terms are incorporated within the different models we reviewed.

2.2.1   Definitions of Terms

- *Collision probability*   The probability that a bird that flies through the rotor-swept area is hit by a rotor blade;

- *Encounter probability* The probability that a bird that flies through a wind farm encounters one or more turbines;

- *Exposure rate*   The rate at which birds fly through the wind farm area, expressed as a number of birds per unit of time;

- *Avoidance rate(s)* The rate at which birds take evasive action to avoid either the entire wind farm (macro-avoidance) or individual wind turbines (micro-avoidance).

2.2.2   Discussion of How Terms have Been Applied in Models

Collision Probability

Perhaps the aspect that has received the most attention in collision modeling is the probability of collision during passage of the rotor area. Several models have used theoretical reasoning to examine the probability of collision with the rotors based on the physical characteristics of the turbine and bird species in question, for example Tucker (1996) and further described by Band (2000), Podolsky (2005, 2008), Holmstrom et al. (2011), Folkerts (*in* Department of Energy & Climate Change [DECC] 2012), Green and Perrow (2012), Band (2012), and Smales et al. (2013). Several of these models also consider the numbers of flying birds that encounter the rotor and an avoidance factor, here referring to avoidance of individual rotors (cf. micro-avoidance).

Several of these models (e.g., Podolsky 2008, Holmstrom et al. 2011, Folkerts [*in* DECC 2012], and Smales et al. 2013), apply a calculation for flights at oblique angles to the rotors, as described in Tucker (1996) and Band (2000), and later in Band et al. (2007) and Band (2012). Whereas Band (2000) and Band (2012) recognize the validity of oblique flight angles and regard it as a relatively minor factor in the model, both Holmstrom et al. (2011) and Folkerts (*in* DECC 2012, Green and Perrow 2012) suggest otherwise, and include oblique flights in addition to perpendicular flights. Holmstrom et al. (2011) suggest that the inclusion of oblique flight can increase the overall collision risk. They do however not mention the reduced number of passages through the rotor area due to the relatively smaller encounter area, as described in Band (2000), Bolker et al. (2006, 2014), Band et al. (2007), and Band (2012). In a comparison for a theoretical offshore wind farm, Folkerts (*in* DECC 2012) produced only slightly lower estimates than Band et al. (2007) (Green and Perrow 2012).

Several authors use Tucker (1996), Band (2000), or Band et al. (2007) for estimating the collision probability within their models (Desholm and Kahlert 2006, Troost 2008, May et al. 2010, Mateos et al. 2011, Sugimoto and Matsuda 2011, Holmstrom et al. 2011, Nations and Erickson 2010, Band 2012). An alternative approach to theoretical modeling is to use empirical data as is described in the first two approaches in Troost (2008). Here, data on number of collisions (either per period of time or per crossing) from a reference wind farm, or wind farms, are used to estimate the potential numbers of collisions in the planned wind farm. The advantage of using empirical data is obvious as this also includes any avoidance of turbines, which are in general difficult to assess and have a large influence on results (Chamberlain et al. 2006). Empirical data however, may be limited by being turbine-, site- and/or species-specific or influenced by environmental conditions and events. Factors relating to location and species are of particular importance as currently only empirical data are available for terrestrial wind farms. In these models, therefore, many 'land-based' assumptions still have to be adjusted to offshore locations, including the use of land-based collision rates.

Encounter Probability

Various approaches exist for deriving the numbers of turbines that are encountered by birds flying through a wind farm. The simplest of these is to assign a proportion based on the proportion of the airspace occupied by turbines, combined with a mean number of turbines encountered (calculated as the square root of the total number of turbines to account for all flight directions) (Troost 2008, Smales et al. 2013). Band (2012) uses a similar method, in which the encounter probability is based on the number of turbines and on the areal density of birds within a risk zone. This risk zone is determined by the size of the rotor and the ground speed of the flying bird in question. Encounter probability is considered in further detail in the 'extended' option of Band (2012), in which the reduced encounter rate of birds passing through the spandrels around the rotor is considered based on the flight heights of the species in question. A more detailed approach is described by Bolker et al. (2006, 2014), who calculate the number of turbines encountered based on the layout of the wind farm in question and on a range of flight angles and wind directions. This approach may represent a more realistic approach for wind farms that deviate from a largely square design and where flight direction is predominantly in a single direction (such as could be the case for migrating birds). For situations where there is no predominant flight direction or where the turbine layout is fairly uniform, using the simpler method is likely to suffice.

All of the methods described above make the assumption that birds are evenly distributed within the wind farm and most assume that birds follow a straight-line flight path. Several models make an adjustment for flight height and consider only those birds at rotor height (Troost 2008, Band 2012). As mentioned below, the level of avoidance in the horizontal and vertical planes also strongly influences the encounter probability. These last two factors are discussed further with regards to exposure and avoidance rates.

Exposure Rate

Exposure rate refers to the numbers of bird flights through the wind energy Facility area over a given unit of time, and we note that this is not equivalent to the number of individual birds exposed. Typically, we adopt a realistic worst-case scenario and assume that each flight of a bird through the wind farm is made by a different individual. However, in some instances, such as for local populations or where the same individuals make multiple flights through the wind farm, individual-based approaches that deviate from this assumption may be appropriate (Mateos et al. 2011, Eichhorn et al. 2012, Smales et al. 2013). For certain

situations where relevant data is available, seasonal and diurnal variation, as well as weather and condition-specific variation can be incorporated into exposure rates and included within models, generating more complex and more realistic representations of the passage rates of birds through wind facilities within models (Hatch and Brault 2007, Nations and Erickson 2010, Gordon et al. 2011).

Avoidance Probabilities

Behavioral avoidance is recognized as one of the most important factors in determining the collision rates of birds (Chamberlain et al. 2006; Drewitt and Langston 2006; Cook et al. 2012, 2014). Various authors have recognized several different types of avoidance behaviors that may be performed by birds interacting with wind facilities, with important consequences for collision risk modeling (Cook et al. 2012, 2014). Herein, we use the concepts of "macro-avoidance" and "micro-avoidance" as defined by Gordon et al. (2011) to classify different avoidance behaviors into two distinct scales, both of which have been incorporated into certain collision risk models. "Macro-avoidance" is defined as the probability of birds approaching the wind energy Facility redirecting their flight to avoid flying into the wind energy Facility altogether. This has the effect of reducing the number of birds that pass through the wind farm, and therefore can be considered to affect the exposure probability. "Micro-avoidance" is defined as the probability of a bird redirecting its flight trajectory within a short distance of a turbine to avoid flying through the rotor-swept area as it flies within the wind Facility. This concept only applies to birds that are already flying within the wind energy Facility, and hence does not impact exposure probability, but it can potentially influence the encounter probability, depending on how this parameter is incorporated into the model.

Both types of avoidance reduce the numbers of birds at risk of collision. The level to which numbers are reduced in reality remains largely unknown, as avoidance has proven difficult to quantify, and is likely to vary in response to a wide range of environmental and ecological factors as well as the configuration of the wind farm (Krijgsveld 2014). It is widely accepted that overall avoidance probabilities (both types of avoidance combined) amongst birds are likely to be high, perhaps on the order of 90% – 99%, or even higher. Several models have used a single avoidance probability to represent both types of avoidance (Band 2000, 2012), whereas most have applied separate macro- and micro-avoidance probabilities (Troost 2008, Nations and Erickson 2010, Smales et al. 2013). These two types of approaches can be compared and interrelated as follows:

$$P(\text{overall avoid}) = 1 - [1 - P(\text{macro} - \text{avoid})] \times [1 - P(\text{micro} - \text{avoid}|\text{no macro} - \text{avoid})]$$

where $P(\cdot)$ denotes probability, "avoid" is short-hand for "avoidance", and the last quantity is the conditional probability of micro-avoidance given there was no macro-avoidance. The use of separate avoidance probabilities for macro- and micro-scale behavioral avoidance phenomena provides greater transparency and model flexibility for incorporating a biologically realistic representation of birds' avoidance behaviors than does the use of single avoidance probability. This conclusion is supported by the work of Petersen et al. (2006) and Krijgsveld et al. (2011), who used radar and visual data to demonstrate the occurrence of both macro- and micro-avoidance behaviors in birds at offshore wind farms. These studies focused mainly on seabirds but show the importance of relating avoidance behaviors to separate, specific avoidance parameters that can be incorporated into collision models at different scales.

With regard to the various components of collision rate models, avoidance probabilities influence both the exposure probability (macro-avoidance) and the encounter probability (micro-avoidance). In theory, collision rate could also be influenced by avoidance behaviors occurring at even finer scales of space and time than micro-avoidance, if birds can evade the moving blades of the rotor during passage through the rotor-swept area. Such avoidance maneuvers at the finest scale affect collision probabilities at the level of birds potentially encountering rotors as both birds and rotors move within the rotor-swept plane, and therefore must be incorporated into the basic geometry of collision probability modeling. All existing models to date have used either the Tucker (1996) model, or the Band (2012) model to represent this level of geometric dynamics, and of these, evasive actions by birds inside of the rotor-swept plane can only be incorporated into the former. For this reason, collision risk models using the Band model to represent basic collision geometry have necessarily incorporated avoidance behaviors only at larger scales (e.g. macro-avoidance and/or micro-avoidance as defined herein), if at all.

It is important to note that because macro-avoidance influences the number of birds that fly through the wind energy Facility, the relationship between macro-avoidance and exposure probability must be carefully considered in developing bird collision risk models at wind farms. This consideration, and the incorporation of avoidance probabilities into collision models, may be constrained by the type of input data on bird passage rates that are incorporated into collision risk models. Band (2012) has been specifically developed for use with density data from ship-based and aerial surveys, which does not include any macro-avoidance behavior, whereas Smales et al. (2013) used point counts as the starting point, from which macro-avoiding birds had already been subtracted, in the case of post-construction observations. Troost (2008) used a general bird passage rate (flux) figure, meaning that visual observations, radar data or expert opinion can be used, and the rate has generally not had macro-avoiding birds pre-removed.

2.3   Description and Comparison of Reviewed Models

2.3.1   General Models

We classify five of the models we reviewed as "general models," meaning that their basic structures are general to a wide variety of specific applications, not tailor-made to one specific case study. The models we classified as general models are those described in Tucker (1996), Band (2000), Bolker et al. (2006, 2014), Troost (2008) and Band (2012). The first two of these models, Tucker (1996) and Band (2000), focus on the collision probability for a bird passing through the rotor-swept area, while the model in Bolker et al. (2006, 2014) provides an approach for calculating encounter probability. The models in Troost (2008) and Band (2012) describe standardized approaches for all four of the core components described previously. Troost (2008) describes three alternatives within a general approach. Two of these alternatives are based on empirical data from existing wind farms on land, which limits their use for offshore areas and for species-specific studies. The third alternative requires the use of a separate model for calculating collision probability (such as Band 2000). Band (2012) provides the most complete model with respect to estimating collision probability from standard input data that is commonly available, but as a consequence, offers little flexibility.

2.3.2   Situation-Specific Models

We classified four of the models we reviewed as situation-specific models, meaning that they incorporated case-specific detail into the model that may, or may not be applicable to other

case studies. While the specific approaches taken in these cases cannot be applied directly to the current study, they are useful for our purposes as they represent examples of how general models can be adapted toward specific cases with the inclusion of case-specific detail. A few examples of such models are described below.

Hatch and Brault (2007) assessed collision rates for Roseate Tern (*Sterna dougallii*) and Piping Plover (*Charadrius melodus*) for an aproved wind farm at Horseshoe Shoal in Nantucket Sound. Encounter probability was based on Bolker et al. (2006), while exposure probability, avoidance probability, and collision rate focused on situation-specific information for each species considered and modeled separately. Species-specific information incorporated into the models included variable flight heights and other behavioral features of each species in relation to weather conditions, breeding phenology, and migration.

Nations and Erickson (2010) modeled collision rates for Marbled Murrelet (*Brachyramphus marmoratus*) at three wind farm variants in Washington State. The model incorporated elements of species-specific biology and data collected at the site to determine the potential number of passages through the wind farm, and in turn, the rotor-swept areas of the turbines, modeled in a spatially explicit configuration. Collision probability was then calculated using Tucker (1996). Besides species-specific data, the model also incorporated specific information relating to the wind farm including wind data and periods of curtailment. Nations and Erickson (2010) also considered the high wing loading of the species with respect to avoidance ability by including a risk associated with the supporting structures and static turbines.

Gordon et al. (2011) developed a model for assessing collision rates specifically for Roseate Tern at offshore wind energy facilities on the Atlantic Outer Continental Shelf. The model was based on Hatch and Brault (2007) and Bolker et al. (2006). The exposure probability, encounter probability, and both micro- and macro-avoidance probabilities were informed using empirical data gathered at field sites in Massachusetts.

Eichhorn et al. (2012) used individual-based spatial models in order to assess the potential collision rate for Red Kite (*Milvus milvus*). This approach assessed flight activity based on the proximity of suitable habitat around a territory. This was combined with an avoidance probability and a model for the probability of collision during passage of the rotor (for which Eichhorn et al. 2012 used Band et al. 2007). Mateos et al. (2011) presented a similar approach for seabirds based on the probability of moving in a certain direction, which was based partly on the presence of turbines. Collision probability was estimated using existing models (Tucker 1996 or Band et al. 2007).

2.4 Evaluation of Model Suitability for Application to Red Knots in Nantucket Sound

In this section, we present an evaluation of the suitability of the five available general models for application to modeling collisions of rufa Red Knots with the approved Facility in Nantucket Sound. Our evaluation is based on six specific criteria, and centers on the completeness and sufficiency of the ways in which the candidate models treat the four main model aspects (collision probability, encounter probability, exposure probability, and avoidance probabilities), as applicable to the case of modeling rufa Red Knot collisions with the Facility approved in federal waters of Nantucket Sound, Massachusetts. The seven model

evaluation criteria are defined below, and a summary of our evaluation of these models is presented in Table 2.2.

Completeness

This criterion relates to the models' completeness with respect to the four core components of collision risk models, as described previously (1 = collision probability, 2 = encounter probability, 3 = exposure probability, 4 = avoidance probabilities).

Acceptance

This criterion relates to how well each model has been accepted, and how widely it has been applied within the scientific field of wind-wildlife interaction science.

Flexibility

This criterion describes how readily the model's structure can be applied to a wide range of potential input data.

Bird Distribution and Directional Assumptions

This criterion describes specific assumptions contained within the candidate models regarding the spatio-temporal distributions of birds, as well as birds' flight directions.

Flight Height Adjustments

This criterion describes whether or not the candidate model has the capacity to incorporate variation in birds' flight altitudes, or flight altitude distributions, as model inputs.

Ability to Incorporate Red Knot Biology

This criterion is a composite consideration of the candidate models' general suitability for application to Red Knots, given certain specific aspects of Red Knot biology that are believed to have important influences on the species' risk of collisions with wind turbines.

Table 2.2 Candidate models (represented in columns) and evaluation criteria (rows) used in the review of candidate offshore wind bird collision models for application to generating quantitative collision rate predictions for Red Knots at the approved Facility in Nantucket Sound, Massachusetts.

Criterion	Tucker (1996)	Band (2000)	Bolker et al. (2006, 2014)	Troost (2008)	Band (2012)
Completeness*	**1**	**1**	**2**	**1-4**	**1-4**
Acceptance	Widely applied and accepted.	Widely applied and accepted.	Widely applied and accepted. Previously used for Piping Plover and Roseate Tern at the Facility.	Widely used in Netherlands.	Widely applied and accepted. Currently widely used for seabirds in several European countries.
Flexibility	Collision probability suitable for incorporation in other models.	Collision probability suitable for incorporation in other models.	Encounter probability suitable for incorporation in other models.	Some flexibility with input data.	Collision probability suitable for incorporation in other models. Rigid in incorporation of number of birds, encounter probability and avoidance probability.
Bird distribution and directional assumptions	Range of flight angles across the rotor area included.	Flight angles assumed perpendicular to rotor area.	Actual distribution and flight directions incorporated in encounter probability	Even distribution, single flight directions assumed. (see Band 2000).	Even distribution with random flight directions assumed, flight angles assumed perpendicular to rotor area
Flight height adjustments	Yes	No	Yes	No (*see* Band 2000)	Yes
Ability to incorporate Red Knot biology	Allows variation in biometry, flight speed.	Allows variation in biometry, flight speed.	Allows inclusion of flight direction.	Includes flight height (see Band 2000).	Includes biometry, flight speed, flight height, flight density (relates to seabirds and not to Red Knots).
Overall suitability for current study	Provides only collision probability.	Provides only collision probability. Too simple compared to Band (2012).	Approach of encounter probability well suited for current case. Collision probability (fixed) less suited, number of birds and avoidance probability not included in model.	Approach is too general.	Approach of collision probability well suited for current case. Encounter probability, exposure probability, and avoidance probabilities not suited for the highly directional flights of migrating Red Knots.

*Completeness = which of the four basic model elements described in text above are included (see text).

2.5   Recommended Modeling Approach for the Current Project

Based on this review, we recommend the development and application of an original, compound model that combines the best available aspects of existing models while being informed by the available data regarding the species- and site- specific information. We believe that the Band (2012) model contains the most suitable representation of collision probability for the current application. In essence, this part of the recommended compound model would encompass the probability that Red Knots that are flying through the rotor-swept areas of the turbines within the approved Facility would collide with wind turbine rotors. We consider that other aspects of the dynamics of the system of interest can be best represented by incorporating additional dynamics into a compound model with the Band (2012) model at its core. For example, site-specific encounter probabilities can be most accurately represented by incorporating a spatially-explicit representation of the specific location and turbine layout of the approved Facility, combined with species-specific information on the migratory patterns of rufa Red Knots. Encounter probability can be further refined by the incorporation of information on the migratory flight altitudes of rufa Red Knots in relation to environmental conditions, as well as the accommodation of non-perpendicular approach flight directions. Macro- and micro-avoidance probabilities can be developed using species-specific information on rufa Red Knot flight behaviors and morphology, as well as site-specific data on wind, precipitation, and visibility conditions during the seasonal time windows, within which rufa Red Knots are expected to pass through the Facility region.

3.   Methods

3.1   Introduction

In this methods section, we present a description of the original model that was developed by the Project's technical team for the purpose of obtaining quantitative estimates of rufa Red Knot collision fatalities at the Facility that has been approved for federal waters of Nantucket Sound, Massachusetts. In Section 3.2: *Model Overview*, we present a basic description of the model's overall structure, as it was realized, guided by the recommendation presented in the previous Chapter. In Section 3.3: *Input Assumptions and Data*, we review the model's basic input variables, assumptions, and other structural elements, as they were incorporated into the model based on the vision for the incorporation of biological and meteorological realism that was collectively developed by the Project's technical team during a series of teleconferences that occurred in fall 2014. In Section 3.4: *Model Description*, we present a detailed and comprehensive description of the structure of the model, as well as a description of the methodology for the simulations that were run to generate the results.

3.2   Model Overview

We have developed a stochastic simulation model for estimating Red Knot fatalities due to collision with wind turbines at the Facility that has been approved in federal waters of Nantucket Sound, Massachusetts. The model is spatially explicit, accounting for the Facility's location in relation to migratory flights of Red Knots through Nantucket Sound, as well as the approved layout of turbines within the Facility. Red Knot flights through the Facility within turbine heights have direct geometric representations, as do collisions with individual turbines.

At its core, the model relies on the Band (2012) model to calculate the probability of collision with active turbine rotors. However, our model explicitly accounts for considerable detail that is not present in Band's rotor model. This detail includes various aspects of Red Knot biology, such as seasonal differences in migration numbers and flight patterns, effects of variable weather conditions on flight patterns, and flocking behavior. Furthermore, Red Knot avoidance behaviors are hierarchical (macro-avoidance of the entire Facility, and micro-avoidance of individual structures within the Facility). Rather than post hoc adjustment of fatality rates based on a single overall avoidance probability, as in Band (2012), avoidance is fully integrated into our model such that the only birds at risk of collision are those that fail to actively avoid both the Facility and then individual structures within the Facility.

In addition to Red Knot characteristics, our model explicitly accounts for wind turbine dynamics including orientation which is dependent on variable wind direction, as well as rotational velocity and blade pitch angle which are dependent on variable wind speed. In addition to collision with active rotors, the model recognizes the potential for collision with stationary structures including rotors (when wind conditions dictate), turbine towers and nacelles, and the electrical service platform (ESP) within the Facility.

Each iteration of the model represents flights of the at-risk migratory populations of Red Knots in spring and fall of a single year. The primary outcome of interest is the number of fatalities, which – for that iteration – is a realization of a process with many random components. Repeating that process many times, that is, generating a large set of independent realizations, yields the distribution of the number of fatalities. We summarize the distribution in several ways including the expected number of fatalities per year and the probability of one or more fatalities in a year.

3.3   Input Assumptions and Data

3.3.1   Red Knot Biology

The sections that follow address the major features of Red Knot biology that we believe will influence the number of birds at risk of collision, as determined by the Project's technical team during a series of teleconferences held in fall 2014. Table 3.1 summarizes the major assumptions in the collision risk model. In some cases, we have assumed a particular characteristic has a fixed value, and we have considered neither natural variation in that characteristic nor any alternative values. Examples of such characteristics include Red Knot body size (wing span and body length) and the number of at risk flights per season (Table 3.1). In other cases such as flight speed and direction, we have assumed the characteristic exhibits natural variation. In simulations, the variation has been represented by generating random variates from a statistical distribution, for instance, a parametric distribution in the case of air speed and a non-parametric distribution in the case of fall flight direction (Table 3.1). In several of the sections below, we refer to the "baseline" condition or assumption, that is, the most reasonable assumption given what is known. We recognized that there was uncertainty inherent in these assumptions and that model output might be sensitive to variation in these characteristics, so we examined alternatives to the baseline. In some cases, the alternatives were additional fixed values. For example, the baseline headwind threshold for 'choosing' to delay departure in the fall migration was 5.0 meters per second (m/s; 16.4 feet [ft] per s), but we also examined alternative thresholds of 10 m/s (33 ft/s) and 15 m/s (49 ft/s). In other cases, the alternatives were randomly generated from a

statistical distribution. For instance, the baseline fall migratory population was fixed at 1,500 Red Knots, while alternative population sizes were simulated from a Negative Binomial (Neg Bin) distribution with expected value of 1,500. Finally, flight altitude was unique in that we assumed natural variation in flight heights under baseline conditions, while the alternatives were similar distributions with different parameters; that is, we also assumed that there was natural variation under the alternatives. Each of the assumptions in Table 3.1 is described in greater detail below.

Table 3.1 Primary assumptions regarding Red Knot biology as incorporated into the collision model.

Feature/Assumption	Baseline	Alternatives
Number of at risk flights	1 per season per individual	--
Migration timing	Non-parametric distributions[1] (see Figure3.2)	--
Flight directions	Fall: Non-parametric distribution [1] (see Figure 3.3b) Spring: Uniform distribution [1] (see Figure 3.4)	--
Body size	0.54 m wingspan, 0.24 m body length	--
Flock size	Discrete Uniform, $\mu = 105$ [1]	--
Flock shape	Chevron	--
Flight speed (air speed)	Gamma, $\mu = 20.1$ m/s [1]	--
Population size		
Current, Fall	1,500	Neg Bin, $\mu = 1,500$ [2]
Current, Spring	150	Neg Bin, $\mu = 150$ [2]
Recovered, Fall	4,500	Neg Bin, $\mu = 4,500$ [2]
Recovered, Spring	450	Neg Bin, $\mu = 450$ [2]
Fall departure delay		
Headwind threshold	5.0 m/s	10 m/s, 15 m/s
Delay sensitive proportion	0.80	0.60, 0.95
Flight altitude		
High	Uniform, $\mu = 1,000$ m [1]	Uniform, $\mu = 500$ m [3] Uniform, $\mu = 1,500$ m [3]
Low	Gamma, $\mu = 19.50$ m [1]	Gamma, $\mu = 13.50$ m [3] Gamma, $\mu = 24.00$ m [3] Gamma, $\mu = 33.75$ m [3]
Headwind threshold	5.0 m/s	10 m/s, 15 m/s
Precipitation threshold	2.5 mm/hr	1 mm/hr, 4 mm/hr
Macro-avoidance probability		
Good weather	0.28	Beta, $\mu = 0.28$ [2]
Poor weather	0.01	Beta, $\mu = 0.01$ [2]
Precipitation threshold	2.5 mm/hr	1 mm/hr, 4 mm/hr
Visibility threshold	1,000 m	500 m, 2,000 m
Micro-avoidance probability (active rotors)		
Good weather	0.93	Beta, $\mu = 0.93$ [2]
Poor weather	0.75	Beta, $\mu = 0.75$ [2]
Headwind threshold	5.0 m/s	10 m/s, 15 m/s

Micro-avoidance probability (stationary structures)		
Good weather	0.99	Beta, $\mu = 0.99$[2]
Poor weather	0.85	Beta, $\mu = 0.85$[2]
Headwind threshold	5.0 m/s	10 m/s, 15 m/s

[1]Distribution representing natural variability
[2]Distribution to account for uncertainty in baseline assumption
[3]Distribution representing natural variability, with alternate parameterization for uncertainty
mm = millimeter; m = meter; hr = hour

Number of at Risk Flights

The number of at risk flights was assumed to be directly related to the numbers of individual Red Knots potentially migrating through the Facility area in each season, as the Project team determined that it was unlikely for Red Knots to utilize the area in the course of activities other than migration (e.g., daily foraging or commuting flights), and hence it was unlikely for any individual birds to cross the Facility area multiple times within a season (L. J. Niles, personal communication [pers. comm.]). For fall, the population of interest was assumed to consist exclusively of the short-distance migrant subset of the rufa Red Knot population that stages at, or near the Monomoy National Wildlife Refuge (MNWR) on Cape Cod, Massachusetts. The rationale for this assumption is that only the short-distance migrants are believed to normally fly in westerly directions, potentially crossing the Facility area in Nantucket Sound, as they progress southward from the MNWR in fall, headed to various destinations along the Atlantic Coast of the US (Harrington et al. 2010, Niles et al. 2012). By contrast, members of the long-distance migrant subpopulation are believed to fly eastward as they fly south from Massachusetts in fall, hence they are not likely to cross the Facility area (Harrington et al. 2010, Niles et al. 2012). We assumed a fixed baseline population size of 1,500 short-distance migrant Red Knots. We did not attempt to represent natural variation in population size, though in additional simulations, uncertainty in fall population size was represented by generating random variates from a Neg Bin ($r = 58.44$, $p = 0.0375$) distribution (Figure 3.1a), with mean = 1,500 and standard deviation = 200, thus, with coefficient of variation of 0.13. This distribution was intended to be consistent with the expert opinion that the current fall population of short-distance migrants staging at the MNWR is between 1,000 and 2,000 birds (Niles, pers. comm.).

Expert opinion held that there was less certainty about the number of Red Knots migrating through Nantucket Sound in the spring, but that the number was probably 5 – 10% of the size of the fall at-risk population, as the vast majority of Red Knot individuals from both the long- and short-distance populations are expected to fly directly over land between spring migratory stopover areas in Delaware Bay and breeding areas in the vicinity of Hudson Bay, Canada, thereby passing entirely to the west of Massachusetts and not flying through the Facility area (Gordon et al. 2011; Burger et al. 2012; Niles et al. 2010, 2012; Niles, pers. comm.). For modeling, we assumed a fixed baseline spring migratory population of 150 Red Knots, i.e., 10% of the size of the fall baseline population. To account for uncertainty in that number, we conducted additional simulations in which the spring population size was randomly generated from a Neg Bin (9.57, 0.06) distribution (Figure 3.1b), with mean = 150 and standard deviation = 50 (coefficient of variation = 0.33).

We also assumed that under full species recovery, the sizes of the migratory populations passing through Nantucket Sound would be three times current population sizes. That is, the expected

fall population of birds potentially passing through the Facility area would be 4,500 Red Knots and the expected spring population would be 450. As for current populations, we accounted for uncertainty by randomly generating population sizes using a Neg Bin (139.2, 0.03) distribution for fall (Figure 3.1c) and a Neg Bin (21.2, 0.045) distribution for spring (Figure 3.1d).

a

b

c

d
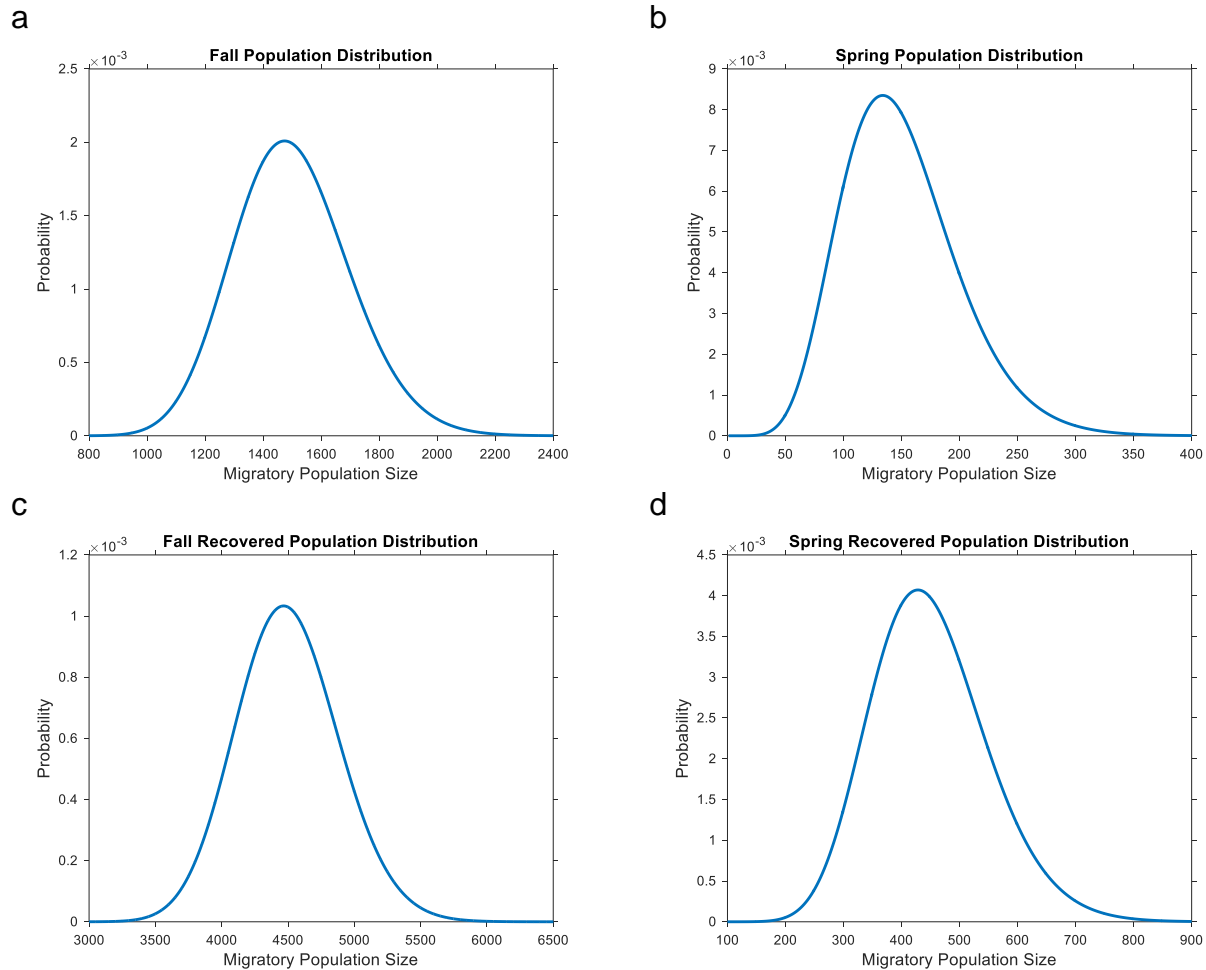
Figure 3.1 Assumed distributions of current numbers of individual Red Knots that potentially cross the Nantucket Sound Facility area.

The "population size" in (a) fall and (b) spring, and recovered populations in (c) fall and (d) spring. All four plots represent Negative Binomial probability mass functions. Note that the X-axis limits differ in each panel.

Migration Timing

Seasonal Timing

We developed non-parametric distributions based on data from eBird, (Sullivan et al. 2009, eBird 2014) as well as expert opinion (Niles, pers. comm.) to represent the timing of Red Knot passage through Nantucket Sound in fall and spring. Fall departures from the MNWR were assumed to begin on July 8 and end on November 21, with early September being the most likely time of departure and with 90% of birds departing between July 28 and November 3 (Figure 3.2a). In the spring, we assumed that the first Red Knots would begin passing over Nantucket Sound on April 28 and that the last day of migration would be June 9, with passage most likely

in mid-May (Figure 3.2b). Note that both seasonal distributions represented Julian dates, i.e., continuous date and time.

a

b
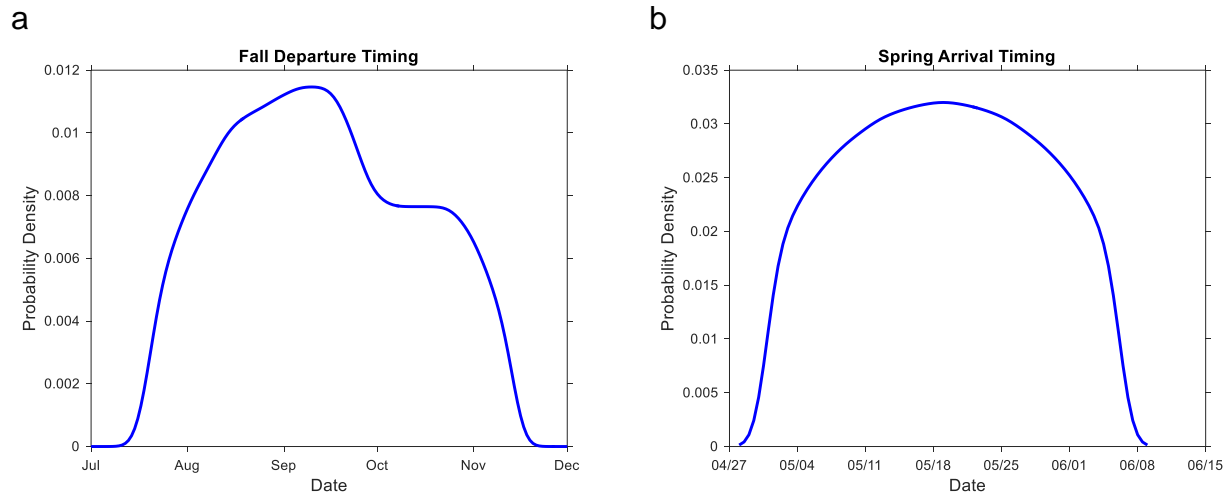
Figure 3.2 Simulation distributions for timing of Red Knot migration at Nantucket Sound.
(a) fall departure from the Monomoy National Wildlife Refuge, and (b) spring "arrival", i.e., passage over Nantucket Sound. Both panels represent non-parametric probability density functions based on expert opinion (Niles, pers. comm.).

Diurnal Timing
The diurnal distribution of flights depended on the season. In fall, birds were assumed to pass over the Facility area not long after (within ca. one hour [hr]) of departing from land, as birds were assumed to initiate these flights from the staging areas in the vicinity of the MNWR. Therefore, fall flights were assumed to occur near sunset, generally in the few hours preceding sunset but occasionally shortly following sunset (Niles, unpublished data). However, depending on wind conditions at the selected time, we used anecdotal observations by experts to develop a structured set of realistic assumptions regarding decisions made by Red Knots to delay fall migratory flight departures under adverse weather conditions, specifically headwinds. If headwinds exceeded a threshold level, most Red Knot flocks were assumed to delay their departure. During simulations in which this threshold was crossed and fall departures were delayed, wind conditions were checked and delay decisions re-evaluated in each subsequent hour until the headwind was less than the threshold, five days elapsed, or the end of the fall season was reached, whichever occurred first. For baseline conditions, we assumed that the headwind threshold was 5.0 m/s and that 80% of flocks (randomly chosen) were *delay sensitive*, i.e., they would delay departure if the threshold was exceeded. Irrespective of wind conditions, the remaining 20% of flocks would depart at the time initially selected. This model feature was designed to mimic observed behavior of Red Knots, which generally tend to delay departure on migratory flights until there is a following wind (Niles, pers. comm.). To examine sensitivity to these parameter choices, additional simulations were conducted in which the headwind threshold for departure was set at alternative values of 10 m/s and 15 m/s, and the percentage of flocks choosing to delay departure was set at alternative values of 60% and 95%.

In spring, flights through Nantucket Sound were assumed to occur with roughly equal probability at any time of day. This assumption was based on the notion that flocks passing through the area

17

would have made long over-water flights of varying distance immediately prior to their Nantucket Sound crossing, and would have encountered differing weather conditions such that synchronized "arrival" would be highly unlikely.

Migration Flight Directions

Fall flight directions were based on a dataset representing 23 "short-distance" migrants among a larger set of Red Knots tagged with geolocators at the MNWR (Niles, pers. comm.). These data consisted of terrestrial endpoints of flights (origin at the MNWR and terminus at various destinations or stop-overs), though not actual flight paths. We assumed straight-line flights between these endpoints in all cases (Figure 3.3a) and calculated the direction from the MNWR to each destination. A linear kernel density (Silverman 1986) was fit to these directions (Figure 3.3b). Note that three of the 23 observed directions crossed the approved Facility (Figure 3.3a) while approximately 11% of the fitted distribution lay between the angular limits of the Facility (Figure 3.3b). During simulations, all flights in fall were assumed to originate from the MNWR and flight directions were generated from the fitted kernel density. That is, simulations were designed to represent natural variability in flight directions.

a   b
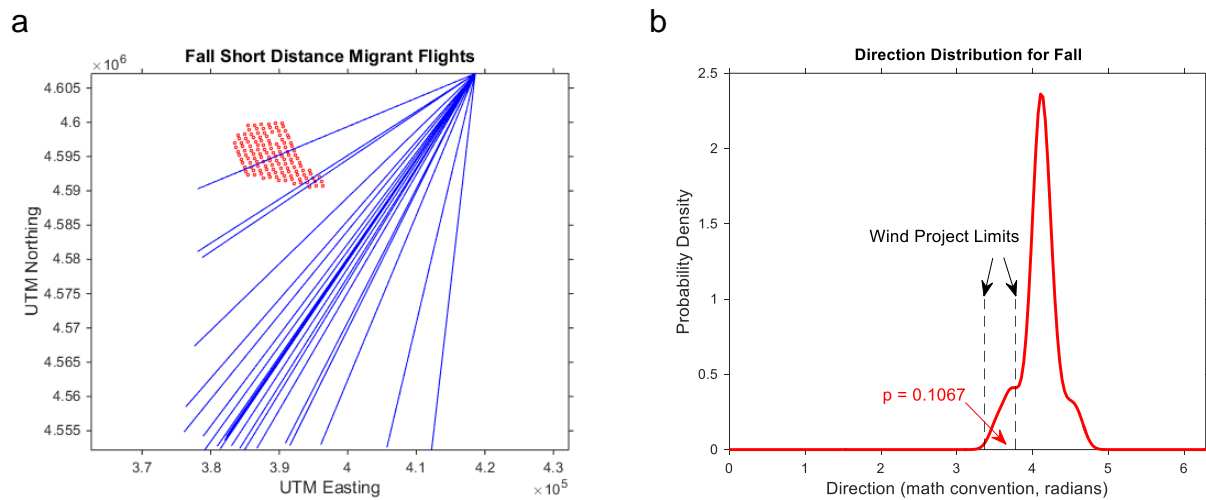
Figure 3.3 Red Knot flight directions in fall.
(a) Flight line segments (blue lines) based on geolocator equipped birds departing from the MNWR, with approved wind turbine layout at the approved Cape Wind Facility (red circles). Flight destinations are not shown; segments have been shortened but preserve origin and direction. (b) Linear kernel density estimated from directions shown in (a). Approximately 11% of the fitted distribution lies between the angular limits of the Facility (dashed vertical lines).

Note that a linear kernel was judged appropriate for these circular data because observed directions were restricted to a relatively narrow arc of 61 degrees (°), or approximately 17% of the circle. Furthermore, the kernel density estimator fit the tails of the distribution (which included directions toward the Facility) better than parametric distributions, including circular distributions such as the Von Mises. Finally, the linear kernel distribution allowed easier and faster generation of random variates than did alternative circular kernel density estimators.

We assumed that in spring Red Knots migrating through eastern Massachusetts would be on trajectories roughly from south-southeast to north-northwest. That is, these migrants would have

flown long distances over water and would be headed towards Hudson Bay (Niles, pers. comm.). Further, we assumed that all these migrants would pass through a 50-kilometer (km; 31-mile) wide "gate" between the eastern end of Martha's Vineyard and the elbow of Cape Cod (Figure 3.4). Bearings were calculated from the center of the approved Facility to the easternmost limit of Hudson Bay ($\alpha_1 = 1.781$ rad $\equiv 348°$) and to the westernmost limit of the bay ($\alpha_2 = 2.153$ rad $\equiv 327°$). We assumed all migrants would have flight directions between these limits.
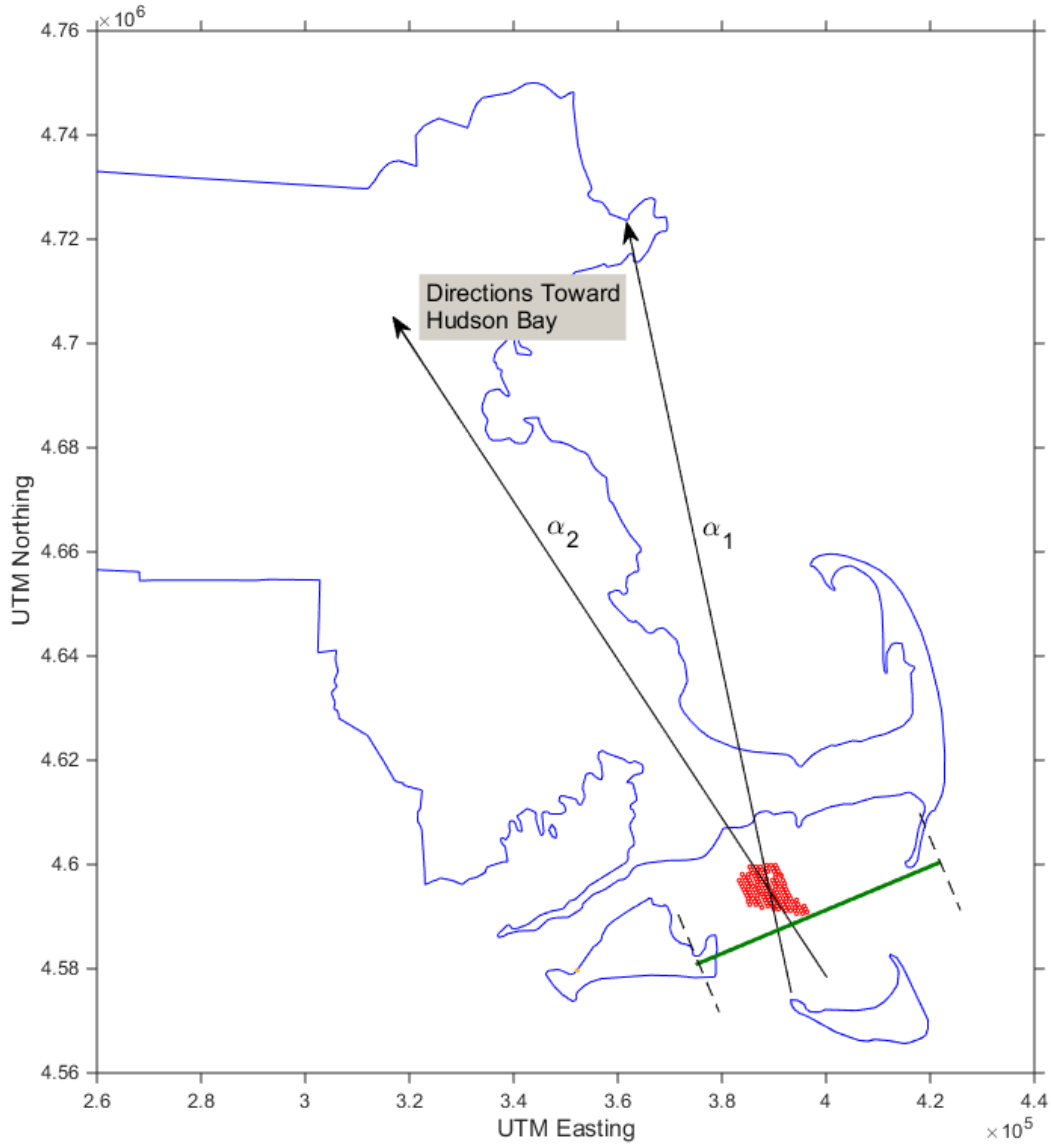
Figure 3.4 Red Knot flight directions in spring.
Turbines within the approved Facility shown as red dots. For simulations, the green line served as a "starting gate"; uniform random locations along this line served as flock starting positions. Flight directions were uniformly distributed between α_1 and α_2 (delimiting angles towards Hudson Bay).

For the purposes of simulation, the gate was effectively a starting line. Each flock was assigned a starting position along the line by generating a Uniform (0, 50) random variate and then calculating the corresponding x,y-coordinate pair. Also, each flock was assigned a direction by

19

generating a Uniform (α_1, α_2) random variate. Note that the actual bearings to the easternmost and westernmost limits of Hudson Bay would vary slightly depending on the starting position within the gate, though the discrepancies with α_1 and α_2 would be small given the great distance between Nantucket Sound and Hudson Bay.

Flight Altitude

Observations of migrating Red Knots indicate that these birds generally fly at altitudes well above wind turbines, often at 500 – 2,000 m (1,640 – 6,562 ft) and sometimes as high as 3,000 m (9,843 ft; Alerstam et al. 1990, Green 2004, Petersen et al. 2006, Piersma and Jukema 1990). We used parametric distributions to represent natural variability in flight heights, though we assumed that Red Knots would adopt two substantially different distributions ("low" and "high") depending on weather conditions. Furthermore, we recognized uncertainty in the parameters underlying both the low and high distributions and, therefore, examined several alternative distributions in each case.

Weather Effects
We assumed that weather conditions influenced Red Knots' preferred flight altitude distribution such that under favorable conditions most birds would be flying according to a "high" altitude distribution, while under less favorable conditions most birds would be flying according to a "low" altitude distribution. Both wind and precipitation were assumed to influence the choice of distribution. Regarding wind, for the baseline condition, we assumed that effective headwinds of 5.0 m/s or greater would trigger choice of the low-altitude distribution. That is, faced with relatively strong headwinds, Red Knots would choose to fly low, generally close to the water surface, to minimize wind resistance. To examine sensitivity to this parameter choice, we also conducted simulations in which the alternative threshold wind speeds were 10 m/s or 15 m/s. Given these greater threshold values, flocks would more frequently choose to adopt the high-altitude distributions and thus would experience lower collision risk relative to the baseline threshold.

Precipitation was also assumed to influence choice of high- or low-altitude distribution, such that if hourly precipitation exceeded a threshold, flocks would select the low-altitude distribution. The baseline threshold value was 2.5 millimeters per hr (mm/hr; 0.1 inch/hr), though alternative values of 1.0 mm/hr (0.4 inch/hr) and 4.0 mm/hr (0.2 inch/hr) were also examined.

High-Altitude Distributions
The assumed baseline high-altitude distribution was a Uniform (0, 2000) such that a flock would be equally likely to select any flight altitude between the sea surface (zero m) and 2,000 m. Given this distribution, the expected proportion of flocks flying within wind turbine heights (0 – 133.5 m [438.0 ft]) was 0.0668. To account for uncertainty in this distribution, we conducted simulations with two alternative high-altitude distributions – a Uniform (0, 1000) and a Uniform (0, 3000). Relative to the baseline, the former doubled the expected proportion within turbines heights to 0.1335, while the latter reduced the expected proportion to 0.0445 (Figure 3.5).

a

Baseline High Altitude Flight Distribution
Uniform(0,2000)

b

Alternative High Altitude Flight Distribution
Uniform(0, 1000)

c

Alternative High Altitude Flight Distribution
Uniform(0, 3000)
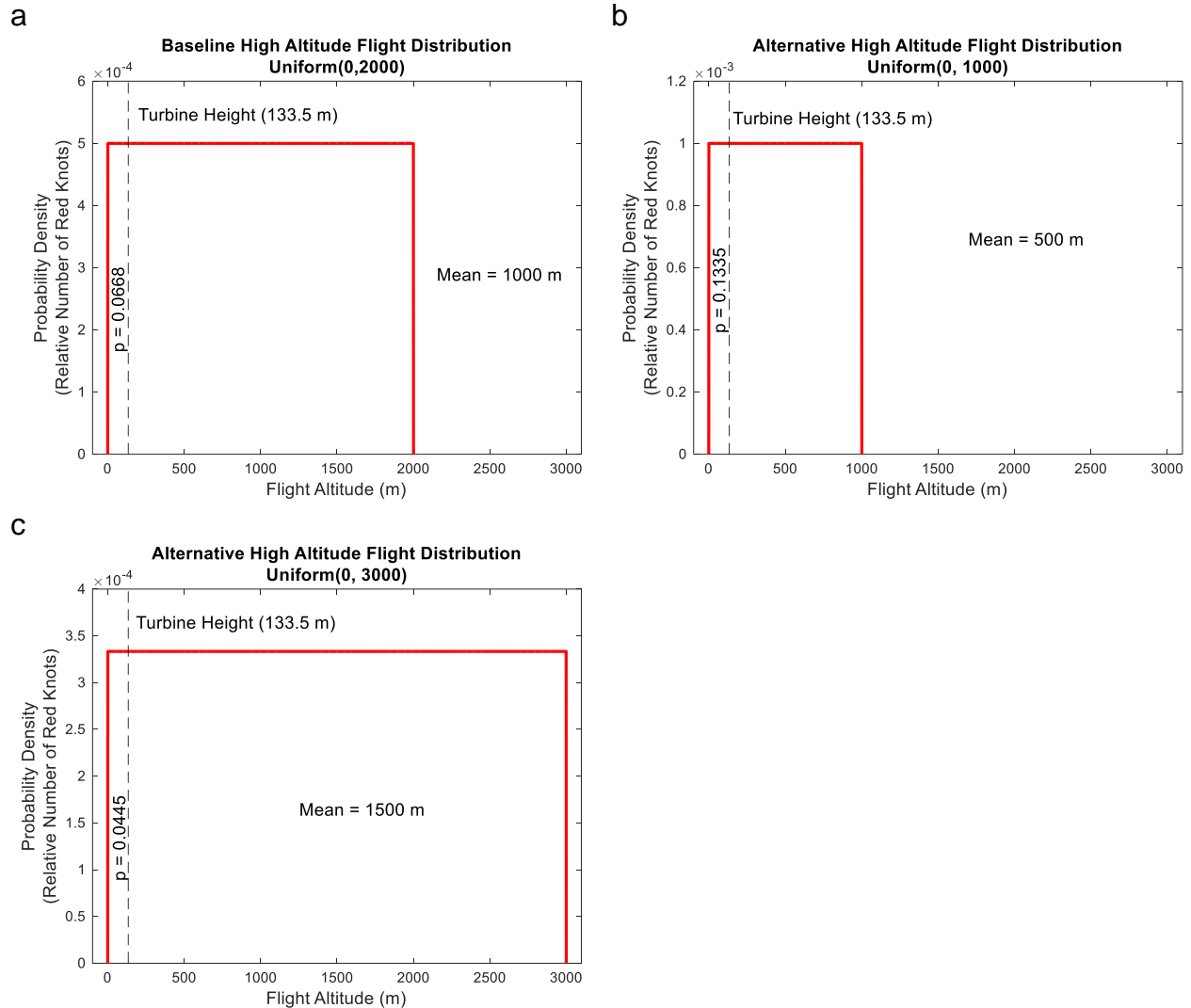
Figure 3.5 High-altitude flight distributions for Red Knots migrating under favorable weather conditions.

(a) baseline, (b) alternative that has higher expected proportion of flights within wind turbine heights, and (c) alternative that has lower proportion within turbine heights.

Low-Altitude Distributions

Low-altitude flight distributions were designed to represent the preferences exhibited by Red Knots, as well as many seabirds, shorebirds, and waterfowl, for flying near the water's surface when flying into a headwind (Niles, pers. comm.; Newton 2010; Finn et al. 2012). The general Gamma distribution (Figure 3.6) was selected for simulation of low-altitude flight because it has a lower bound of zero (birds cannot fly below the surface), and depending on parameter choice, most of the distribution's mass can be 'placed' near zero (most birds fly near the surface), with a long, unbounded right tail (fewer birds fly at greater heights). The baseline low-altitude distribution was a Gamma (1.5, 13) with nearly 75% of the distribution less than 26.5 m (Figure 3.6a); that is, the expected proportion of flocks flying below rotor-swept heights was 0.7467. Three alternative low-altitude distributions were also used – one which increased the proportion of flights below rotor-swept heights, and two which had lower expected proportions at heights

21

less than 26.5 m (86.9 ft) and correspondingly higher expected proportions within rotor-swept heights. Note that in all four cases (Figure 3.6), the modal height is close to 10 m ([33 ft] within a few meters) and that at least half of all flights are expected to be below the lower rotor limit. Table 3.2 provides a summary of all high- and low-altitude flight distributions.

During simulations, each flock was assigned either a high- or low-altitude distribution dependent on weather conditions at the fall departure or spring arrival time. Then, the flight altitude for that flock was determined by generating a random variate from the appropriate distribution. Altitude was assumed to be the same for all birds within the flock, and to be constant as the flock traversed the Facility.
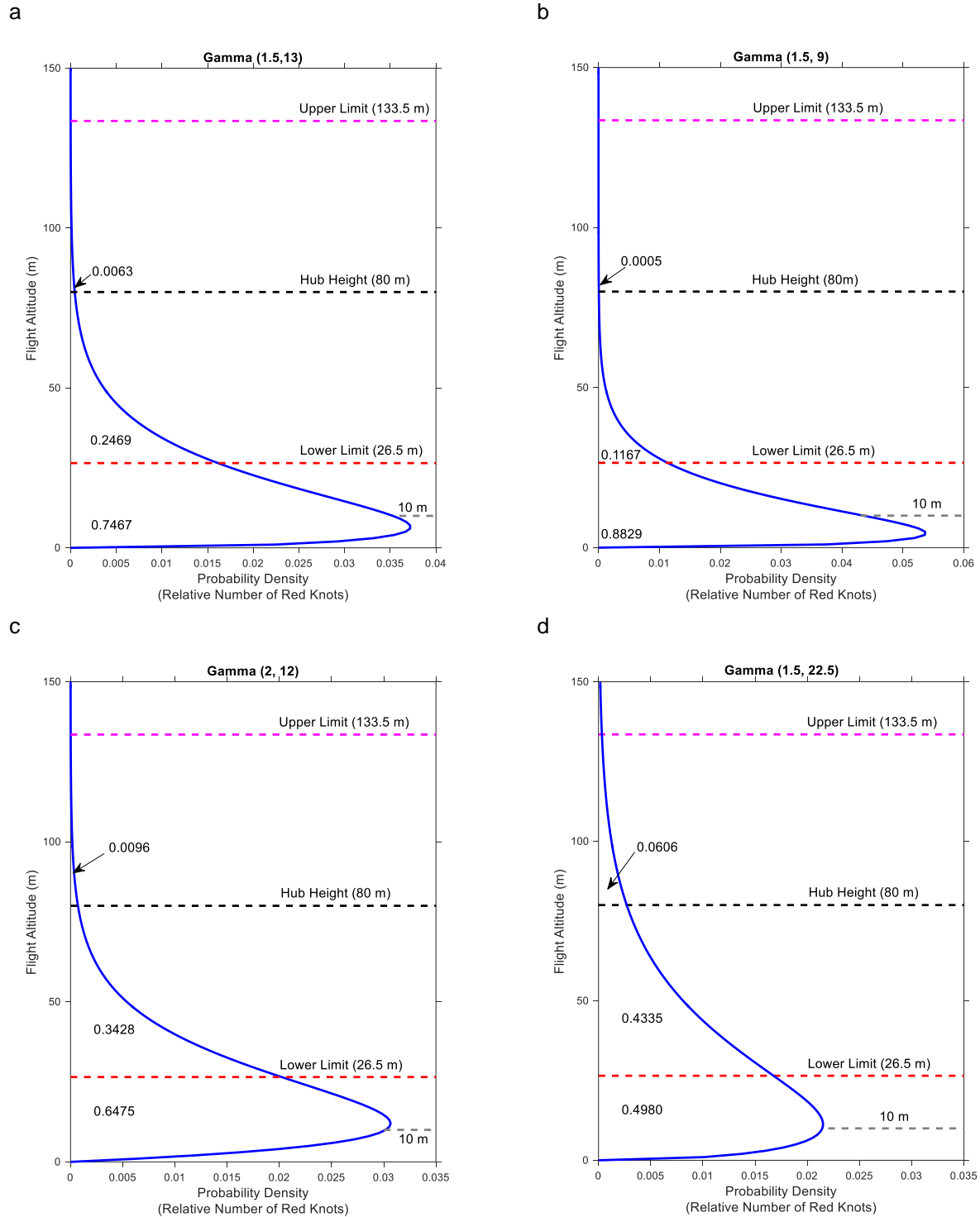
Figure 3.6 Gamma distributions for low-altitude flight distributions of Red Knots passing through the approved Cape Wind Facility area during unfavorable weather conditions.

Note that X and Y axes are reversed compared to typical probability density functions. (a) baseline, (b) alternative that has lower expected proportion of flights within rotor-swept heights, and (c) and (d) alternatives that have higher proportions within rotor-swept heights.

Table 3.2 Summary of flight altitude distributions used to model migratory flight altitudes of Red Knots passing through the approved Facility area in Nantucket Sound.

The right-most columns indicate the probability (i.e., the expected proportion of simulated flights) within three height classes: (1) below rotor-swept height (less than 26.5 m), (2) between the lower rotor-swept limit and hub height (26.5 – 80 m [262 ft]), and (3) between hub height and the upper rotor-swept limit (80 – 133.5 m [438 ft]).

Class	Alternative	Distribution	Mean Height (m)	Probability		
				< 26.5	26.5−80	80−133.5
High-altitude	Baseline	Uniform (0, 2000)	1,000	0.0133	0.0268	0.0268
	Alt. 1 (lower)	Uniform (0, 1000)	500	0.0265	0.0535	0.0535
	Alt 2 (higher)	Uniform (0, 3000)	1,500	0.0088	0.0178	0.0178
Low-altitude	Baseline	Gamma (1.5, 13)	19.50	0.7467	0.2469	0.0063
	Alt. 1 (lower)	Gamma (1.5, 9)	13.50	0.8829	0.1167	0.0005
	Alt 2 (higher)	Gamma (2, 12)	24.00	0.6475	0.3428	0.0096
	Alt 2 (highest)	Gamma (1.5, 22.5)	33.75	0.4980	0.4335	0.0606

Avoidance

We assumed that Red Knot flocks exhibited hierarchical active avoidance behaviors, as in Gordon et al. (2011). In particular, macro-avoidance entailed avoidance of the entire Facility. Flocks exhibiting macro-avoidance behaviors did not fly through the Facility area, and hence had no collision risk. Flocks that entered the Facility (no macro-avoidance) and flew within turbine heights might then have potential encounters with one or more turbines or with the ESP. Active avoidance of any such structure once a flock was already flying within the Facility area represented micro-avoidance. We note that the concept of micro-avoidance, as we included it in the model, corresponds most closely to the concept of "meso-avoidance" as defined by Cook et al. (2014) and May (2015), referring to evasive maneuvers taken by birds to avoid wind turbine rotors while they are already flying within the wind farm. Cook et al. (2014) and May (2015) define "micro-avoidance" as instantaneous "escape" maneuvers taken by birds that have already elected to fly through the rotor-swept zone of a turbine. In omitting this type of avoidance behavior, our model makes the conservative assumption that birds entering the rotor-swept zones of wind turbines are subject to a collision probability determined only by simple geometric considerations, unaffected by avoidance behaviors at this scale.

The model treated avoidance exclusively as an active behavior. Some simulated flocks might have had flight directions and/or flight altitudes such that there was no collision risk. Other flocks might have flown through the Facility between rows of turbines and, thus, would not have encountered a turbine. Such flights might be considered to have passively avoided collision, though we prefer to consider them as flights without risk, or simply successful flights. In our model, macro-avoidance was an option only for those flocks that otherwise would have encountered the Facility and entered it within turbine heights. Similarly, micro-avoidance was an option only for those flocks that otherwise would have encountered a turbine (or the ESP) and risked collision with it.

If a flock randomly "chose" to avoid, then the flock operated as a cohesive unit and completely avoided the Facility (macro-avoidance) or the turbine (micro-avoidance). Partial avoidance, in which some flock members successfully avoided while others failed to avoid, did not occur.

<u>Macro-Avoidance</u>
As noted above, macro-avoidance implied that a flock on a course toward the Facility made an evasive maneuver and thereby avoided the Facility completely. However, within the model there was no explicit representation of macro-avoidance movements. Depending on the outcome of a random draw, a flock headed toward the Facility either avoided the Facility or it failed to avoid, and thus entered the Facility. Flocks that avoided the Facility incurred no risk and received no further consideration.

We assumed a fixed baseline macro-avoidance probability of 0.28 in favorable weather conditions, based on data for wading birds from the Egmond aan Zee offshore wind energy facility in the Netherlands (Krijgsveld et al. 2011), as well as data reported in Cook et al. (2012). In additional simulations accounting for the uncertainty in this parameter, the probability was assumed to be distributed as a Beta (14, 36) random variable with expected value of 0.28 (Figure 3.7a).

In unfavorable weather conditions (heavy precipitation and/or low visibility), we assumed a fixed baseline macro-avoidance probability of 0.01. That is, in such weather, we assumed only 1% of flocks would avoid the Facility. In additional simulations, poor weather macro-avoidance probability was randomly generated from the Beta (0.01, 0.99) distribution (Figure 3.7a).

Under the baseline assumption, the heavy precipitation threshold was 2.5 mm/hr. That is, if hourly precipitation exceeded this threshold, macro-avoidance probability was low. Alternative thresholds of 1.0 mm/hr and 4.0 mm/hr were also examined. The low visibility threshold was 1,000 m with the baseline assumption. That is, if visibility was 1,000 m or less, macro-avoidance probability was low. Alternative thresholds of 500 m and 2,000 m were also examined.
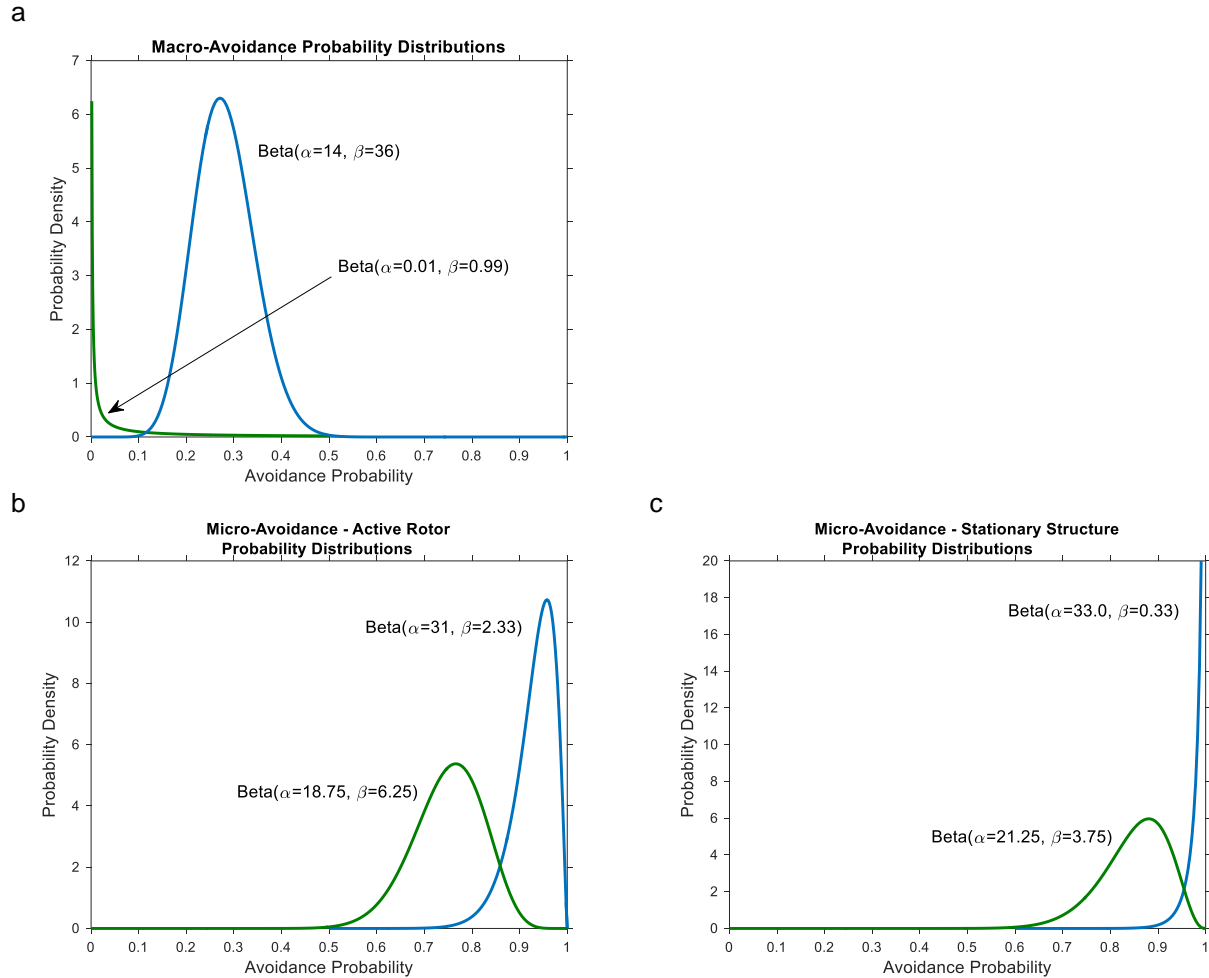
Figure 3.7 Assumed distributions for Red Knot avoidance probabilities.

(a) macro-avoidance; (b) micro-avoidance for active rotors; (c) micro-avoidance for stationary structures. In each panel, the blue line represents the distribution under favorable weather conditions, while the green line represents the distribution under unfavorable conditions.

Micro-Avoidance

We developed a baseline assumption for micro-avoidance based on parameter values for various types of birds in published literature, further assuming that micro-avoidance was higher for stationary structures than for active rotors, and that micro-avoidance ability was reduced when flocks encountered strong headwinds. Active rotor avoidance was based on consideration of the flight morphology and behavioral characteristics of Red Knots in the context of previously published micro-avoidance parameters for various types of birds at wind energy facilities. For this consideration, it was important to distinguish between published overall avoidance probabilities, which typically incorporate both macro-and micro-avoidance, and published avoidance probabilities that specifically refer only to micro-avoidance. We settled on a default value of 0.93 for the Red Knot micro-avoidance of active rotors under favorable weather conditions in our model, which was the average of Petersen et al.'s (2006) average micro-avoidance value for sea ducks at the Nysted Wind Project in Denmark (0.886) and the overall average micro-avoidance probability for all birds (0.976) in the studies reviewed by Cook et al. (2012), which is heavily weighted toward highly maneuverable species, such as gulls and terns.

In essence, we assumed that Red Knots had micro-avoidance capacity somewhere in between that of sea ducks and that of gulls and terns. Thus, 93% of Red Knot flocks in our model avoided active rotors when wind conditions were favorable. In the simulations, we assumed that good weather active rotor probability had a Beta (31, 2.33) distribution (Figure 3.7b), with expected value of 0.93. When headwinds crossed a threshold value of 5.0 m/s, the micro-avoidance probability was reduced to 0.75. The lower probability (compared to favorable weather) was intended to account for the relatively high wing-loading in Red Knots (Harrington 1996) and assumed lower maneuverability when flying into a headwind. In the simulations, this avoidance probability was generated from the Beta (18.75, 6.25) distribution (Figure 3.7b), with mean value of 0.75. Alternative headwind thresholds of 10 m/s and 15 m/s were also examined.

Micro-avoidance of stationary structures (towers, static rotors, ESP) was treated similarly, though it was typically higher than avoidance probability for active rotors. The favorable weather baseline value was 0.99, with corresponding uncertainty distribution given by a Beta (33, 0.33) distribution (Figure 3.7c). The unfavorable weather (headwind above threshold value) baseline value was 0.85, with a corresponding Beta (21.25, 3.75) distribution to account for uncertainty (Figure 3.7c). The headwind thresholds for triggering lower micro-avoidance probability were the same as described above for the micro-avoidance of moving rotors.

Because wind turbines comprise both stationary components and rotors which are frequently, but not always, active, we made some simplifying assumptions regarding micro-avoidance. If a flock was flying at low height beneath the rotor-swept zone, then the only turbine component presenting risk was the tower and, therefore, the model applied stationary structure avoidance probability irrespective of rotor status. If a flock was flying at any height within the rotor-swept zone, then the effective avoidance probability depended on rotor status and, thus, on wind speed. At wind speed either below the turbine cut-in speed or above the cut-out speed, the rotor was assumed to not be turning and the model applied stationary structure avoidance probability. Otherwise, at intermediate wind speed, the rotor was assumed to be turning. In this case, active rotor avoidance probability was applied even though stationary structures (both the tower and nacelle) presented additional collision risk in the lower half of the rotor-swept zone. Stationary structure avoidance probability was in effect at all times for the ESP.

Weather Effects on Red Knot Behavior
Table 3.3 summarizes assumptions regarding the influences of various weather variables on important features of Red Knot biology that were incorporated into our model, as discussed in preceding sections.

Table 3.3 Summary of weather effects on Red Knot behavior.

Includes flight altitude, avoidance, and fall departure.

Weather Variable	Weather Threshold Value		Biology Aspect	Consequence
	Baseline	**Alternatives**		
Headwind[1]	≥ 5.0 m/s	≥ 10 m/s ≥ 15 m/s	Fall departure	Delay hourly, up to five days
			Flight altitude	Low-altitude distribution
			Active rotor micro-avoidance	Probability lowers from 0.93 to 0.75
			Stationary structure micro-avoidance	Probability lowers from 0.99 to 0.85
Precipitation	≥ 2.5 mm/hr	≥ 1.0 mm/hr ≥ 4.0 mm/hr	Flight altitude	Low-altitude distribution
			Macro-avoidance	Probability lowers from 0.28 to 0.01
Visibility	≤ 1,000 m	≤ 500 m ≤ 2,000 m	Macro-avoidance	Probability lowers from 0.28 to 0.01

[1]refers to effective headwind speed, or the speed of the vector of total wind speed that is directly (180⁰) opposed to birds' flight direction. Therefore, effective headwind speed is usually less than actual wind speed, unless the direction of the wind is directly opposed to the birds' flight direction.

Assumption of Static Weather Conditions and Red Knot Flight Height, Speed, and Direction

Our model represents a dynamic system and some dynamic components are explicitly included in the model. In particular, weather conditions determine both turbine state (orientation and rotational velocity) and Red Knot flight height, avoidance behavior, and fall departure delay behavior. The model is dynamic in that different flocks are likely to experience different conditions. However, the conditions experienced by an individual flock are static. For each flock, spring arrival or fall departure date and time are randomly generated, and then weather conditions for that date and time are obtained via random sampling (see Section 3.3.2: *Weather Data*). Those conditions are assumed to be constant during the flock's passage through the Facility and, in the fall, during the implicit passage across Nantucket Sound between the MNWR and the Facility site. We recognize that this simplifying assumption sacrifices some realism, particularly in the fall, because weather conditions could change during the time required for Red Knots to reach the Facility site from the MNWR. On the other hand, given the distance of the Facility from the MNWR (approximately 28 km [17 miles]) and typical flight air speeds of Red Knots (20 m/s [66 ft/s] ≡ 72 km/hr [45 miles/hr]), we would expect most flocks in most conditions to reach the Facility in less than an hour (the time resolution of our weather data).

Body Size and Shape

Red Knots were assumed to have wing span of 0.54 m (1.78 ft) and body length of 0.24 m (0.79 ft; Gudmundsson et al. 1991, Baker et al. 2013). Body size was held constant, that is, these dimensions were the same for all individuals in all simulations. Within the Band (2012) sub-model for active rotors, birds were treated as 2-dimensional crosses, with length and width but without height. In the Band sub-model, length is important because it affects a bird's residence time within the rotor disc. Otherwise, in assessing collisions with stationary structures, time

played no role and, thus, body length was ignored; in effect, birds were represented as 1-dimensional, having width (wing span) only.

Flock Size and Shape

All Red Knots were assumed to migrate in single-species flocks (Piersma and Jukema 1990) ranging in size from 10 to 200 birds (Niles, pers. comm.). As a starting point, we assumed flock size had a discrete uniform (10, 200) distribution, with a mean size of 105 birds. However, the realized size distribution was constrained by the additional assumptions that the number of flocks was random and the total number of birds in all flocks must equal the migratory population size. For instance, a spring population size of 150 clearly implied that the any flock greater than 150 had true probability of zero. Therefore, flock sizes were generated by an iterative process that relied on the discrete uniform (10, 200) distribution but made adjustments to satisfy the constraint on total number of birds. In brief, flocks were generated incrementally until the total was within a specified tolerance of population size, and then at most one bird was added to or subtracted from one or more flocks such that the total equaled the population size. If the population size plus tolerance was exceeded, the flock closest in size to the exceedance was removed and the tolerance was re-checked. If the tolerance check failed a second time, the iteration was rejected and a new one was initiated. In general, the generating process was quite rapid (only requiring one or few iterations) for the larger fall population and yielded the intended distribution (Figure 3.8a). However, the process was slower for the spring and yielded a non-uniform distribution biased towards the maximum size of 150 (Figure 3.8b).

a
b
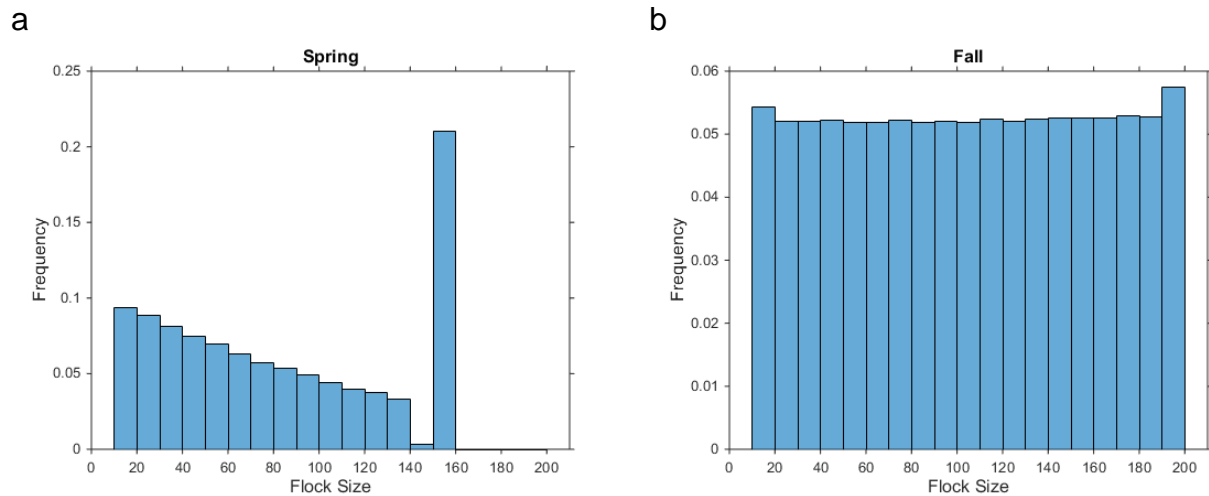
Figure 3.8 Realized distributions of flock size from 100,000 iterations for (a) spring and (b) fall.

Flocks were modeled with a classic chevron- or V-shape (Barter and Tonkinson 1997, Alerstam et al. 1990, Swennen 1992). Within the chevron, wing tips were assumed to be perfectly aligned tip-to-tip, that is, with neither overlapping wing tips nor any gaps between wing tips, as consistent with optimal energetic efficiency (Seiler et al. 2003). Bird bodies were assumed to be regularly spaced such that the distance between the head of one bird and the tail of the bird in front of it was 25% of body length. Figure 3.9 illustrates flock shape and the positioning of birds within the flock within the model.
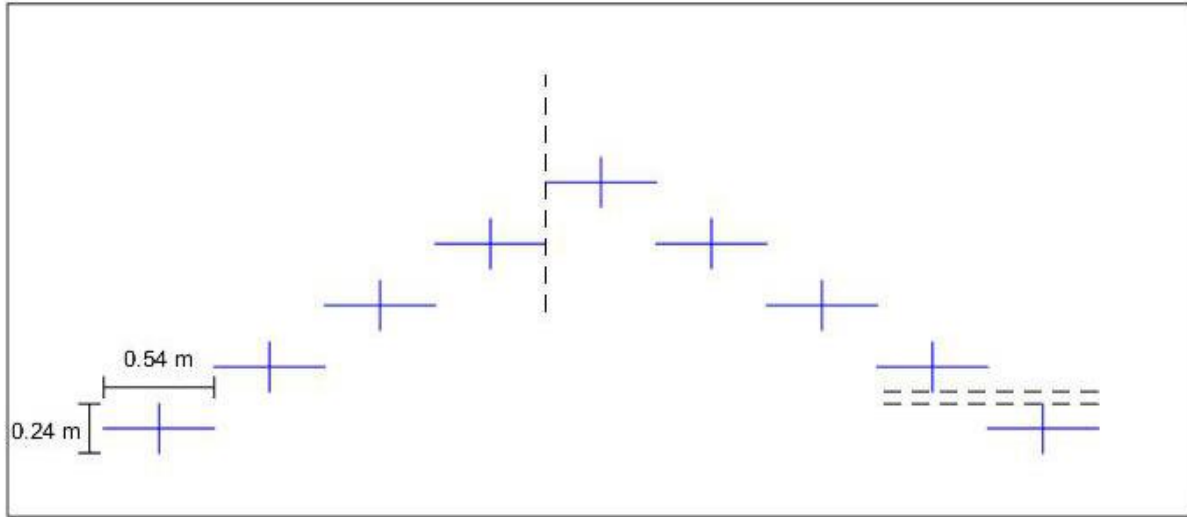
Figure 3.9 Diagram illustrating modeled size and shape of individual Red Knots, and flock shape (modeled flock sizes ranged from 10 to 200 birds).

Vertical dashed line indicates wing-tip alignment and horizontal dashed lines indicate gap between bird bodies.

Flight Speed

We used a default flight air speed value of 20 m/s for Red Knots in our model, based on data reported in literature, particularly from measurements made using radar. We took into consideration the fact that without any adjustment, radar measurements yield ground speed, but in some cases, the variable of interest is air speed. If there is no wind, the air speed of birds can be assumed to be the same as ground speed. Under calm conditions, Alerstam et al. (2007) measured Red Knot flight ground speeds with a mean of 20.1 m/s (65.9 ft/s) and standard deviation of 1.9 m/s (6.2 ft/s). Similarly, Green (2004) measured mean ground speeds of 20.7 m/s and 20.9 m/s (67.9 ft/s and 68.6 ft/s) during calm conditions. In the presence of headwinds or tailwinds, measured ground speeds of flying Red Knots include lower or higher values, ranging from 18.3 m/s to 25.6 m/s (60.0 ft/s and 84.0 ft/s; Gundmundsson 1994, Petersen et al. 2006). We assumed that Red Knot air speed followed a Gamma distribution fit to the mean and standard deviation reported by Alerstam et al. (2007), i.e., a Gamma (111.91, 0.1796) (Figure 3.10). The distribution was truncated at 10 m/s and 30 m/s (98 ft/s), though there is extremely low probability in the tails (e.g., 99.9% of all flocks would have air speed between 14.43 m/s and 26.94 m/s [47.34 ft/s and 88.39 ft/s]).
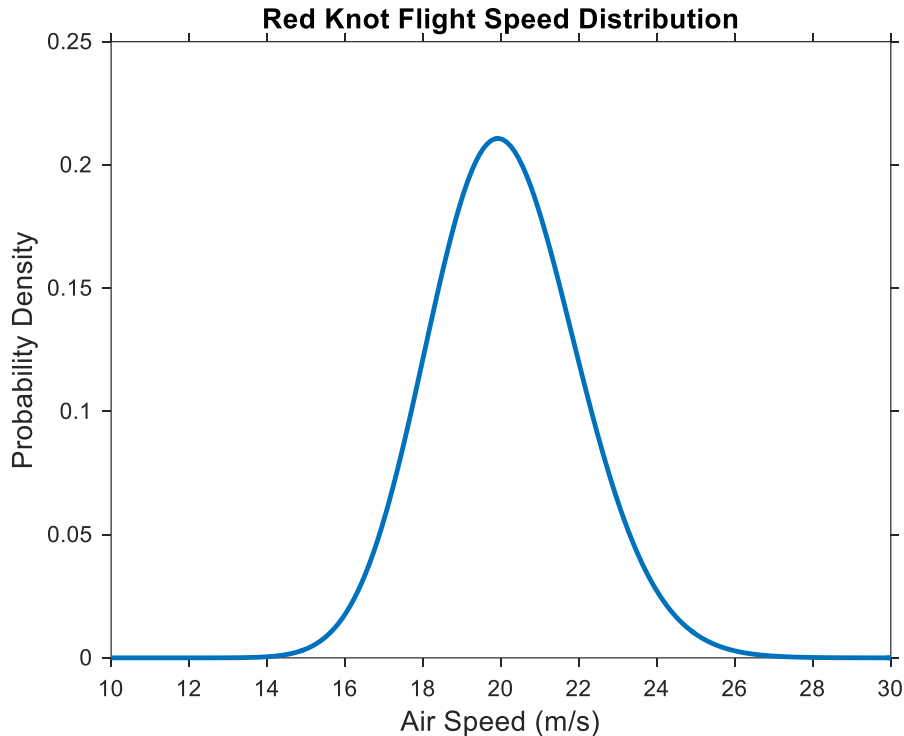
Figure 3.10 Assumed distribution for Red Knot air speed, with mean = 20.1 m/s (65.9 ft/s) and standard deviation = 1.9 m/s (6.2 ft/s).

During simulations, each flock's air speed was generated as a random variate from the distribution shown in Figure 3.10. Dependent on the flock's selected air speed and flight direction, as well as wind speed and direction, the flock's ground speed was calculated secondarily (see Section 3.4.3: *Structural Elements of the Model*, subsection: *Ground Velocity*). Ground speed was the flight speed variable incorporated into our model, applied within the Band (2012) sub-model for active rotors.

3.3.2   Weather Data

In order to generate a realistic representation of weather conditions as they affect modeled various features of Red Knot behavior in our model, we developed a spatially and temporally-explicit weather "landscape" for the Facility area during the time periods in which Red Knots pass through the area. We developed this landscape using weather data for the vicinity of the Facility, obtained from publicly available sources.

Data Sources

Wind

Wind data were obtained from the National Data Buoy Center (National Data Buoy Center 2015), which maintains current and historical data from a worldwide network of marine buoys. In particular, data were obtained for Station 44020, which is a buoy in Nantucket Sound located at 41.443°N, 70.186°W. Hourly wind speed and direction data from this buoy were downloaded for the 5-year period 2009 – 2013, inclusive.

<u>Visibility</u>
Hourly visibility observations were obtained from the National Climatic Data Center (NCDC; 2015a). Data were obtained from three land-based stations near the Facility site: Barnstable on Cape Cod, the Martha's Vineyard Airport, and the Nantucket Memorial Airport. "Global Hourly" data, including observations of visibility, were downloaded from all three stations for the period 2009 – 2013, inclusive.

<u>Precipitation</u>
Hourly precipitation data were obtained from the NCDC (2015b). There are three land-based weather stations near the Facility site: Hyannis on Cape Cod, Edgartown on Martha's Vineyard, and the Nantucket Memorial Airport on Nantucket Island. While recent "Precipitation Hourly" data were available from Hyannis and Edgartown, there were many observations that were either missing or corrupted. The best available 5-year dataset was for the period 1965 – 1969, inclusive, from Nantucket; there were no missing or corrupt observations in this dataset.

Data Processing
<u>Wind</u>
Time was converted from Coordinated Universal Time (UTC) to Eastern Standard Time (EST). Wind direction was converted from geographic convention (i.e., degrees clockwise from north) to mathematical convention (i.e., radians counter-clockwise from the positive X-axis). Both wind speed and wind direction were linearly interpolated to observations on the hour (e.g., from 00:50, 01:50, 02:50, 03:50, … to 01:00, 02:00, 03:00,…). Since direction is a circular variable, the sine and cosine transformations of direction were linearly interpolated and then the direction was recovered from the arc-tangent transformation of the interpolated values. Wind speed at hub height was calculated using the power law relationship (Bailey et al. 1997):

$$V_h = V_b \left(\frac{H_h}{H_b}\right)^{\alpha}$$

where V_h was the unknown wind velocity at hub height, V_b was measured wind velocity at buoy height, H_h was hub height (80 m [262 ft]), H_b was buoy height (5.0 m), and α was the wind shear exponent (assumed to be 0.10), appropriate for open water (Hsu et al. 1994).

<u>Visibility</u>
Time was converted from UTC to EST. Irregular observations (generally more than one observation per hour) at each station were linearly interpolated to observations on the hour. To obtain a single value representing visibility, the minimum value for the three stations was calculated. Note that the minimum is also a more conservative measure than the average, for example, because it is more likely to trigger a threshold response.

<u>Precipitation</u>
Time observations required no adjustment (observations in the NCDC dataset were recorded on the hour in EST). Consequently, interpolation of precipitation values was not conducted. However, by NCDC dataset design, periods without measurable precipitation are not recorded. Therefore, zero values were imputed for all hours in such periods. For the purpose of merging with the wind and visibility data, calendar year was changed from 1965 – 1969 to 2009 – 2013,

while month, day, and time of day were otherwise unchanged. Note that merging data from different years ignores any potential correlation between precipitation and either wind or visibility, though, as described above, NCDC hourly precipitation data otherwise had limited availability.

Combined Data

Each of the three datasets was seasonally subsampled according to the definitions of the migratory seasons for Red Knots, that is, April 28 – June 9 for spring and July 8 – November 21 for fall (see Section 3.3.1: *Red Knot Biology,* subsection: *Migration Timing*). In addition, fall data were further subsampled to include only the 4-hr period near sunset each day. Daily sunset times for Nantucket Sound were obtained from the US Naval Observatory (2015). Sunset times were rounded to the nearest hour for consistency with the weather data. That hour and the preceding three hrs represented the 4-hr period for each day of the fall migratory season. The three weather datasets were merged into a single dataset based on date and time. Thus, the final dataset consisted of hourly observations of wind, precipitation, and visibility, only for those dates and times during which Red Knots were assumed to be migrating through Nantucket Sound.

Weather Summary

Plots of hourly wind speed and direction based on the final weather dataset are shown in Figure 3.11. Wind speed at wind turbine hub height in both spring and fall was typically between 5.0 m/s and 10 m/s (Figure 3.11a, b). The distributions of wind speed were similar in the two seasons, though the fall distribution is shifted right (toward higher speed) compared to the spring distribution; mean wind speed was 7.89 m/s (25.89 ft/s) in the spring and 8.67 m/s (28.44) in the fall. In the spring, wind speed was less than the turbine cut-in speed (3.0 m/s [9.8 m/s]) 10.3% of the time, while wind speed never exceeded the turbine cut-out speed (25 m/s [82 ft/s]). In the fall, wind speed was less than the cut-in speed 6.8% of the time and greater than the cut-out speed 0.3% of the time. Thus, turbines would have been operating about 90% of the time in the spring and about 93% of the time in the fall (neglecting other factors, such as maintenance down-time).

Headwind speed determined several threshold responses, namely fall departure delay, low or high flight altitude distribution, and micro-avoidance probability. In each case, the baseline threshold value was 5.0 m/s and the two alternative values were 10 m/s and 15 m/s. Because we were primarily interested in headwind speeds that *exceeded* the threshold, we calculated the empirical complementary cumulative distribution function (CCDF) (Figure 3.11c, d). Hourly wind speeds exceeded 5.0 m/s about 75% of the time in the spring (Figure 3.11c) and about 82% of the time in the fall (Figure 3.11d). By contrast, in the spring wind speed exceeded 15 m/s about 5% of the time, while in the fall, it was exceeded about 6.5% of the time. It is important to note that the actual threshold of interest in our model refers not just to wind speed, but to headwind speed, defined as the component of the wind speed vector that is diametrically (180°) opposed to the direction of the flock's flight. Therefore, the actual frequency of threshold crossings is a combined function of wind speed, direction, and the direction of the birds' flight in a particular simulation. Frequencies of wind speed threshold crossings were therefore analyzed in relation to simulation results, and are discussed in a later section in relation to the results.
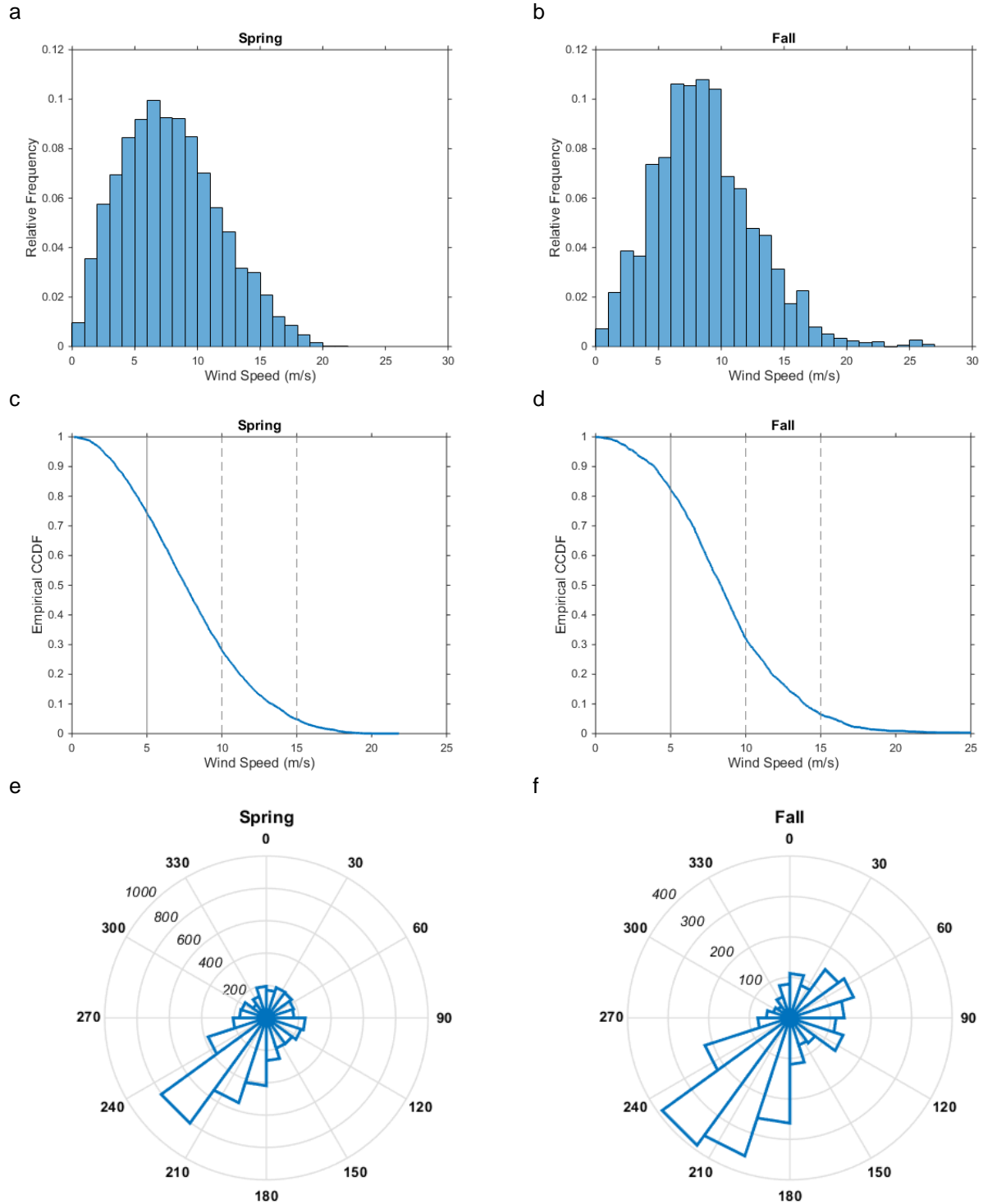
Figure 3.11 Wind conditions in Nantucket Sound, based on 5-year dataset used in collision risk model.

Histograms of hourly wind speed at hub height in (a) spring and (b) fall. The complementary empirical cumulative distribution function (1 –ECDF) of hourly wind speed observations in (c) spring and (d) fall. Rose plots of hourly wind direction in (e) spring and (f) fall; italicized numbers in rose plots indicate absolute frequencies.

Wind direction was generally from the southwest in both seasons. Indeed, the distributions of wind direction in spring and fall appear similar (Figure 3.11e, f), except that in the fall there was a small, secondary mode indicating wind blowing from the northeast and east. Mean wind direction was 205° in the spring and 191° in the fall. As another indication of the southwesterly tendency, wind direction was in the 90° arc between south and west about 46% of the time in the spring and about 48% of the time in the fall.

Hourly visibility data were used exclusively in determining threshold behavior; in particular, if visibility was less than the threshold, then macro-avoidance probability was assumed to be much lower than if visibility was greater than the threshold. Since we were interested in values less than the threshold, the empirical cumulative distribution function (ECDF) of visibility (Figure 3.12a, b) provided a useful summary relevant to the threshold behavior. For instance, given the baseline assumption of a 1,000 m visibility threshold, the ECDF for spring shows this condition was met about 13% of the time (Figure 3.12a). Similarly, spring conditions satisfied the alternative thresholds of 500 m and 2,000 m about 8% and 18% of the time, respectively. Low visibility conditions were rarer in the fall. Assuming the 1,000-m baseline value, low visibility conditions triggering very low macro-avoidance occurred about 3.5% of the time (Figure 3.12b).

In similar fashion, hourly precipitation data were used in determining threshold behavior for macro-avoidance and flight altitude. Since we were interested in values that exceeded the threshold, the CCDF provided the more useful summary (Figure 3.12c, d). Hourly precipitation that exceeded the threshold was rare in both seasons. In spring, the baseline value of 2.5 mm/hr was exceeded about 1.6% of the time (Figure 3.12c), while in the fall the baseline was exceeded less than 1% of the time (Figure 3.12d). Therefore, only rarely was precipitation heavy enough to trigger either low macro-avoidance probability or the low flight altitude distribution.
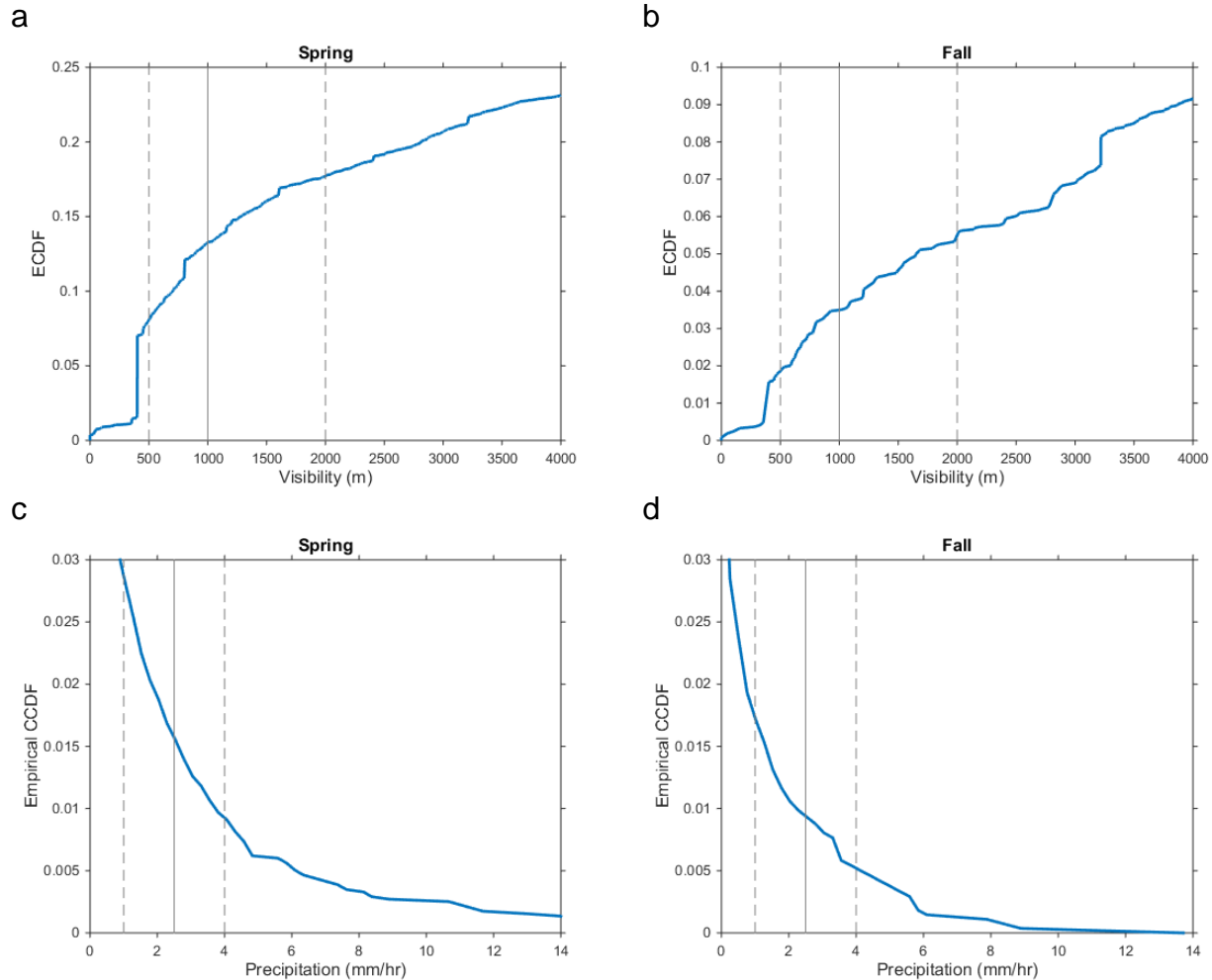
Figure 3.12 The cumulative distribution function of hourly visibility and precipitation observations in spring and fall.

The empirical cumulative distribution function (ECDF) of hourly visibility observations in (a) spring and (b) fall. The empirical complementary cumulative distribution function (CCDF) of hourly precipitation observations in (c) spring and (d) fall. In all panels, the solid vertical line represents the baseline threshold value for Red Knot behavioral switches, while the dashed vertical lines represent two alternative threshold values (see text).

3.3.3　Wind Facility, Wind Turbines, and Electrical Service Platform

In order to create a realistic representation of collision probabilities in our model, we used a spatially-explicit representation of the approved layout of turbines and other structures in Nantucket Sound, through which to "fly" Red Knot flocks in simulations. We also incorporated design specifics of the approved infrastructure to incorporate accurate information on the sizes and shapes of structures approved for installation.

Facility Layout

Locations of wind turbines and the ESP within the Facility were obtained from the Construction and Operation Plan (COP) Revision #1 (Cape Wind Associates 2014). Each turbine point location was interpreted as the center point of the tower; the ESP point location was interpreted as the center of a rectangle. Latitude and longitude were converted to Universal Transverse Mercator coordinates in Zone 19T (Figure 3.13). The COP describes a potential phased development in which 101 wind turbines would be installed in the first construction season and the remaining 29 turbines would be installed in the next construction season. However, phased development was not considered in our collision risk model; all 130 turbines were assumed to be installed and operational in all simulations.
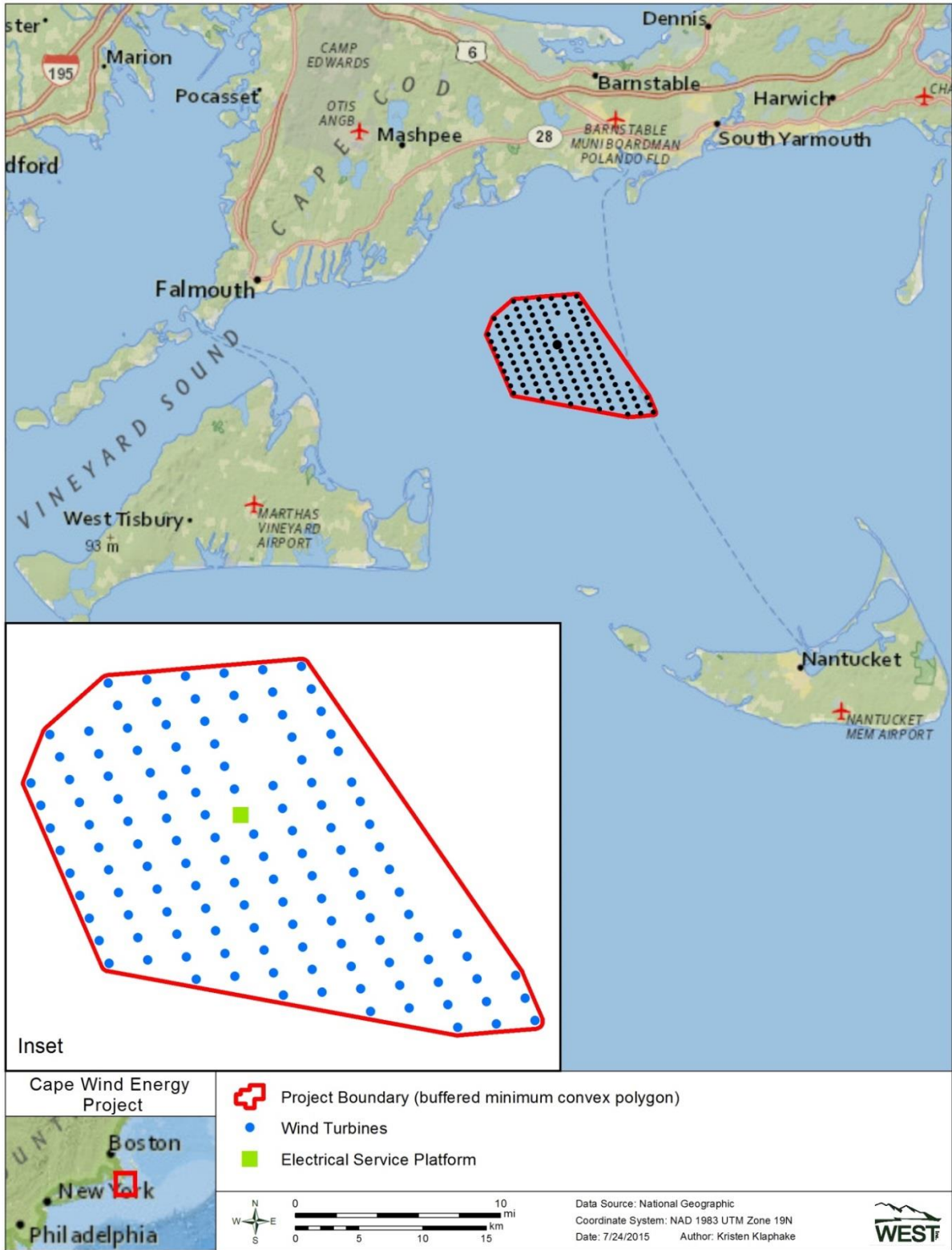
Figure 3.13 Location of the approved Cape Wind Facility in Nantucket Sound, Massachusetts, and approved spatial configuration of turbines and electrical service platform (ESP).

Electrical Service Platform

The COP Revision #1 (Cape Wind Associates 2014) specifies that the ESP will be supported on eight piles, each with diameter of approximately 107 centimeters (42 inches), and that the superstructure will be about 35 m (115 ft) by 40 m (132 ft), with the first deck approximately 10.7 m (35 ft) above mean lower low water and the roof 154 m (47 ft) above mean lower low water. Within the model, these dimensions were translated into meters and rounded to the nearest tenth of a meter (Table 3.4). Furthermore the superstructure was assumed to be shaped like a rectangular box that occupied the entire deck area and had constant roof height (Figure 3.14).

Table 3.4 Dimensions of the electrical service platform (ESP) of the approved Facility.

	COP Revision #1 (feet)	**Model (meters)**
Superstructure		
Length	132	40.2
Width	115	35.0
Height of first deck	35	10.7
Height of roof	47	14.4
Pile Diameter	3.5	1.2
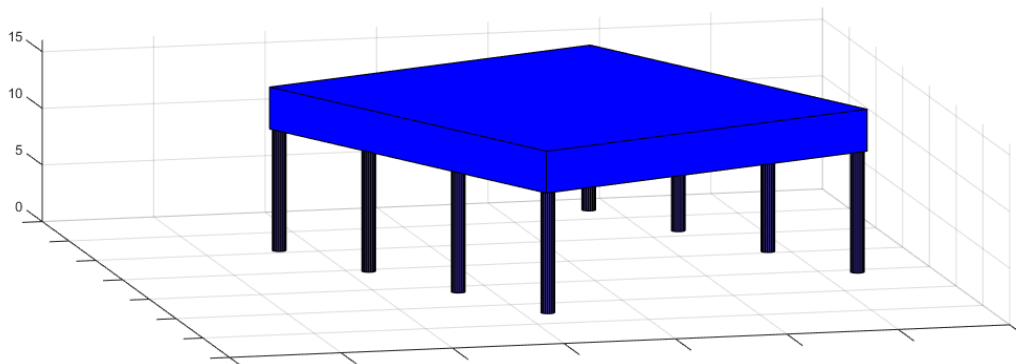
Figure 3.14 Model representation of the electrical service platform (ESP) of the approved Facility.

Wind Turbines

As specified in the final COP (Cape Wind Associates 2011), the wind turbine model selected for the Facility is the Siemens SWT-3.6-107. We developed our representation of this turbine within the collision risk model using publicly available design specifications for this turbine model, with some details modified for the sake of simplicity or to fill in gaps where information from the manufacturer was unavailable. As an example of the latter, the towers were assumed to have diameter of 4.0 m (13.1 ft) at the base and to taper linearly to a 2.75-m (9.02-ft) diameter at the top. Tower cross-section was treated as a decagon (10 line segments) rather than a circle for modeling simplicity. The turbine nacelle was simplified to a regular rectangular box 10 m long by 4.0 m wide by 4.0 m tall. The rotor blades had highly simplified geometry (Figure 3.15), with maximum chord length of 4.2 m (13.8 ft) at a distance of 11 m (36 ft) from the hub center, and minimum chord length of 1.0 m (3.3 ft) at the blade tip. We assumed that the rotor blades were

pitched at 80° (feathered) below the cut-in wind speed of 3.0 m/s and above the cut-out wind speed of 25 m/s, and thus that the rotor was stationary. Between the cut-in and rated wind speeds, i.e., between 3.0 and 13 m/s (9.8 and 43 ft/s), rotor speed was modeled as a logistic function of wind speed (Figure 3.16). Between the rated and cut-out wind speed, rotor speed was constant at 13 revolutions per minute (rpm). We assumed pitch control followed a relationship similar to that depicted by Hansen et al. (2005). Variable pitch came into effect as rotor speed approached the plateau at 13 rpm; that is, speed control transitioned to pitch control near the rated wind speed. Pitch angle increased from 0.5° at lower wind speed to a maximum of 30° at the cut-out wind speed (Figure 3.16). A summary of how turbine structural and operational parameters were incorporated into our model is presented in Table 3.5.
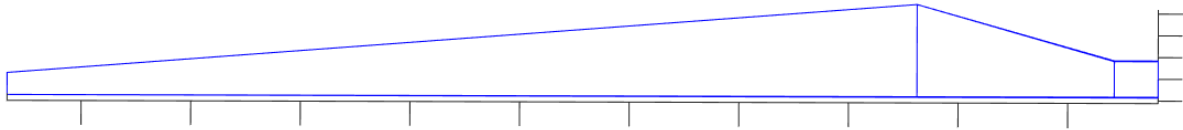
Figure 3.15 Two-dimensional view of modeled wind turbine blade.

Tick marks on horizontal axis indicate 5.0-m intervals; tick marks on vertical axis indicate 1.0-m intervals.
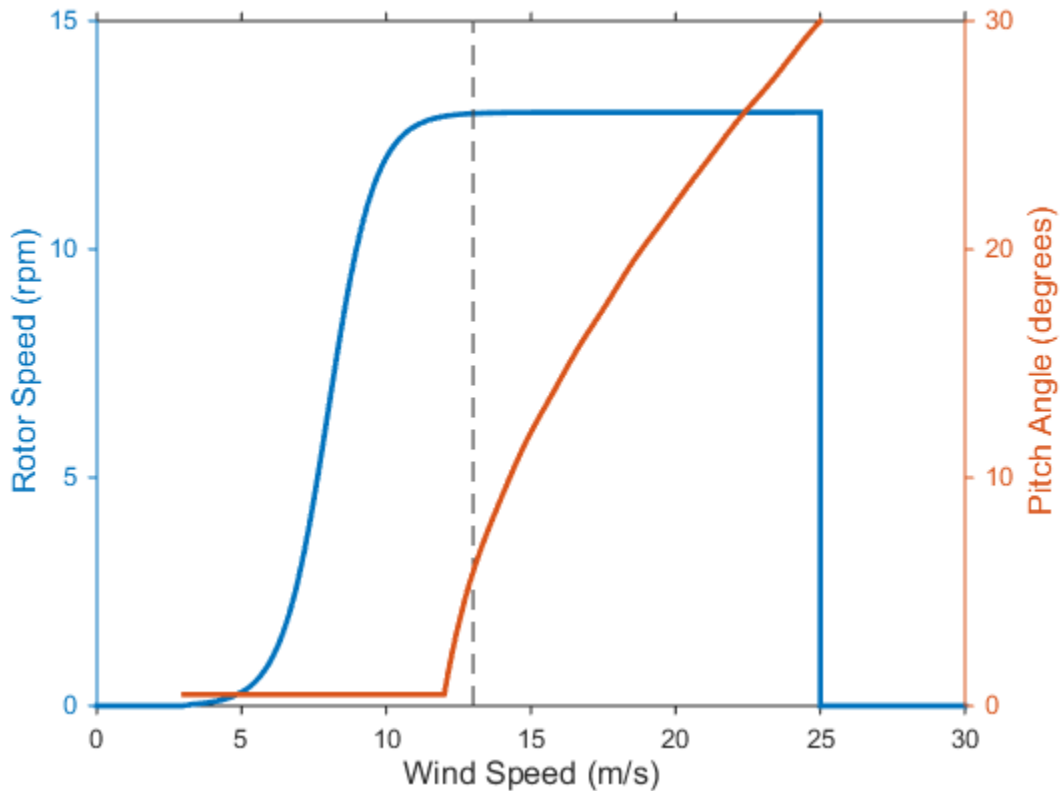
Figure 3.16 Modeled relationships between wind speed and rotor speed (blue line), and between wind speed and blade pitch angle (orange line).

Table 3.5 Wind turbine design assumptions as incorporated into the collision risk model.

Feature	Value / Comment
Rotor diameter	107 m
Rotor speed	0 – 13 rpm [1]
Blade pitch angle	0.5 – 30 degrees [1]
Blade maximum chord length	4.2 m [2]
Blade feathered position	80 degrees
Hub height	80 m [3]
Tower diameter base	4.0 m
Tower diameter top	2.75 m
Nacelle dimensions	10 m × 4.0 m × 4.0 m (length × width × height)
Cut-in wind speed	3.0 m/s
Cut-out wind speed	25 m/s
Rated wind speed	13 m/s

[1] See Figure 3.16.
[2] See Figure 3.15.
[3] 80.5 m (264.1 ft) according to COP (Cape Wind Associates 2011)

3.4 Model Description

3.4.1 General Overview

We constructed an original simulation model to represent the dynamics of Red Knots potentially passing through the approved Facility and potentially colliding with the Facility's structures during the Red Knot's spring and fall migrations. The basic operation of this model is summarized and illustrated in Figure 3.17.
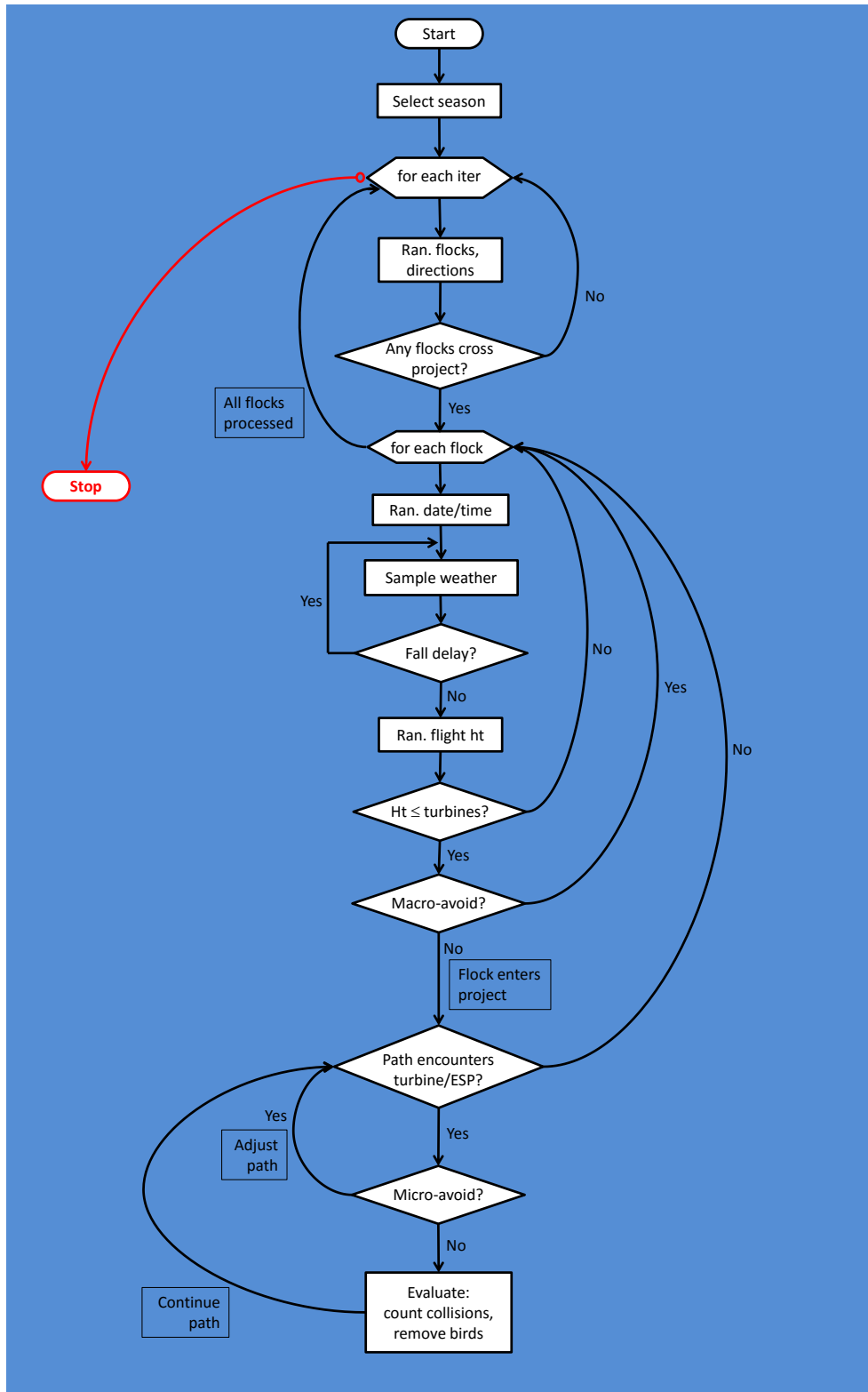
Figure 3.17 Flow chart representing the operation of the collision risk model.

This model was developed to represent collision probabilities for Red Knots potentially interacting with the approved Facility in Nantucket Sound, Massachusetts.

We performed a series of simulations with this model to develop an understanding of Red Knot collision risk at the approved Facility. The basic unit of our simulation testing was an "iteration," which consisted of running the entire potentially-exposed population of Red Knots through the model one time during one single, entire migratory season (either spring or fall). At the onset of each iteration, flock sizes, initial flock positions (in spring), and flock flight directions were all randomly generated as appropriate for the chosen season. If none of the flight paths crossed the Facility site, then the model proceeded to the next iteration. On the other hand, if one or more flight paths crossed the Facility, then those crossing flights were processed sequentially, as follows. For the flock in question, the departure (or arrival) date and time were randomly generated, again, as appropriate for the season. Weather conditions were then randomly sampled based on the selected date and time. If delay conditions were satisfied, that is, if the selected season was fall, if the flock was *delay sensitive*, and if the flock would experience a headwind exceeding a specified threshold, then departure was delayed (see Section 3.3.1: *Red Knot Biology,* subsection: *Migration Timing*), generally until weather was more favorable. Irrespective of whether a flock had been delayed or not, depending on a further test of the headwind experienced by the flock, the appropriate flight height distribution was selected and a flight height for the flock was generated from that distribution. If the height was above wind turbine heights, then that flock was judged to have no collision risk and the model proceeded to the next flock with flight path crossing the Facility. However, if the randomly generated flight height was within wind turbine heights, then macro-avoidance was evaluated for the flock. Depending on the outcome of a random draw, if the flock "decided" to avoid the entire Facility, then, again, that flock had no risk and the model proceeded to the next flock.

On the other hand, if the flock decided to enter the Facility, then its path through the Facility was evaluated. If the path encountered no structures (any turbine or the ESP), then that flock was judged to have no risk and the model proceeded to the next flock. However, if the flock encountered at least one structure, its path was evaluated in stages. For the first structure encountered, the flock made a micro-avoidance decision based on the outcome of a random draw. If the flock chose to avoid the structure, then its path shifted laterally (the avoidance maneuver) and the new path was re-evaluated to determine whether it encountered any additional structures. If the flock chose not to avoid the first structure encountered, then its path carried it "through" the structure. In this case, the flight path of each bird in the flock was evaluated separately using the modeled spatial dimensions and configuration of flocks and birds. If any individual birds collided with a structure, the collision was assumed to be fatal, and that bird was removed from the flock. After removing any collisions, the flock's path continued through the Facility. The evaluation process was the same for each structure encountered. That is, a new decision was made either to avoid the structure or not − avoidance was accompanied by a lateral shift of the path, while non-avoidance was accompanied by assessment of collisions and removal of birds that collided. This process continued until no further structures were encountered and, implicitly, the flock had passed out of the Facility. Since this flock had no further risk, the model proceeded to the next flock that crossed the Facility.

When all flocks in the entire potentially-exposed population had been evaluated for the entire season, the model proceeded to the next iteration, that is, random generation of a new set of flocks and evaluation of the outcomes for the entire set of flocks within a season as described above. For each set of modeled conditions that we examined, we typically performed 100,000

such iterations in order to generate robust output distributions (numbers of fatalities). Furthermore, we typically repeated this process 10 times for each set of modeled conditions, in order to characterize confidence intervals around mean fatality levels observed in each set of 100,000 iterations. In the sections that follow, we discuss details of model operation that were not addressed in Section 3.3: *Input Assumptions and Data*.

3.4.2 Software

We developed the collision risk model using MATLAB® software (MathWorks 2014). We wrote the primary functions, though we also relied on the Statistics Toolbox (Mathworks 2014) for various tasks associated with probability distributions, particularly generating random variates. In addition, we made use of a number of functions from the MatGeom library (Legland 2014) for geometric computing, particularly those functions designed for intersection computation in 2-dimensional space. We modified some of the MatGeom functions to obtain different or additional output, and to improve computational speed.

3.4.3 Structural Elements of the Model

Coordinate System, Distances, and Directions

All locations, both real and simulated, were expressed in the Universal Transverse Mercator coordinate system, Zone 19T. Correspondingly, all distances and lengths were expressed in meters. Furthermore, all angular measurements were based on Cartesian geometry. Angles followed mathematical convention, increasing counter-clockwise from the positive X-axis. Directions followed the meteorological convention for wind, that is, the direction from which the wind originates. Red Knot flight directions followed the same convention; thus, for example, a flock heading due north had direction $3\pi/2$.

Date and Time Randomization

During simulations, flight dates and times were randomly generated from the distributions shown in Figure 3.2. Both of these distributions represented date and time continuously, essentially Julian date. Therefore, random variates from these distributions were rounded for consistency with the weather data and our assumptions regarding fall departure times. For each flock passing through Nantucket Sound in spring, a date/time was generated from the spring distribution (Figure 3.2b) and rounded to the nearest hour. For each flock departing in fall, a date/time was generated from the fall distribution (Figure 3.2a) and rounded to the nearest date, depending on the sunset time. Then, the departure time was randomly selected from the sunset hour and the preceding three hrs. For instance, if the randomly generated date/time was September 25 at 03:15, then the nearest sunset was on the previous day, so date was rounded to September 24. Sunset on this date occurred at17:35, therefore the rounded sunset hour was 18:00. That hour and the preceding three hrs (15:00, 16:00, and 17:00) were considered equally likely, so the departure hour was selected from the four available hrs by simple random sampling.

Sampling Weather

For each flock, the selected departure or "arrival" date (month and day) and hour were combined with a year chosen from the interval (2009 - 2013) by simple random sampling. The complete date/time (year, month, day, and hour) was then used to retrieve the weather data (wind, visibility, and precipitation) for that flock. Thus, weather conditions were sampled from a specially-constructed 5-year dataset for Nantucket Sound.

Effective Headwind

Headwind magnitude was calculated from vector components based on wind speed and the angular difference between wind and flock directions. For instance, with wind direction directly opposite flock direction, the angular difference was 180°, and under that condition the wind speed (for example, 10 m/s) was the effective headwind experienced by the flock. If the flock was headed obliquely into the wind such that the angular difference was 135°, then the effective headwind was lessened. A wind speed of 10 m/s at 135° yielded an effective headwind of 7.07 m/s (23.20 ft/s). In general, for angular differences, α, greater than 90°, the headwind velocity, V_h, was calculated as $V_h = V_w \times abs(\cos(\alpha))$ where V_w was wind velocity. For angular differences of 90° or less, the effective headwind was zero; that is, the flock experienced a tailwind.

Ground Velocity

As noted above, flock ground velocity was calculated secondarily from sampled wind velocity and direction as well as randomly generated air velocity and flock flight direction (i.e., direction with respect to the ground). If wind and flight were parallel, then ground velocity was the sum or difference of wind velocity and flock air velocity. Otherwise, the ground velocity was calculated using basic trigonometry. As illustrated by the wind triangle (Figure 3.18), the known quantities were wind direction (α_w), wind velocity (v_w), flight direction (α_g), and air velocity (v_a). Unknown quantities, including the interior angle*s* of the triangle, were calculated as:

$A = |\alpha_g - \alpha_w| = \min[\alpha_g - \alpha_w, 2\pi - (\alpha_g - \alpha_w)]$, from the corresponding angles postulate;

$W = \sin^{-1}(v_w \times \sin A / v_a)$, from the law of sines; and

$G = \pi - (A + W)$.

Finally, ground velocity was calculated as:

$v_g = \sin G \times v_a / \sin A,$ again from the law of sines.
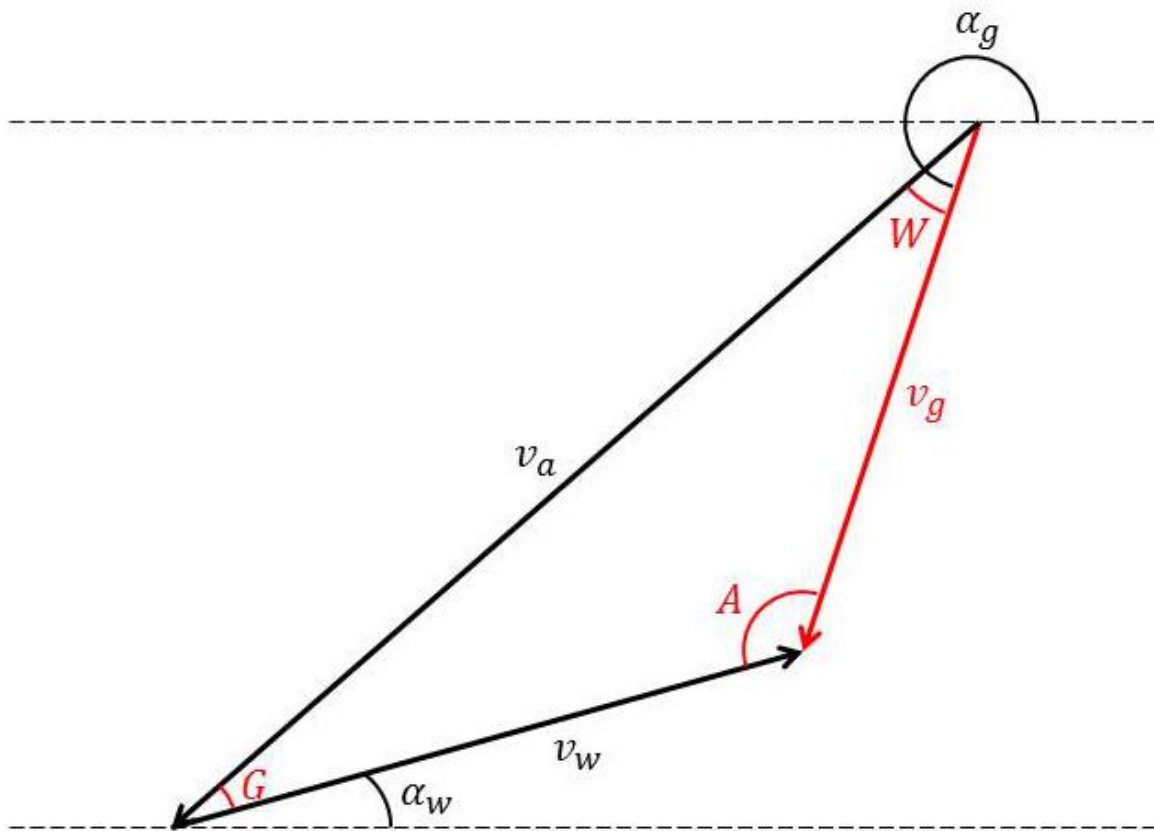
Figure 3.18 Wind triangle diagram illustrating quantities used in calculation of Red Knot ground velocity.

Known quantities (black) include wind velocity (v_w), bird air velocity (v_a), wind direction relative to origin (α_w), and bird direction relative to origin (α_g). Unknown quantities (red) include interior angles of triangle (A, G, and W) and bird ground velocity (v_g).

Determining Whether Flight Paths Crossed the Facility

For the collision risk model, the Facility boundary was determined by calculating the minimum convex polygon for all wind turbine locations and then adding an external buffer of 200-m (656-ft) width. Initial flight paths for all Red Knot flocks in an iteration were defined as line segments from the originating points (MNWR in fall, along the "starting gate" in spring), with randomly generated directions, and with length of 40 km ([25 miles] sufficient length to cross the entire Facility from any origin). The set of paths that crossed the Facility boundary was determined from line segment – line segment intersection (Legland 2014).

Determining Flight Path Encounters with Wind Turbines or the Electrical Service Platform

In this context, "encounter" did not imply collision, but rather the *potential* for collision if the structure was not avoided. To assess encounters, flight paths that crossed the Facility within turbine heights were represented as rectangles with 40 km length (again, sufficient to cross the entire Facility from origin) and width equal to flock width (e.g., a flock of 100 Red Knots had

46

path width of 54 m [177 ft] – see Section 3.3.1: *Red Knot Biology*, subsection: *Flock Size* and *Shape*). Furthermore, bounding polygons (specifically, decagons) were centered on all turbine locations and the ESP location. Turbine decagons had 53.5-m (175.5-ft) radius (the same as rotor radius) and the ESP decagon had 26.65-m (87.43-ft) radius (sufficient to circumscribe the rectangular platform). Any intersection of path rectangle and bounding decagon was flagged as an encounter, and each encounter was evaluated successively. If the flock avoided the structure, then the path was shifted laterally (see Section 3.4.3: *Structural Elements of the Model*, subsection: *Micro-Avoidance Maneuvers*) and re-assessed for new encounters. On the other hand, if the flock did not avoid the structure, then each the flight path of each bird within the flock was evaluated for potential collision, but the flock's path was unaltered and any subsequent encounters were similarly evaluated.

Initializing Wind Turbines
Turbine rotors were rotated to face into the wind (accompanying nacelles were also rotated appropriately) in order to create a realistic representation of the angle at which the flock encountered the rotor. For computational efficiency, this operation was only performed for rotors encountered by particular Red Knot flight paths and flight altitudes.

Micro-Avoidance Maneuvers
Maneuvers for micro-avoidance were explicitly represented in the model. In particular, avoiding flocks shifted laterally without changing either flight height or primary direction. Lateral maneuvers are consistent with observations of seabirds (Cook et al. 2012, 2014). Considering collision risk within the model, such movements were conservative in that an avoiding flock remained within turbine heights and, thus, may have encountered additional structures as it continued through the Facility. In contrast, vertical movements would alter the chance of encountering any additional structures. A downward movement would reduce or eliminate the risk of encountering additional rotors (though not turbine towers), while an upward movement would reduce or eliminate the chance of encountering any structures at all.

Modeled lateral movements were sufficient to clear the bounding decagon around a turbine or the ESP by a minimum of 10 m (i.e., the nearest bird would be 10 m from the bounding polygon). Shifts were either left or right (relative to flock heading), depending on which direction required the least total movement. Geometrically, the shift required calculation of new coordinates for the flock's flight path rectangle and, similarly, new coordinates for all birds within the flock. Otherwise, the new path was parallel to the previous path. That is, the flock continued in its original flight direction (Figure 3.19).
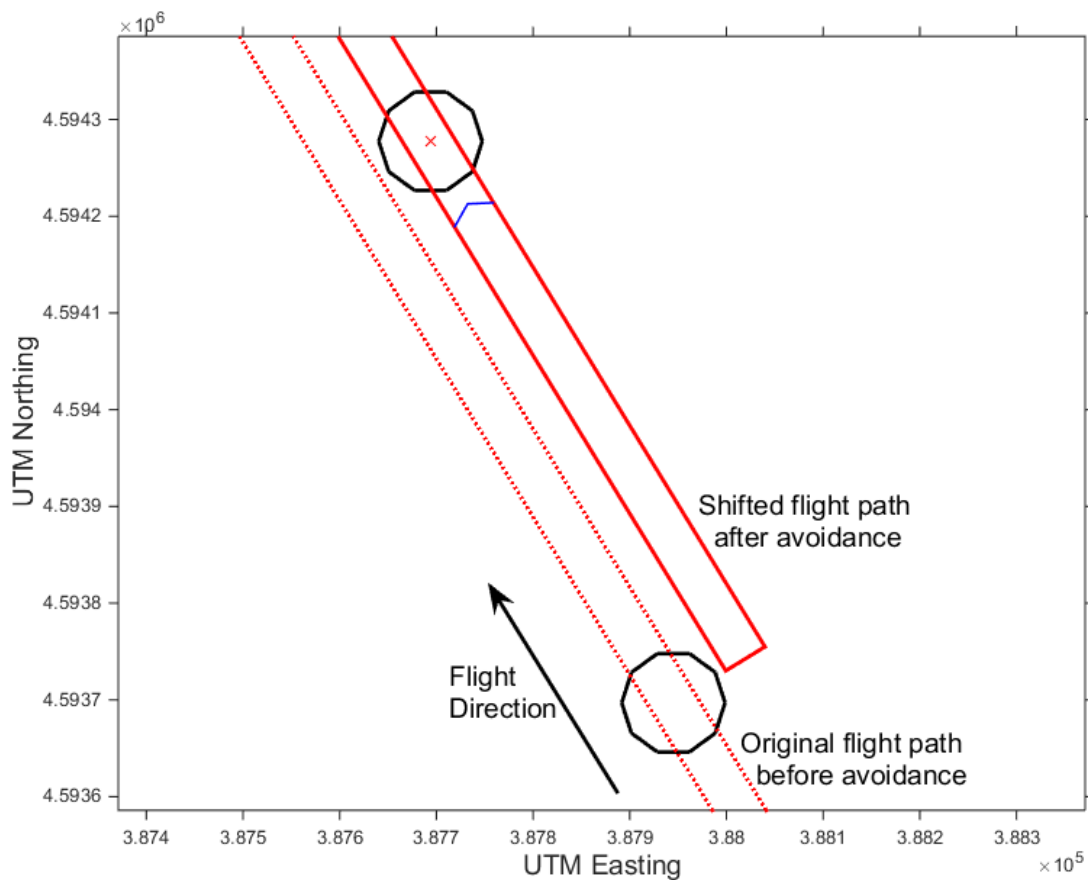
Figure 3.19 Example of micro-avoidance maneuver as represented in the collision model.
Black decagons are bounding polygons for two wind turbines. The flock's original flight path (dotted red lines) would have encountered the more southern turbine (path polygon intersected turbine bounding polygon). The decision to avoid this turbine was implemented by shifting the flight path to the right. The new path (solid red lines) continues in the same direction as the original path and intersects the bounding polygon for another wind turbine. The blue chevron within the new path represents the flock.

Following avoidance, the flock might have encountered one or more additional structures. At each encounter, the decision to avoid or not was determined by a random draw, treated independently of all previous draws. That is, the decision to avoid did not depend on previous decisions or previous outcomes (e.g., collision and removal of some members of the flock).

Evaluating Collisions with the Electrical Service Platform
If a flock did not avoid a wind turbine or the ESP, then the flight path of each individual bird was evaluated for collision. Individual structural components were evaluated as appropriate for the flock height. First, consider the ESP, which was assumed to have no moving components. If a flock failed to avoid the ESP and flight height was less than 10.7 m (35.1 ft), then the components presenting risk were the eight support piles (Table 3.4, Figure 3.14). In two dimensions (as if viewed from above) each pile was represented by a decagon. In general, each bird's flight path was represented by a line segment extending from the bird's left wing tip; the rightmost bird in the flock also had a line segment extending from its right wing tip. A line

segment intersection test (Legland 2014) was used to determine which flight paths intersected pile polygons. (Note that single line segments were used to represent individual flight paths whenever possible to minimize the computational burden.) If the bird immediately to the right of the leftmost bird had intersecting flight path, then the leftmost bird was automatically flagged as also having intersecting flight path (recall that flocks were assumed to fly in tight formation). Any intersection was interpreted as a collision, and the corresponding birds were removed from the flock.

If a flock approaching the ESP had flight height between 10.7 m and 14.4 m (47.2 ft; Table 3.4), then the superstructure presented risk. The superstructure was represented in two dimensions by a rectangle, thus, with only four line segments. Otherwise, evaluation of collision was the same as for the piles: a test for line segment intersections was conducted and those birds with intersecting flight paths were removed from the flock.

Flock shape was invariant during simulations. Even when individual birds were removed due to collision, a flock retained its overall dimensions and shape; birds did not close rank to fill empty positions. Assuming constant flock dimension and shape sacrificed some realism for simplicity, and was also more conservative with respect to collision risk – all else being equal a larger flock was more likely to encounter subsequent turbines in its passage through the Facility.

Evaluating Collisions with Wind Turbine Towers and Nacelles

Evaluating collisions with turbines was more complicated than with the ESP because of multiple structural components, varying dimensions with height, differing orientation depending on wind, and the probabilistic nature of collision with the rotor. Considered alone, tower collisions were simplest. Tower diameter was calculated based on a flock's flight height, and the tower's cross-section was generated as a 2-dimensional decagon. Collisions were determined from flight path line segment intersections with the decagon (Figure 3.20), and the corresponding birds were removed from the flock. Flocks flying below rotor-swept height might only collide with the tower, but failure to avoid the turbine did not guarantee collision even in this case. Recall that the avoidance decision was based on encounter with the bounding polygon. However, intersection might involve only a portion of the flock and the outer portion of the polygon. Thus, even if the flock failed to avoid, those birds whose paths intersected the bounding polygon might pass to the side of the tower. For flocks flying within rotor-swept height but below hub height, collisions with the tower were evaluated before potential collisions with the rotor even when the rotor would have been encountered first because, having failed to avoid the turbine, collision with the tower was certain.

a
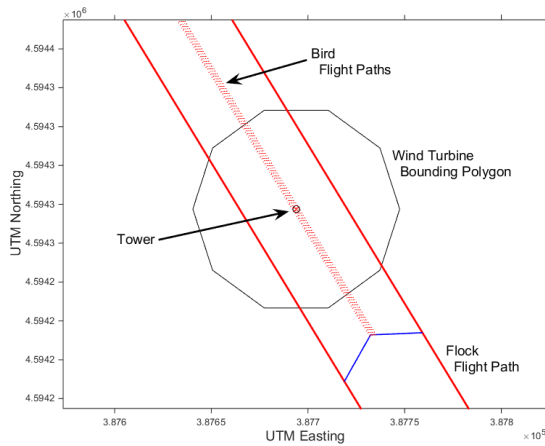
b
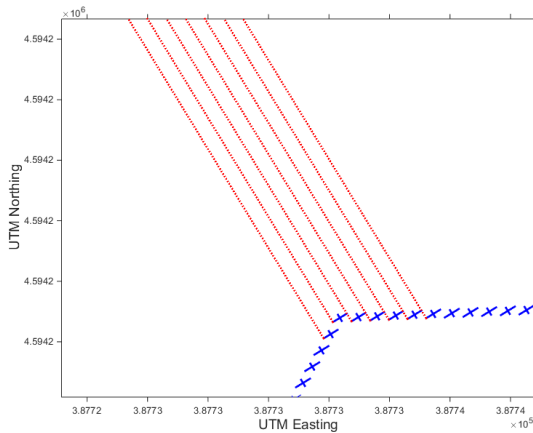
c
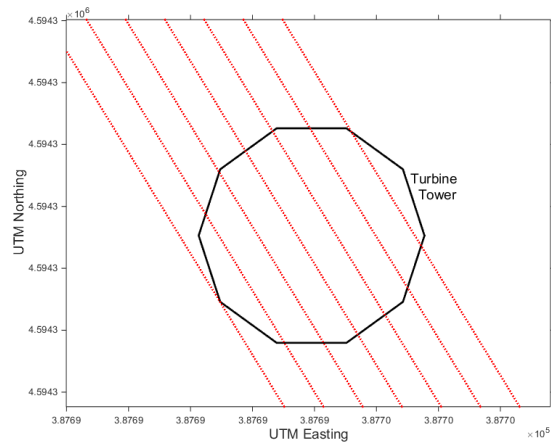
Figure 3.20 Example of collision of Red Knots with a wind turbine tower as represented in the collision model.

(a) View of entire flock, flock flight path, and individual bird flight paths that intersect the tower polygon.
(b) Close view of birds within flock and the flight paths of individual birds that intersect the tower polygon.
(c) Close view of tower and intersecting flight paths.

Similarly, collisions with the nacelle were evaluated before potential collision with the rotor. The nacelle was represented in 2-dimensional cross-section as a rectangle, which was oriented on the turbine according to wind direction. Otherwise, nacelle collisions were similar to tower collisions, i.e., based on line segment intersection, followed by removal of the appropriate birds from the flock.

Evaluating Potential Collisions with Rotors

Collision evaluation for rotors was a 2-stage process. In the first stage, individual flight paths that intersected the rotor were flagged as potential collisions. The second stage employed either the Band (2012) sub-model for active rotors, or a geometric sub-model for stationary rotors. The first stage intersection test was similar to the intersections tests for stationary components (ESP piles and superstructure, towers, and nacelles) described above. For flocks within rotor-swept heights, determining which birds within the flock were at risk depended in part on the flock's

height relative to hub height. The "width", w, of the rotor at flock height, h, was calculated as $w = 2\sqrt{r^2 - |h - H|^2}$, where r was rotor radius and H was hub height (note this is the formula for the length of a horizontal chord in a circle of radius r with center at H). Thus, w defined the length of a line segment representing the rotor cross-section at flock height. For example, for the Siemens SWT-3.6-107 wind turbine with $r = 53.5$ and $H = 80$ and for a flock flying at a 50-m (164-ft) height (30 m below the hub), the rotor width would be $w = 88.6$ m (290.7 ft). The rotor segment was oriented perpendicularly to the wind direction and assigned coordinates for the turbine in question. If line segments representing individual bird flight paths intersected the rotor segment (Figure 3.21), the intersection points were calculated. Thus, for each bird at risk of collision (with an intersecting path), stored information included the bird's height and its lateral displacement from the hub, i.e., the bird's exact point of entry into the rotor. Further, the angle between the flock's flight path and the rotor segment was calculated and stored; approach angle affected the calculation of collision probability in some cases. In the second stage of collision evaluation, the appropriate rotor sub-model was invoked to determine which of these birds, if any, collided with the rotor.
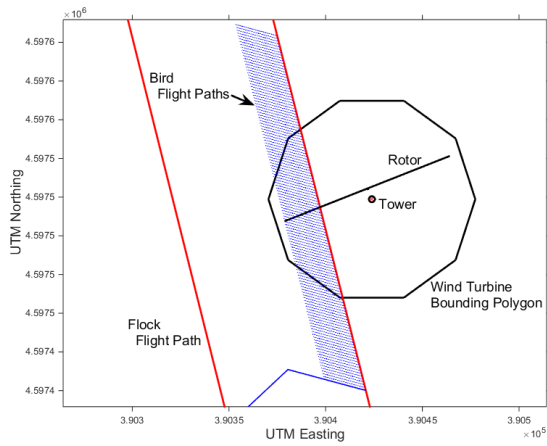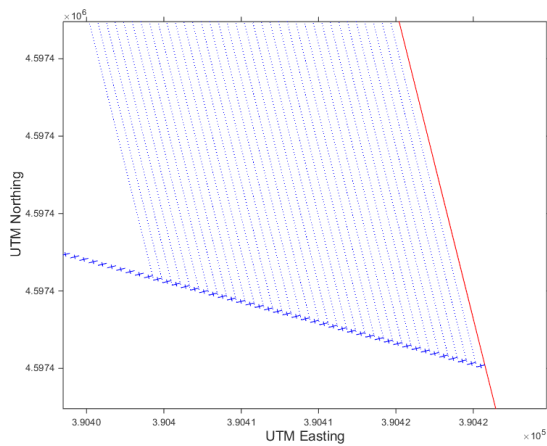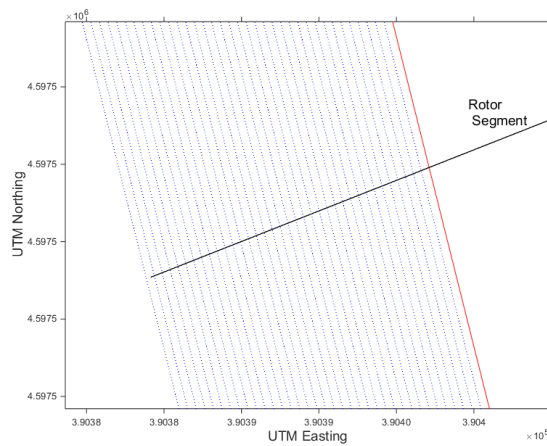
Figure 3.21 Example illustrating potential collisions with a wind turbine rotor.
(a) View of flock, flock flight path, and individual bird flight paths that intersect the rotor line segment. Note that the flock is flying upwind in this case. (b) Close view of birds within flock and the flight paths of individual birds that intersect the rotor segment. (c) Close view of rotor segment and intersecting flight paths.

Band Sub-Model for Active Rotors

The primary component of the Band (2012) model is a mathematical description of bird flight through an active rotor with the objective of estimating the probability that the bird will collide with a rotor blade. The intent of this component and some of the mathematical details are similar to those of Tucker's (1996) model. Collision probability depends on blade rotational velocity and blade pitch and, thus, indirectly on wind speed. The probability is also dependent on the bird's point of entry into the rotor disc, in particular, the radius or distance from the hub center, and the blade chord length at that radius. Bird characteristics that influence collision probability include size (body length and wing span) and ground speed. Finally, the direction of approach (whether upwind or downwind) affects collision risk. Band's equation for collision probability, *p*, accounting for blade chord length (Band's 3-dimensional model) is:

$$p = \left(\frac{b\Omega}{2\pi v} \right) \Big[\, | \, dc \sin\gamma + \alpha c \cos\gamma \, | + \max\left(L, W\alpha F \right) \Big] \tag{1}$$

where:

b = number of rotor blades (three)

Ω = angular velocity of rotor (radians/second)

v = bird ground velocity

d = +1 for upwind flight, −1 for downwind flight

c = blade chord length

γ = blade pitch angle

L = bird body length

W = bird wing span

$\alpha = v/(r\Omega)$, where r = radius at bird's point of entry

F = 1 for a bird with flapping wings, cos φ for a gliding bird, and φ is the angle of the entry point with 0 directly above the hub and π directly below the hub

Band's model incorporates a number of secondary components to allow estimation of the number of bird fatalities at a wind facility. These components include: (1) bird passage rate ("flux", i.e., the number of birds expected to pass through a rotor per unit time); (2) flight height distribution; (3) multiplication to account for passage through multiple turbines in a wind facility, (4) avoidance probability; and, (5) a large array correction factor. An estimate of flight height distribution (2) takes advantage of the basic model prediction of varying collision probabilities depending on point of entry into the rotor. In the absence of such information, one uses the average collision probability over the entire rotor. The last two components are applied after calculation of unadjusted fatalities. In the case of avoidance (4), the adjustment is obtained by multiplying the unadjusted number of fatalities by one minus the overall avoidance probability. Similarly, the large array correction factor (5) is a post-hoc adjustment to account for the fact that collision risk is not additive, as is assumed by the multiplication in (3). This is

because the outcomes of multiple turbine encounters are not independent events – if a bird collides with a turbine, it is not available to collide with any subsequent turbines it might have otherwise encountered.

We retained Band's primary component, Equation (1) (Eq. (1)), as a sub-model to estimate risk of collision for individual encounters with active rotors. However, we did not retain any of the other components described above because our model accounts for these features and a number of others with greater precision. When all or some portion of a flock passed through an active rotor, each bird's flight path was evaluated within the Band model. The collision probability was calculated based on each bird's known point of entry (see Section 3.4.3: *Structural Elements of the Model*, subsection: *Evaluating Potential Collisions with Rotors*). To determine the outcome (collision or not), a random variate from the Uniform (0, 1) distribution was generated for each bird and compared to that bird's Band collision probability; if the random value was less than the probability, a collision was tallied and that bird was removed from the flock.

Figure 3.22 shows representative collision probabilities yielded by the Band model using the assumed dynamic characteristics of our modeled turbines (Table 3.5, Figure 3.16), wind speed of 15 m/s, fixed Red Knot dimensions (see Section 3.3.1: *Red Knot Biology*, subsection: *Body Size and Shape*), flapping flight, and Red Knot air speed of 20 m/s. As a consequence of flapping flight, collision probabilities are radially symmetric (dependent only on radius) in both panels of Figure 3.22. Downwind flight under these conditions generates probabilities of 0.05 or less over most (approximately 75%) of the rotor area (Figure 3.22a). Unsurprisingly, probabilities increase towards the hub, and there is a very small area of very high probability (near 1.0) near the hub. Collision probabilities are higher with upwind flight (Figure 3.22b), primarily due to slower ground speed. Probabilities are not less than 0.06 even near the blade tips.

a

b
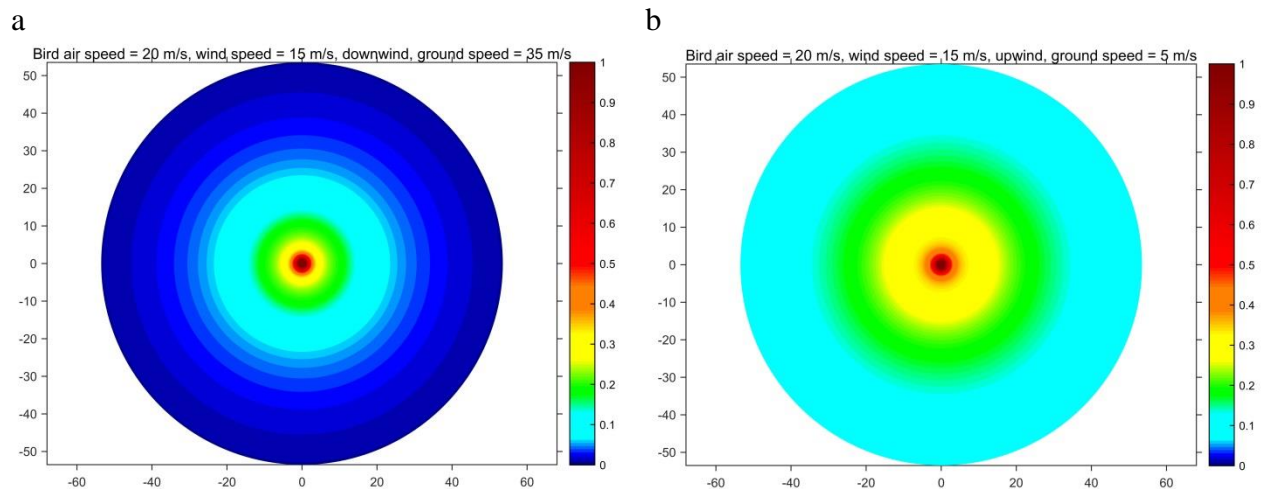
Figure 3.22 Collision probabilities yielded by the Band model for a Red Knot flying through the rotor of a wind turbine.

Turbine model is similar to the Siemens SWT -3.6-107 turbine, with wind speed of 15 m/s and bird air speed of 20 m/s in (a) downwind flight and (b) upwind flight. Axes indicate distance from the center of the rotor hub in meters (i.e., the circles represent rotor-swept areas of a single, idealized turbine).

Adjustments for Non-Perpendicular Approach Angle

An important limitation of Band's Eq. (1) is that it assumes the bird flight is perpendicular (90°) to the plane of the rotor. Frequently, this will not be the case, and as Band (2012) recognizes, collision probability will be higher for angles of approach that are less than 90° and will likely "rise steeply" for angles close to 0°. We decided to relax this assumption, incorporating realistic approach angles and bird-rotor encounter geometry, as we hypothesized it could have a significant effect on collision probabilities. In essence, when a bird approaches a rotor at a non-perpendicular angle, it faces a smaller surface, but has a higher chance of colliding with that surface. Taken to extreme, when the bird's approach is directly parallel to the orientation of the rotor (i.e., the bird's flight is directly perpendicular to wind direction), the collision risk surface of the rotor is equivalent to the silhouette of one blade headed up from the hub, and one blade headed down. Although this surface is much smaller than the circle a bird faces when it approaches the rotor head-on (flight direction parallel with wind direction), a bird headed for the rotor in the parallel orientation has a very high probability of striking that surface, whereas the bird headed for the rotor in the perpendicular orientation has a reasonable chance of surviving, particularly if it is not close to the hub (Figure 3.22).

Approach angles were easily calculated in our model because each flock flight had explicit direction and wind conditions at the time of flight determined rotor orientation. We made two independent adjustments for non-perpendicular approach angles (Figure 3.23). The first adjustment was for those cases when the approach was nearly parallel to the rotor plane. In the absence of any published estimates of this effect, we made the assumption that under baseline conditions, for all approach angles of 25° or less, the odds of collision increased by five compared to the Band model prediction for perpendicular approach (Figure 3.23a). For instance, if the Band model yielded a collision probability of 0.05, then the adjusted probability was approximately 0.22; similarly, if the Band model probability was 0.40, then the adjusted probability was approximately 0.77. We also conducted additional simulations using alternative odds ratios of 10 and 20, which yielded correspondingly larger adjustments (Figure 3.23a).

a

b
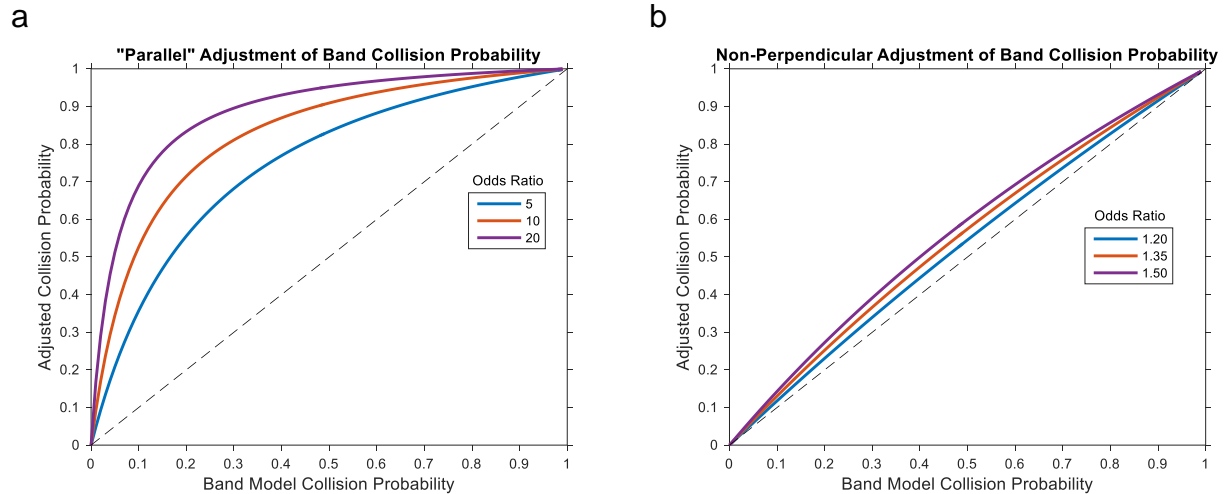
Figure 3.23 Adjustments to Band model collision probabilities based on angle of approach relative to wind direction (rotor orientation).

(a) Adjustments when the approach angle was 25° or less (nearly parallel). Baseline simulations assumed the odds ratio was 5; alternative odds ratios of 10 and 20 were also examined. (b) Adjustments when the approach angle was 25° − 90°. Baseline simulations assumed no adjustment, i.e., odds ratio = 1 (dashed line); alternative odds ratios of 1.20, 1.35, and 1.50 were also examined.

The second adjustment was for those cases when the approach angle was greater than 25°, up to and including 90°. For this adjustment, we relied on a recent modification of the Tucker (1996) model. Like the Band model, Tucker's model assumed perpendicular approach, though modifications by Holmstrom et al. (2011) account for the angle of approach. We note that both Band (2012) and Holmstrom et al. (2011) define the approach angle as the complement of the approach angle in our collision risk model; that is, in the Band (2012) and Holmstrom et al. (2011) models, perpendicular approach is 0° and parallel approach is 90°. Holmstrom et al. (2011) found that collision probability varied as approach angle varied between perpendicular and roughly 45°, and that probability was lowest with perpendicular approach. Holmstrom et al.'s Figures 14 and 15 show probability as a function of approach angle for two different raptor species flying through a GE 1.5-se wind turbine. We noted the maximum and minimum probabilities on each of Holmstrom et al.'s figures and calculated the associated odds ratios: 1.21 for Figure 14 and 1.35 for Figure 15. That is, in the worst case, with non-perpendicular approach the odds of collision increased by 1.35 compared to perpendicular approach.

Under baseline conditions, we made no adjustment to Band probabilities; in effect, we assumed an odds ratio of one. That is, all approach angles greater than 25° were treated as if they were perpendicular. In additional simulations, we used alternative odds ratio adjustments partly based on Holmstrom et al.'s (2011) findings; in particular, we used odds ratios of 1.20, 1.35, and 1.50 (Figure 3.23b). These adjustments were applied uniformly to all probabilities when the approach angle exceeded 25°; otherwise, the adjustment value did not depend on the approach angle. As would be expected, the adjustments in Figure 3.23b were smaller than those in Figure 3.23a. For instance, if the Band model predicted collision probability was 0.20, then the adjusted probability was approximately 0.25 using an odds ratio of 1.35; similarly, if the Band probability was 0.5 and if the odds ratio was 1.5, then the adjusted probability was 0.6.

Geometric Model for Stationary Rotors

Our collision risk model accounts for collisions with stationary structures as well as active rotors. An encounter with a fixed structure (turbine tower, turbine nacelle, and the ESP) has a certain outcome if the structure is not avoided. By contrast, an encounter with a stationary rotor has a probabilistic outcome − even if the rotor is not avoided – on the assumption that the blades stop in a random position. To estimate collision probability with a stationary rotor in a manner consistent with the assessment of encounters between flight paths and rotors (see Section 3.4.3: *Structural Elements of the Model*, subsection: *Evaluating Potential Collisions with Rotors*), we constructed a simplified 3-dimensional model of the rotor consistent with the assumptions in Table 3.5 (e.g., 107-m [352-ft] radius and 4.2 m [13.8 ft] maximum blade chord length). The rotor could be rotated about the hub in 1-degree increments to represent the full range of stopped blade positions. Similarly, the rotor could be rotated about the vertical axis in 1-degree increments to represent the full range of approach angles.

The model was initiated with approach angle of 90° (perpendicular approach) and one of the blades oriented vertically. In two separate stages, the rotor was rotated about the hub in 1-degree increments through an arc of 120° (sufficient to represent a complete rotation since there are three blades). At each position, the 3-dimensional rotor was projected onto two dimensions – essentially the "bird's eye" view. In the first stage, the minimum convex polygon was calculated for the set of all projected points representing the rotor. This polygon was buffered in the horizontal direction by the Red Knot wing span (0.54 m). The resulting bounding polygon represented a 2-dimensional risk space. Assuming straight-line, horizontal flight perpendicular to the projection plane, birds within this space would have finite risk of collision, while birds outside the polygon would have zero probability of colliding with the rotor.

In the second stage, the rotor was once again rotated about the hub in 1-degree increments and projected onto two dimensions (Figure 3.24). A bird was represented as a 1-dimensional horizontal line segment with length equal to wing span. At each rotor position, a large field of birds was generated within the bounding polygon at regular 0.25 m (0.82 ft) height increments and random horizontal position. Birds that either fell entirely within the polygon representing the rotor, or intersected a rotor edge were considered to have collided with the rotor. Each collision was tallied, as was its position relative to the hub (horizontal and vertical displacement). The total number of simulated birds within the bounding polygon was also tallied. Figure 3.24a shows the 2-dimensional projection of the rotor with a 90° approach angle and blades in the initial position (one blade oriented vertically). Birds within the bounding polygon are represented as horizontal line segments – red segments indicate birds that collided with the rotor while black segments indicate birds that did not collide.

Next, the rotor and bounding polyhedron were rotated about the vertical axis in 1-degree increments from 90° to 0° (i.e., ending with approach parallel to the plane of the rotor). At each of these positions (i.e., approach angles), the entire 2-stage process described above was repeated: first, a bounding polygon was generated for the new angle of approach and, second, at each blade position (blades rotated about the hub in 1-degree increments) birds were generated within the polygon and collisions were assessed. Figures 3.24b and 3.24c illustrate approach angles of 45° and 0°, respectively; in both cases, the rotor is in its initial position.

a

Approach Angle: 90°

b

Approach Angle: 45°

c
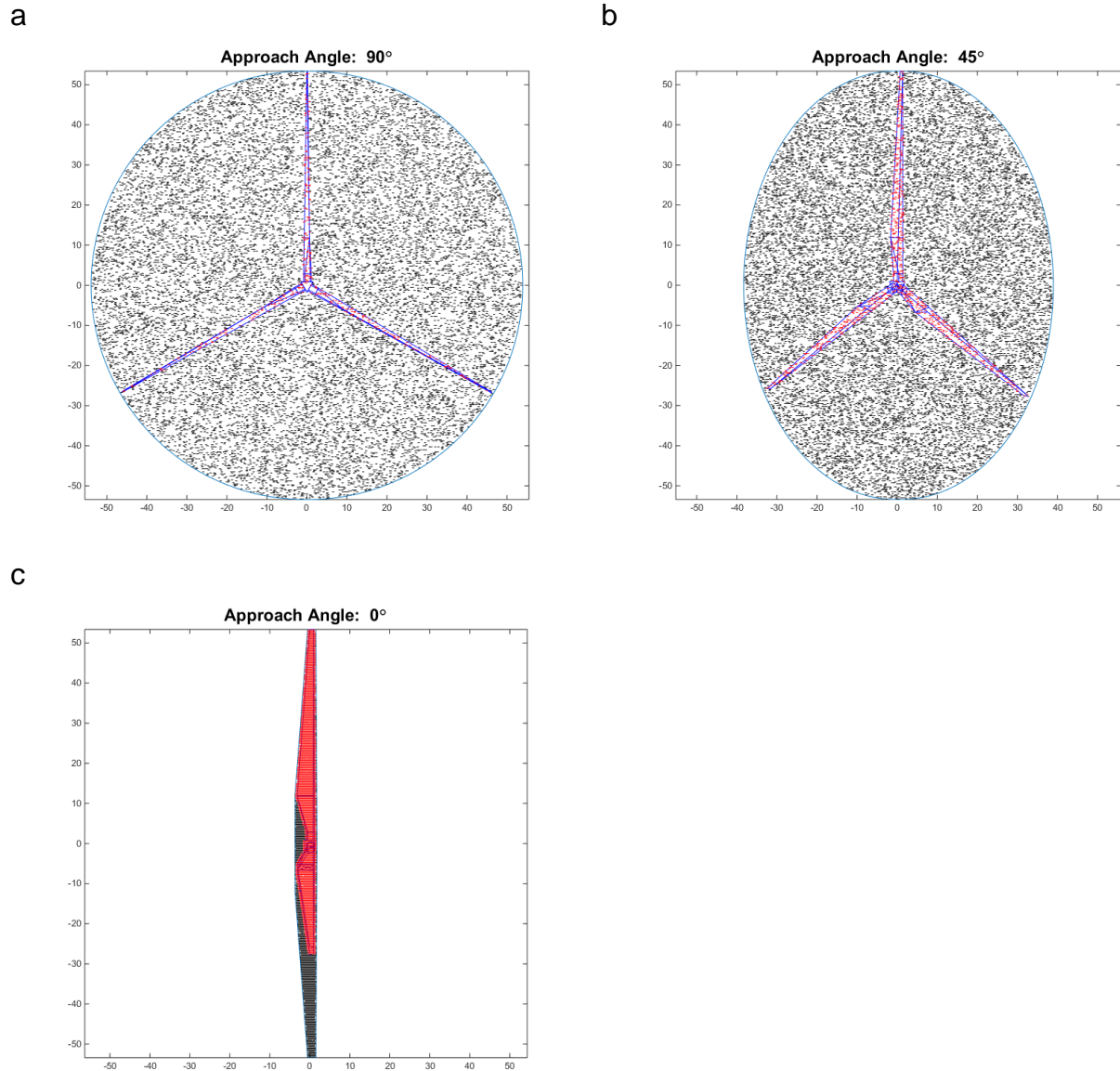
Approach Angle: 0°

Figure 3.24 Stationary rotor model with approach angles.

Model approach angles are (a) 90°, (b) 45°, and (c) 0°. Red horizontal line segments represent birds that collided with the rotor; black segments represent birds within the bounding polygon that did not collide. Axes indicate distance from the center of the rotor hub in meters.

In general, mean collision probability for the entire rotor increased as approach angle decreased (Figure 3.25). When the approach was perpendicular to the plane of the rotor, mean collision probability was approximately 0.024. At an approach angle of 20°, mean collision probability was approximately 0.102, and when the approach was parallel to the rotor collision probability was approximately 0.75.

58
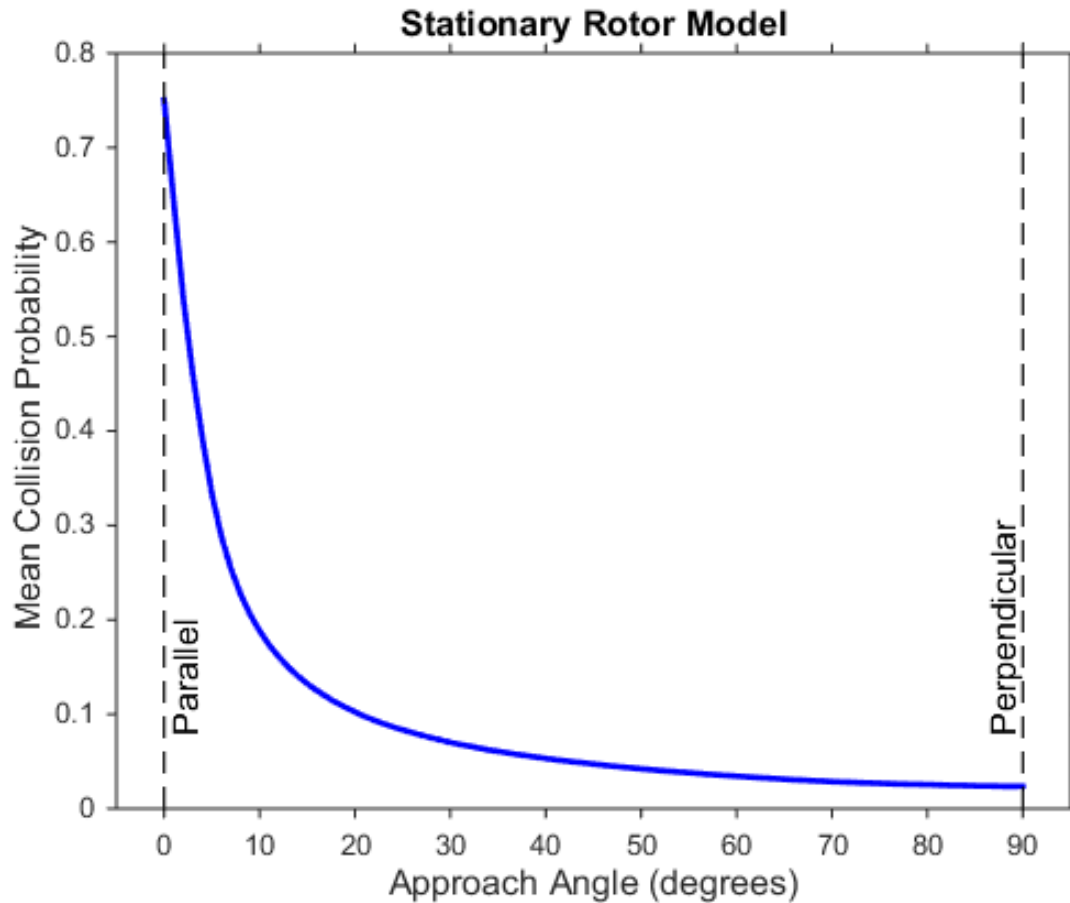
Figure 3.25 Mean collision probability as a function of approach angle for the stationary rotor model.

For use within the main collision risk model, analysis of results from this simulation was directed at estimating collision probability as a function of both approach angle and position of the bird relative to the hub. At each approach angle, data were pooled across all blade positions. Further, because collision risk was symmetric above and below the hub, data were pooled by absolute value of height, e.g., numbers of collisions and total numbers of birds at 1.0 m below and 1.0 m above the hub were pooled together.

For shallow angles of approach (less than or equal to 25°), collision probability was assessed as a function of approach angle and height only. For a given angle and height, the empirical collision probability was calculated as the number of collisions divided by the total number of birds within the bounding polygon at that height. Then, for each approach angle, non-parametric regression based on a local polynomial kernel estimator (Martinez and Martinez 2002) was used to obtain predicted collision probability as a function of height (Figure 3.26). Results show that as approach angle decreases from 25° to 0°, collision probabilities vary more widely with changes in height relative to the hub. Maximum collision probabilities near heights of 10 m become more prominent at shallower angles and are a consequence of blade shape (Figure 3.26). Blade maximum chord length occurs approximately 10 m from the blade root; thus, collision probability is somewhat lower toward the center of the rotor and at heights less than 10 m.

Predicted probabilities from the nonparametric regressions were stored in a look-up table with two dimensions – approach angle and height.

a

b

c

d
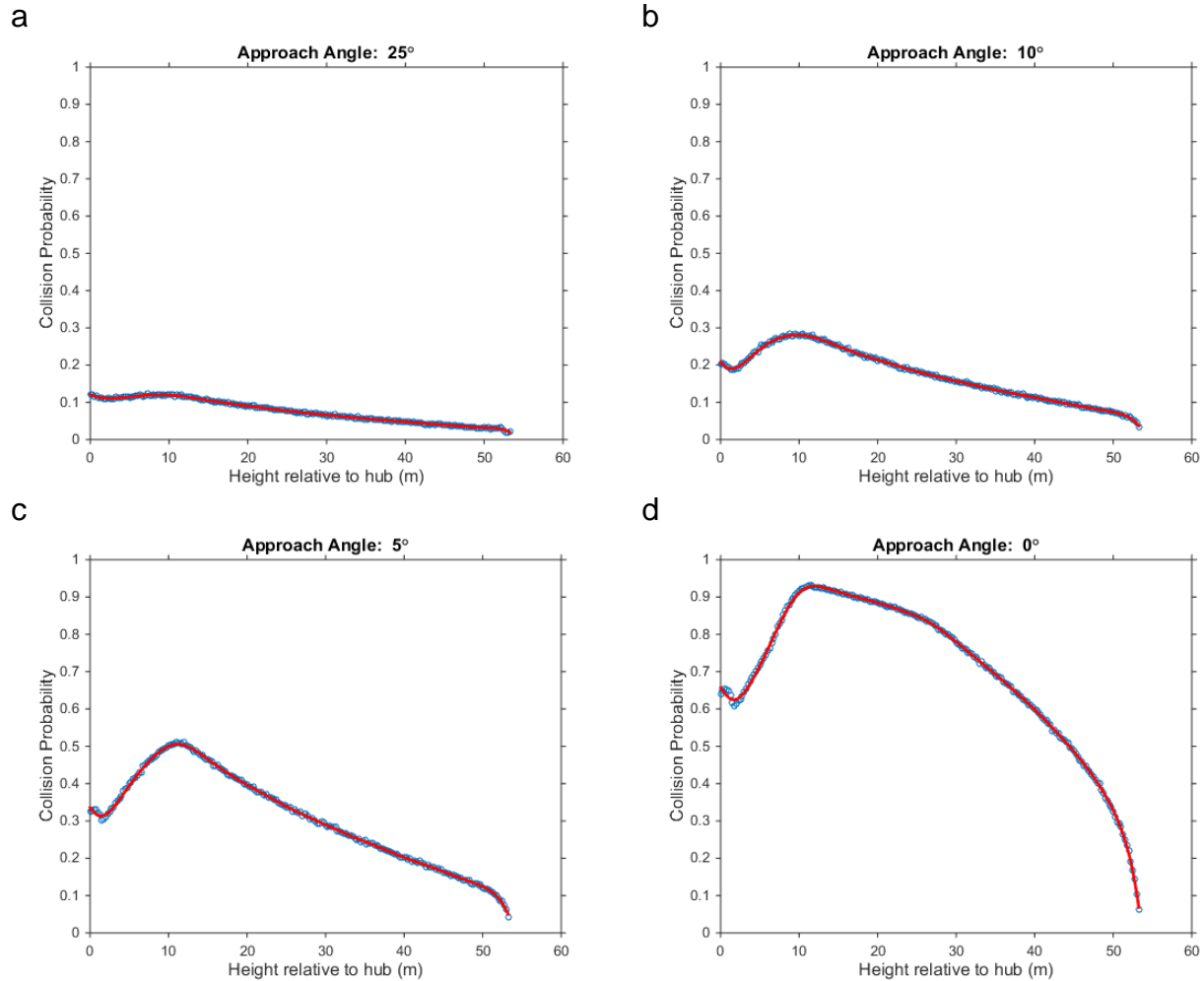
Figure 3.26 Stationary rotor collision probability as a function of height relative to the hub for shallow approach angles.

Approach angles are (a) 25°, (b) 10°, (c) 5°, and (d) 0°. Blue circles represent empirical estimates at each height, and red line represents predicted values from nonparametric regression.

For larger approach angles (more than 25°), collision probability was analyzed as a function of horizontal displacement from the hub in addition to approach angle and height. For this analysis, data from both sides of the hub were pooled together, since collision probability was expected to be laterally − as well as vertically − symmetric. Further, horizontal displacement values were binned (20 equal-width bins) and expressed as the proportion of the rotor half-width. Using proportional rather than absolute distance was consistent with the intersection tests (see Section 3.4.3: *Structural Elements of the Model*, subsection: *Evaluating Potential Collisions with Rotors*) which expressed intersection points with the rotor segment in terms of relative segment length. Continuing the example above (see Section 3.4.3: *Structural Elements of the Model*, subsection: *Evaluating Potential Collisions with Rotors*), for a flock flying at a 50 m height, the rotor half-width was 44.3 m (145.3 ft). A bird from this flock entering the rotor plane 20 m to either side of

the hub would have been placed in the 10th bin, representing proportions 0.45 – 0.50 (since 20/44.3 = 0.4515). For each combination of approach angle and height (0.25-m increments), non-parametric regression models were fit to these binned data (empirical collision probability versus [vs.] relative horizontal displacement), and then used to generate predicted collision probability. Example results for perpendicular approach at several heights show that collision probability decreases as horizontal distance from the hub increases (Figure 3.27).

a

b

c

d
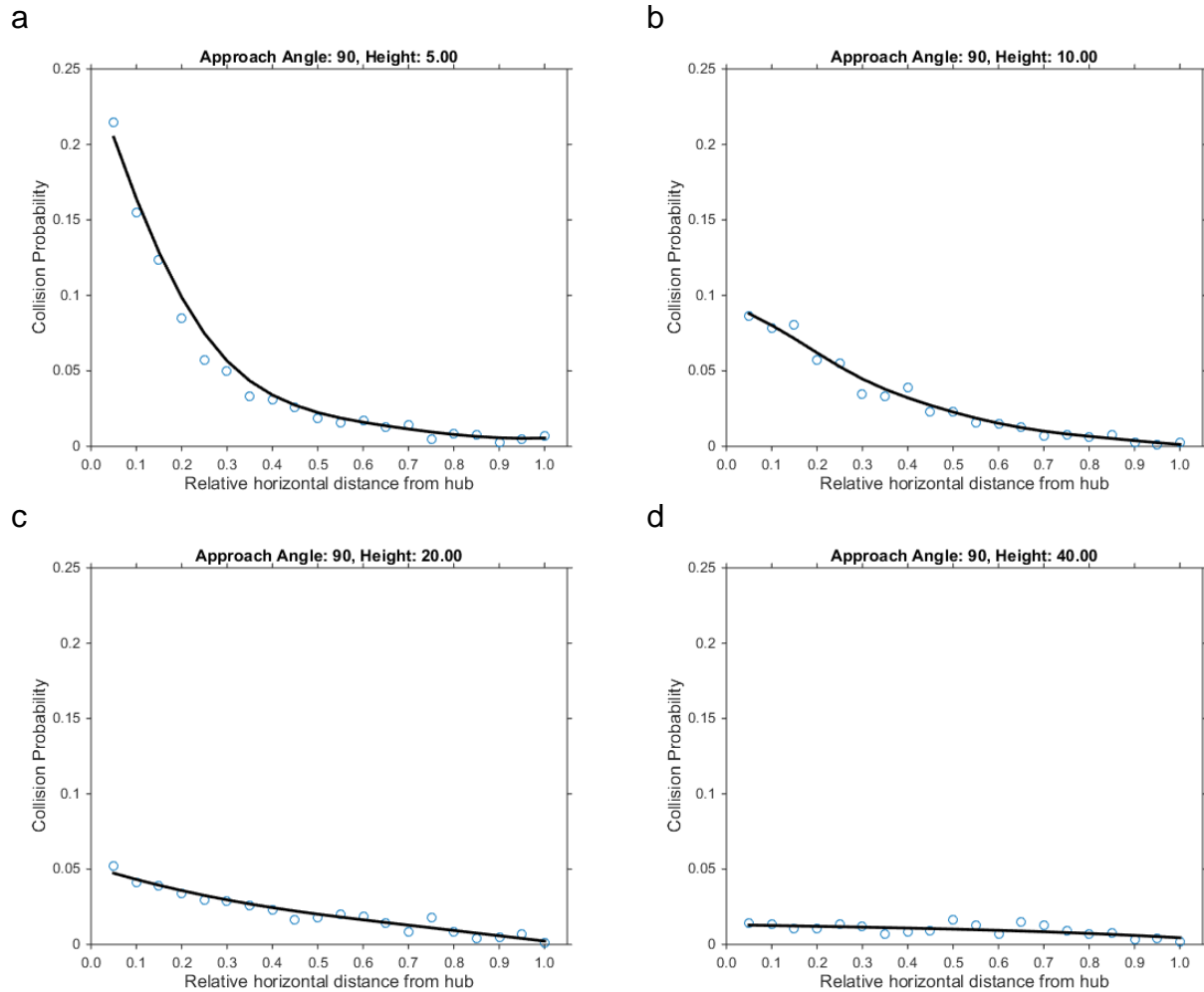
Figure 3.27 Stationary rotor collision probability as a function of relative horizontal distance from the hub for 90° approach angle.

Approach angle heights are (a) 5.0 m, (b) 10 m, (c) 20 m, and (d) 40 m. Blue circles represent empirical estimates at each height, and the black line represents predicted values from nonparametric regression. Similar regressions were fit for all approach angles greater than 25° and for all heights relative to hub height from zero m to 53.5 m (rotor radius).

Predicted probabilities from the regression models were stored in a look-up table with three dimensions – approach angle, height, and relative horizontal displacement.

During simulations of the main collision risk model, when a flock flew through a stationary rotor, the approach angle was used first to select the appropriate look-up table. If the approach angle was less than 25° and the 2-way table was selected, approach angle and height were used

as indices into the look-up table to retrieve a common collision probability for all individual birds whose flight paths intersected the rotor. If the 3-way table was selected because the approach angle was greater than 25°, approach angle, height, and horizontal displacement were used to retrieve collision probabilities that could vary among the birds depending on their horizontal distances from the hub. In both cases, a random variate was generated from the Uniform (0, 1) distribution for each bird and compared to the selected collision probability; if the random value was less than the probability, a collision was tallied and the bird was removed from the flock.

Independent Collision Probabilities

Our main collision model simulates flocks and thereby introduces some dependencies into collision outcomes for birds within a particular flock. However, both the Band (2012) and geometric sub-models treat collision risk as independent among individuals in a flock. This is undoubtedly an over-simplification because if one bird in a flock (particularly, a well-formed flock with regular spacing) collides with a blade, then its closest neighbors are more likely to also collide with the same blade at nearly the same time. By the same token, if a particular bird passes through the rotor without colliding with a blade, then its close neighbors are also more likely to successfully pass through unharmed. That is, for flocking birds, collision risk likely exhibits spatial and temporal dependencies that are not accounted for by the rotor models.

3.5   Simulation Protocol

A single iteration of the collision risk model involved running all of the potentially exposed birds through the model for a single migratory season, by generating flocks with total size equal to the assumed seasonal size of the potentially exposed population. For the fall, the baseline exposed population size was 1,500 Red Knots, so that, given an average flock size of 105, the expected number of flocks would be about 15 flocks. Similarly, for the spring, the baseline exposed population was 200 and the expected number of flocks would be about two flocks. Each of these flocks was assigned a random date of departure or "arrival", random direction, random flight height, macro-avoidance outcome, and so on. For each of those flocks that flew into the Facility within turbine heights, the model examined its passage through the Facility in detail. Stored output included information about each encounter (with a turbine or the ESP) and the outcome of that encounter, in particular the number of collisions.

A simulation consisted of 100,000 iterations under the same set of assumptions, though with random variation in many model components. In some cases, a particular simulation was repeated 10 times for estimation of means and variances of model outcomes. Each such set of 10 simulations was initiated with a new random number stream, and random stream states were stored along with model output. In other cases, a set of simulations consisted of 100 closely related simulations, though each was at a randomly generated population size or a randomly generated avoidance probability. These sets of simulations were designed to assess model sensitivity given uncertainty in population sizes and avoidance probabilities. Again, each such set was initiated with a new random number stream.

4. Results and Discussion

4.1 Overview

In this section, we provide a summary of the results of simulations that were performed with the model, intended to produce a robust, quantitative prediction for the annual take of rufa Red Knots that is likely to result from collisions of Red Knots with structures associated with the approved Facility in Nantucket Sound, Massachusetts. To this end, we first review the results achieved for one million iterations of the "baseline condition," defined as the complete set of default inputs and assumptions developed by the Project's technical team on the basis of best available scientific information, intended as a realistic representation of the dynamics of the rufa Red Knot population's interactions with the approved Facility. In the sections that follow, we present the results of additional simulations that were performed with alternate inputs and assumptions, as designed by the Project team to encompass reasonable levels of variation in certain structural elements of the model that were hypothesized to have important influences on the results. These sections comprise an informal sensitivity analysis of the model. They are organized by topics, with results and discussion integrated within each topic.

As a general preface to this section, we note that the accuracy of the model's predictions is constrained by the limits of available data and existing knowledge of the dynamics of the system. We are hopeful that our model may help illuminate specific areas where additional data gathering efforts would result in significant improvements to our ability to predict collision fatalities of Red Knots at offshore wind energy facilities. Our expectation is that as additional data becomes available, collision models and their resulting fatality predictions will be improved.

4.2 Baseline Conditions

The baseline simulation was repeated 10 times, each time with a different random sequence, and with 100,000 iterations performed in each simulation. Simulation results for baseline conditions are shown in Figure 4.1. The grand means and standard deviations of three output variables (see below) were calculated from the 10 repetitions, separately for each season. Bar heights in Figure 4.1 represent grand means, while the error bars show ± one standard deviations for the output variable of interest.

a

b

c
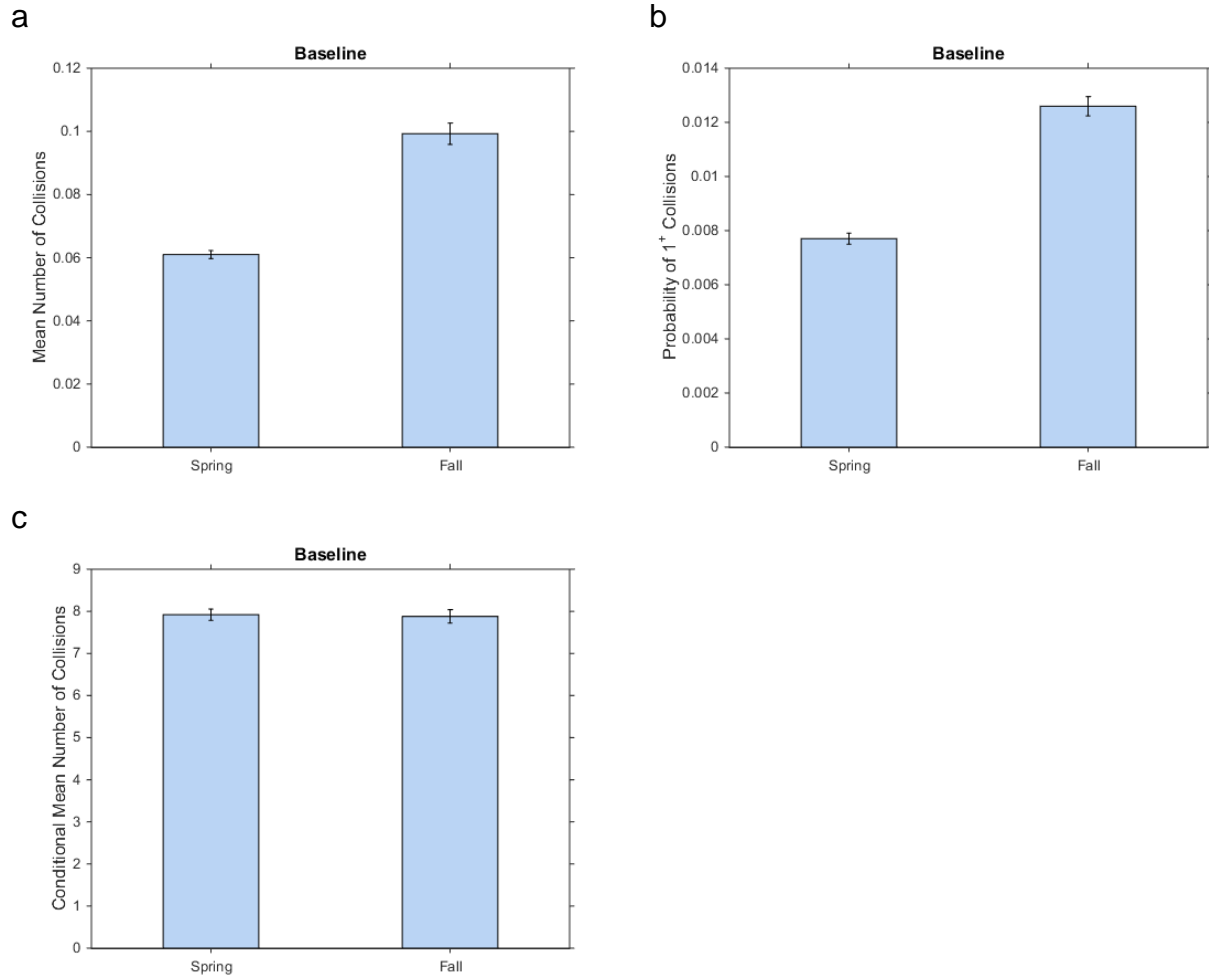
Figure 4.1 Model simulation results under baseline, or default conditions.

Simulation results showing (a) mean number of Red Knot collisions, (b) probability of at least one collision, and (c) conditional mean number of collisions. Bar height represents the grand mean of 10 repeated simulations, each with a unique random number seed, and each simulation representing 100,000 iterations. Error bars indicate ± one standard deviation, based on the 10 repetitions. See text for additional explanation.

To understand the results, we examined the behavior of three distinct output variables, defined as follows:

mean number of collisions (fatalities) per iteration

This output variable was calculated as the total number of Red Knot collisions divided by 100,000 (for a simulation consisting of 100,000 iterations). This represents the mean number of Red Knots killed in the entire population during a single migratory season.

probability of at least one collision occurring during a single iteration

This output variable was calculated as the total number of iterations in which one or more collisions occurred divided by 100,000 (in a simulation consisting of 100,000 iterations). This variable represents the frequency of Red Knot fatalities. It addresses the question, "in what fraction of iterations did at least one Red Knot fatality occur?"

conditional mean number of collisions per iteration

This output variable was calculated as the total number of collisions divided by the total number of iterations in which one or more collisions occurred. As such, this variable reflects the average number of Red Knots killed during the iterations in which at least one fatality occurred.

The mean number of collisions was approximately 0.06 in the spring and 0.10 in the fall (Figure 4.1a), resulting in a total predicted mean annual Red Knot collision fatality rate for the Facility of 0.16 Red Knots/year, or 16 predicted fatalities over a period of 100 years. The probability of at least one collision showed a similar seasonal pattern (Figure 4.1b); the probability was 0.0077 in spring and it was 0.0126 in fall. In other words, the model predicted that Red Knot collisions would only occur in fewer than eight of 1,000 years during the spring migration, and in fewer than 13 of 1,000 years during the fall migration. The conditional mean number of collisions represents the average number of Red Knots killed during migration seasons in which there was at least one collision. In this regard, spring and fall were very similar, as the conditional mean was approximately eight Red Knot collisions in both seasons (Figure 4.1c). In other words, if any Red Knots collided during a particular iteration, often eight Red Knots collided. In essence, the mean number of collisions can be thought of as the product of the collision frequency (probability of at least one collision) and the conditional mean number of collisions per iteration.

In part, the explanation for the value of the conditional mean number of collisions is revealed by histograms showing the relative frequencies of each number of collisions in individual iterations (0, 1, 2, …; Figure 4.2). As expected from the results above, the most frequent outcome of single iterations was zero collisions. This occurred in approximately 99% of iterations in both seasons. (Note that the height of the first bar, for zero collisions, is truncated in Figure 4.2, so that height differences among remaining bars are clearer. Also, note that the last bar represents collisions of 20 or more Red Knots.) The second most frequent outcome of single iterations in both seasons was exactly eight Red Knot collisions. There were exactly eight collisions in approximately 2.8 of every 1,000 iterations in the spring (Figure 4.2a) and in approximately 4.5 of every 1,000 iterations in the fall on average (Figure 4.2b). The third most likely outcome was exactly seven collisions in an iteration, occurring in one of every 1,000 iterations in the spring and in 1.5 of every 1,000 iterations in the fall, on average.

a

Spring Baseline

b
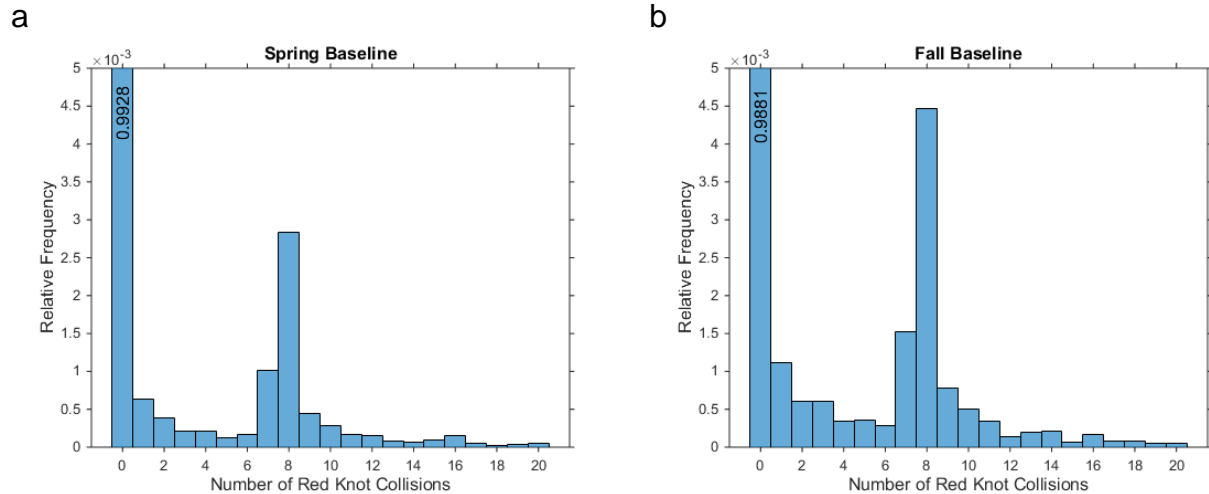
Fall Baseline

Figure 4.2 Histograms showing relative frequencies of number of collisions in single iterations across 10 simulations of 100,000 iterations each of the baseline model.

Separate results are shown for (a) spring and (b) fall iterations. In each panel, the Y-axis and the zero collision bars are truncated because the height of the zero collision bar would otherwise dwarf all other bars. Numbers within the zero bars indicate the relative frequency.

Examination of the structures involved in collisions (Figure 4.3) provides further explanation of why the number of collisions is most often seven or eight during iterations containing at least one collision. Note that due to the method of storing simulation output, collisions with the nacelle and any additional collisions that might have occurred with the rotor were combined, and were not separable in later analysis. Similarly, collisions with the portion of the tower within rotor-swept heights were combined with any additional collisions with the rotor, and the two were not separable later. These categories are labelled "Nacelle+Rotor" and "Tower+Rotor", respectively, in Figure 4.3. The category labelled "Rotor" includes all rotor collisions above hub height, as well as collisions below hub height in those cases where there were no concurrent collisions with the nacelle or tower (that is, when the flock passed through the rotor to either side of the tower). The category labelled "Tower" includes only those collisions with the tower below rotor-swept heights. The Tower category – collisions with the lower part of the tower – accounts for a high proportion of all collisions, approximately 48% in the spring (Figure 4.3a) and approximately 44% in the fall (Figure 4.3b). Collisions with the rotor alone were far less frequent, approximately 4% of all collisions in the spring (Figure 4.3a) and 6% of all collisions in the fall (Figure 4.3b). Given these results and the generally low probabilities of rotor collisions, whether with active rotors (Figure 3.22) or stationary rotors (Figures 3.25-3.27), we conclude that most of the collisions in the "Nacelle+Rotor" and "Tower+Rotor" categories were due to the nacelle and tower, respectively. Therefore, the tower almost certainly accounts for the majority of collisions.
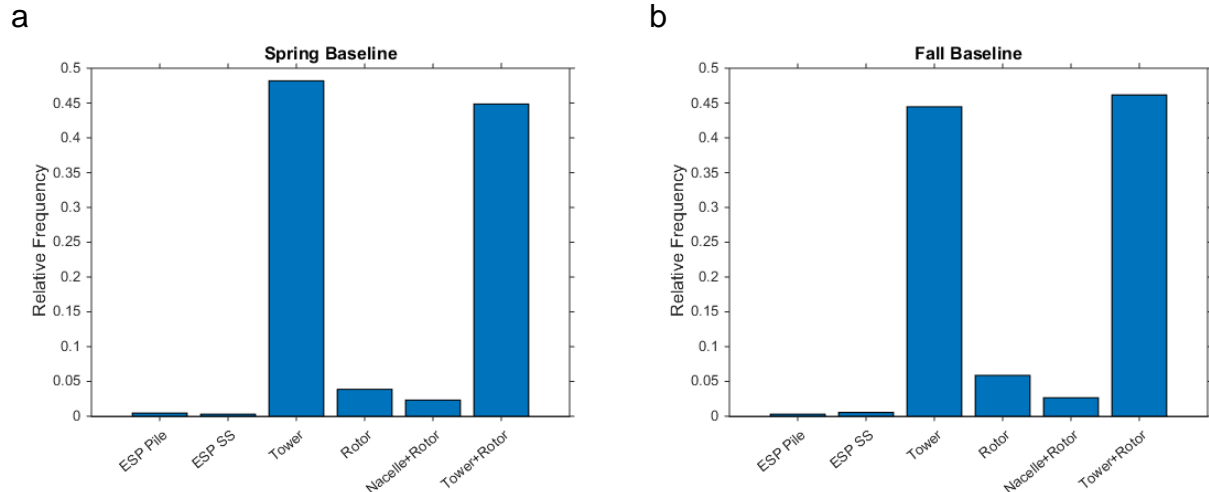
Figure 4.3 Bar charts showing relative frequencies of number of collisions with different components of turbines and the Electrical Service Platform (ESP).

Relative frequencies of collisions are from 10 repeated simulations (each consisting of 100,000 iterations) under baseline conditions in (a) spring and (b) fall. "Tower" indicates collisions with the tower beneath rotor-swept heights. "Tower+Rotor" indicates collisions with the tower within the lower half of the rotor-swept zone and concurrent collisions with the rotor in the same zone. Collisions with the ESP are subdivided into collisions with the piles ("ESP Pile") and collisions with the superstructure ("ESP SS"; see text for additional explanation).

Considering the fact that most of the collisions occurred with the tower rather than the rotor (Figure 4.3), together with the result that when any collisions occurred during an iteration, there were usually seven or eight collisions (Figure 4.2); the most common collision result can be understood as the collision of a Red Knot flock with a pole that has a diameter of seven or eight Red Knots, as depicted in Figure 3.9, as Red Knots were represented with 0.54-m wing spans and aligned wingtip to wingtip in flocks. It is also important to consider that the modal altitude of the low-altitude (poor weather) flight distribution placed most flocks near the water's surface, or below rotor height, where collisions with the relatively wide portion of the turbine towers represented the only collision risk other than the ESP. For example, a flock flying 8.0 m (26.2 ft) above the water surface (approximately the modal height assuming the baseline low-altitude flight height distributions in Figure 3.6a) that failed to avoid a turbine would encounter a tower diameter of 3.9 m (12.8 ft), equivalent to 7.2 Red Knot wing spans. Thus, eight Red Knots would likely collide with the tower (in rarer circumstances, the edge of the flock might encounter the tower such that fewer than eight individuals would collide).

As expected, Red Knots collided with the ESP less frequently than with wind turbines. The ESP accounted for less than 1% of all collisions in each season. There were more collisions with the ESP piles than with the superstructure in the spring (Figure 4.3a), while in the fall there were more collisions with the superstructure (Figure 4.3b).

Histograms of the relative numbers of collisions as a function of height (Figure 4.4) are consistent with the results described above. In each season, the highest proportion of collisions occurred near the sea surface (zero – 10 m) and the proportion generally decreased with increasing height. The exception, a slight increase in collisions in the 30 – 40 m height bin is most likely due to the additive effect of rotor collisions. The distribution of collisions as a

function of height is shifted left slightly in the spring (Figure 4.4a) compared to the fall (Figure 4.4b). That is, collisions tend to occur at slightly lower heights in the spring. The seasonal height difference likely accounts for the relative difference is collisions with the ESP components, namely, proportionally fewer collisions with the superstructure in the spring. Similarly, the height difference would account for the facts that there were relatively more collisions with the lower portion of the tower and relatively fewer collisions with the rotor alone in the spring (Figure 4.3). The most likely explanation for this difference in collision height across seasons is the seasonal difference in Red Knots' exposure to the poor weather conditions that cause them to switch to the low-altitude flight distribution. In fall, if weather conditions are poor, Red Knots most often delay their departure until favorable weather conditions occur. This element of the baseline model was based on field observations of Red Knots at migratory stopover sites, whence they are known to depart almost exclusively when there are following winds (Niles, pers. comm.). In our model, this meant that fall flights through the Facility area occurred almost exclusively during favorable weather conditions when birds were typically migrating at higher altitudes, selecting altitudes from the high-altitude flight distribution (see Figure 3.5). This high-altitude flight in fall had the effect of putting most flocks above rotor-swept altitudes during fall, where they were not exposed to any risk of collision with structures of the wind energy Facility. By contrast, during spring migration, birds passing through the Facility area were assumed to have initiated their migratory flights so far to the south, and so many hours before crossing the Facility area, that they were unable to exhibit any selectivity of weather conditions. They were stuck with whatever weather happened to be occurring in the Facility region when they got there. As a result, a greater proportion of migrating birds in the spring were exposed to poor weather conditions (see earlier discussion of headwind and precipitation thresholds) that caused them to fly close to the water's surface, selecting flight altitudes from the low-altitude distribution in our model (Figure 3.6). This seasonal difference in flight altitudes, driven by season difference in weather-related selectivity, is the most likely explanation not only for the lower collision altitudes in spring compared with fall, but also the overall higher proportion of potentially exposed birds colliding in spring compared with fall. In fall, the average total potentially exposed population size was assumed to be 1,500 birds, and the average number of fall collisions in the baseline model was 0.10 birds/fall (0.0067% of exposed birds colliding), while in spring, the average total potentially exposed population size was assumed to be 150 birds, and the average number of spring collisions in the baseline model was 0.06 birds/spring (0.04% of exposed birds colliding). In effect, the collision risk in spring was effectively six times higher for any given bird than it was in fall, but the number of potentially exposed birds was 10 times lower, resulting in an overall seasonal mean fatality rate that was only slightly lower in spring (0.06 birds/year) than it was in fall (0.10 birds/year).
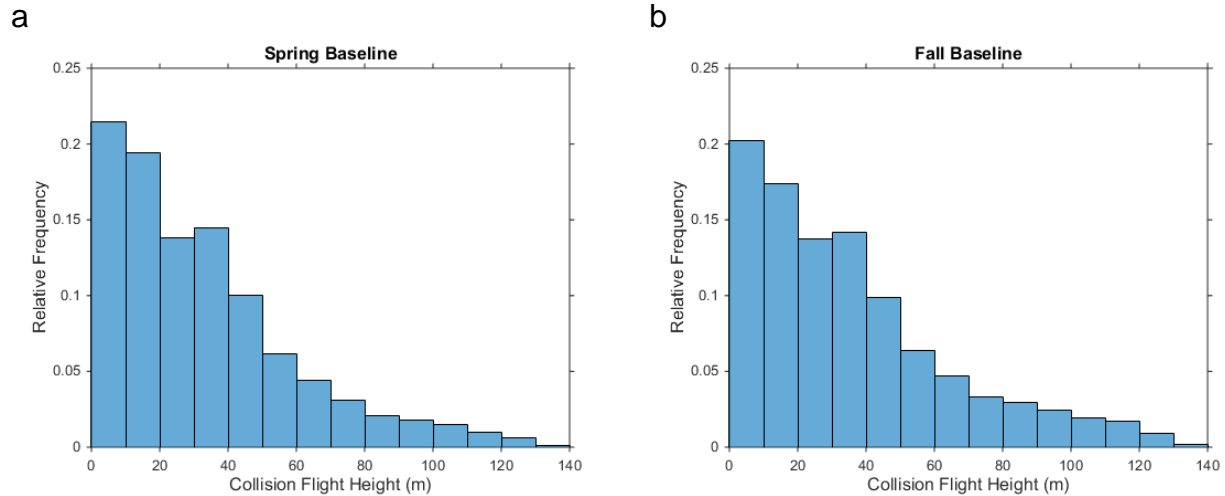
Figure 4.4 Histograms showing relative frequencies of number of collisions by height category.

Relative frequencies of number of collisions by height from 10 repeated simulations (each consisting of 100,000 iterations) under baseline conditions in (a) spring and (b) fall.

4.3   Sensitivity Analysis

In the final section of this report, we present and discuss the results of additional simulations that were performed for the purpose of examining the sensitivity of the model's outputs to variation in certain model assumptions and inputs. The primary objective of these additional simulations was to gain a more robust understanding of potential variation in Red Knot collision rates under certain alternative conditions that had been hypothesized by the Project's technical team to potentially be of interest. This section is organized by topic, with results and discussion integrated for each topic

4.3.1   Precipitation and Visibility Thresholds

Precipitation and visibility were hypothesized to increase collision risk for Red Knots, and this influence was built into our model in several ways. Visibility decreased Red Knots' ability to exhibit macro-avoidance behavior as a function of whether or not visibility levels were above a default, or baseline value of 1,000 m. When visibility was above the threshold value, macro-avoidance probability was 0.28. That is, 28% of the flocks headed for the wind energy Facility saw it from a distance as they were approaching, and made a decision to avoid flying through it altogether, thereby avoiding all collision risk. When visibility was below the threshold (i.e., under foggy conditions), macro-avoidance probability was 0.01. That is, only 1% of flocks headed for the wind farm were able to see it from a distance and avoid flying through it altogether. In order to examine the model's sensitivity to this assumption, we examined alternative visibility thresholds of 500 m and 2,000 m. Visibility conditions ought to meet the higher threshold, for instance, more frequently, so that fewer flocks would avoid the Facility and more collisions would result, while the lower threshold value should result in fewer collisions, as the Red Knots' ability to see and avoid the wind farm from a distance is maintained over a larger range of visibility conditions.

Precipitation was also hypothesized to influence Red Knots' ability to see and avoid the wind energy Facility from a distance (macro-avoidance), and it was also hypothesized to affect the birds' choice of flight altitudes. Under the baseline condition in our model, if precipitation exceeded a threshold value of 2.5 mm/hr, Red Knots were subject to the same low macro-avoidance probability as under low visibility conditions (0.01), while they enjoyed the same high macro-avoidance probability (0.28) when precipitation was below the threshold value. The same baseline threshold value of 2.5 mm/hr precipitation was used to "switch" Red Knots between the high-altitude flight distribution (Figure 3.5) and the low-altitude flight distribution (Figure 3.6), based on the hypothesis that the birds were likely to fly low, tending to hug the water's surface, during stormy conditions. In order to examine the sensitivity of model outputs to variation in Red Knots' sensitivity to precipitation, we also examined alternative precipitation thresholds of 1.0 mm/hr and 4.0 mm/hr for both behavioral switches. Precipitation conditions ought to meet the lower threshold more frequently, such that fewer flocks would avoid the Facility and more flocks would fly at lower altitudes. Both of these circumstances would result in more collisions. By contrast, applying the higher threshold value would have the effect of reducing collisions by increasing the birds' ability to exhibit macro-avoidance behaviors as well as their tendency to remain at high migratory flight altitudes.

We explored the sensitivity of the fatality rate to variation in visibility and precipitation thresholds by conducting a set of additional simulations using a fully factorial combination of the alternative threshold values for these behavioral switch thresholds described above. That is, we conducted a set of 10 simulations, each consisting of 100,000 model iterations, with each unique combination of the three visibility threshold values (500 m; 1,000 m; 2,000 m) and the three precipitation threshold values (1.0 mm/hr, 2.5 mm/hr, 4.0 mm/hr). The results of these simulations are shown in Figure 4.5. Contrary to expectations, changing the precipitation and visibility thresholds had very little effect on mean number of collisions (Figure 4.5) in either spring or fall. Bar heights in Figure 4.5 generally increased with increases in the visibility threshold, as expected (except in spring when the precipitation threshold was 1.0 mm/hr). However, these increases were very small, particularly in relation to the simulation standard deviation. Similarly, mean collision probability decreased slightly with increases in the precipitation threshold in the fall (Figure 4.5b) as expected, but not in the spring (Figure 4.5a). Again, in both seasons, the variation in mean collision probability with precipitation threshold was small in comparison to the simulation variation.

a

b
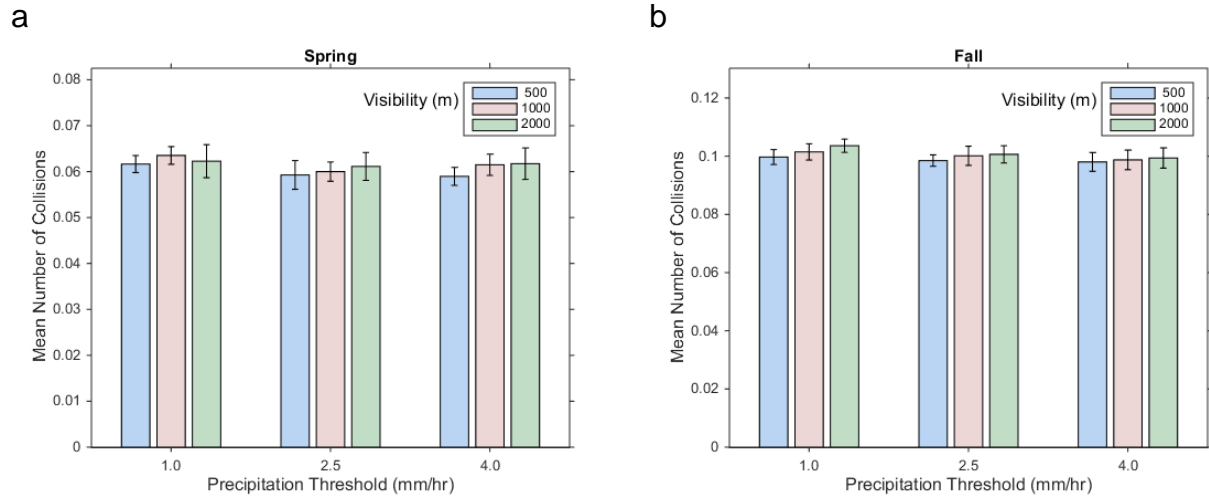
Figure 4.5 Bar plots showing the mean number of Red Knot collisions as a function of precipitation threshold and visibility threshold.

Bar plots showing (a) spring and (b) fall. Baseline conditions were precipitation threshold = 2.5 mm/hr, and visibility threshold = 1,000 m. Bar height represents the grand mean of 10 repeated simulations that were performed for each unique combination of threshold values, each with a unique random number seed, and each simulation representing 100,000 iterations. Error bars indicate ± one standard deviation, based on the 10 repetitions.

The most likely explanation for the insensitivity of the model's outputs to variation in visibility and precipitation thresholds is the rarity of triggering events, as defined by the empirical weather data analyzed for the Facility site over the migration date ranges of interest. Heavy precipitation, as defined by our threshold values occurred less than 3% of the time, even for the lowest alternative threshold value of 1.0 mm/hr (Figure 3.12c, d), infrequent enough that even relatively large behavioral responses to these rare events did not exert a strong impact on the overall number of collisions. Low-visibility conditions were also relatively infrequent, though not as rare as high-precipitation conditions (Figure 3.12a, b). In fall, the visibility threshold was crossed between approximately 2% and 5% of the time, depending on the threshold value, while in spring, the visibility threshold was crossed between approximately 8% and 17% of the time, depending on the threshold value (Figure 3.12). The relative rarity of the precipitation and visibility threshold triggering events in the Facility area during the migratory seasons of interest is further illustrated in Figure 4.6, which shows separate event frequencies for birds flying at all altitudes, and specifically for birds flying within the altitudes of wind energy Facility structures in each season. The relative infrequency of low visibility conditions, combined with the model's relative insensitivity to variation in macro-avoidance probability (see below) had the effect of generating a relatively low sensitivity of model output (predicted fatality rates) to variation in the visibility threshold.

a

b
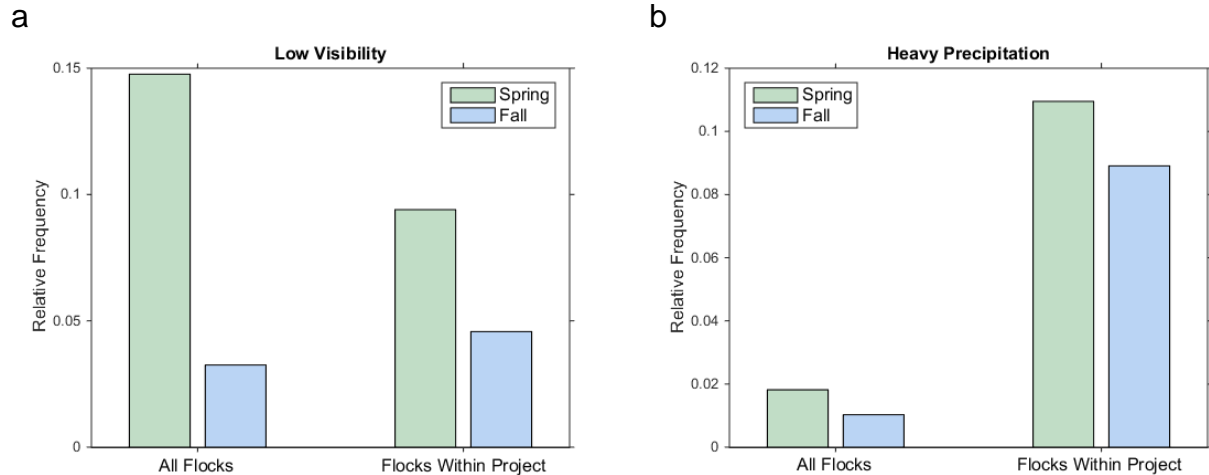
Figure 4.6 Relative frequencies of (a) low visibility and (b) heavy precipitation under baseline conditions in spring and fall.

Relative frequencies are shown separately for all flocks flying directly above the Facility at all heights and for flocks flying through the Facility within turbine heights. Results from the 10 repeated baseline simulations for each season were pooled; each simulation represented 100,000 iterations.

4.3.2   Flight Altitude Distribution

Flight altitudes were hypothesized to affect Red Knot collision probabilities by influencing the number of birds flying through the Facility area at the heights of wind energy Facility structures with which they could potentially collide. The model employed two fundamental migratory flight altitude distributions, a high-altitude distribution that Red Knots adopted when weather conditions were favorable and a low-altitude distribution adopted under less favorable conditions. The high-altitude distributions were uniform distributions, with a baseline mean altitude of 1,000 m, and the low-altitude distributions were Gamma distributions with a baseline mean value of 19.5 m (64.0 ft). These baseline values and the types of distributions were selected by the Project's technical team to represent realistic hypotheses of the migratory flight heights of Red Knots under different weather conditions, as indicated by best available scientific information. In order to explore the model's sensitivity to variation in these distributions, we conducted a set of additional simulations with alternative mean flight altitude values for each of these distributions, as follows: we explored alternative with high-altitude mean values of 500 m and 2,000 m, and we explored alternative low-altitude means of 13.5, 24.0, and 33.8 m (44.3, 78.7, and 1,11 ft). We explored these alternatives by conducting 10 simulations of 100,000 iterations each, with each of these alternative mean values, and the results of these simulations are presented in Figure 4.7.
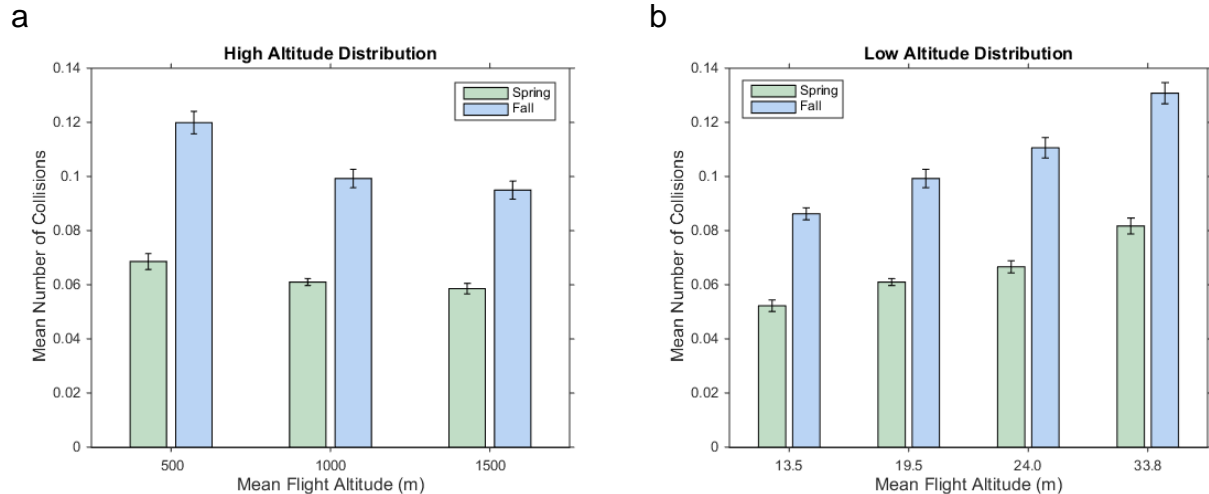
Figure 4.7 Bar plots showing the mean number of Red Knot collisions in spring and fall as a function of (a) high flight altitude distribution and (b) low flight altitude distribution.

Baseline conditions corresponded to high-altitude distribution with mean = 1,000 m, and low-altitude distribution with mean = 19.5 m. Bar height represents the grand mean of 10 repeated simulations, each with a unique random number seed, and each simulation representing 100,000 iterations. Error bars indicate ± one standard deviation, based on the 10 repetitions.

The mean number of Red Knot collisions decreased with increasing mean of high-altitude distribution (Figure4.7a), as expected, since these increasing means corresponded with fewer Red Knot flights within turbine heights (Table 3.2, Figure 3.5). The mean number of collisions was more sensitive to differences in the high-altitude distribution in the fall than in the spring. For instance, in the fall the mean number of collisions was approximately 20% higher at the lowest distribution (mean = 500 m) than at the baseline distribution, while in the spring the relative increase was approximately 12%. One potential explanation for this pattern is that most of the spring fatalities occur under the low flight altitude distribution, as migrating birds in the spring cannot select favorable weather conditions for crossing the Facility because they are crossing the Facility after a very long northward flight. By contrast, in fall, birds cross the Facility area only an hour after their departure from land; hence, they are able to delay their departure under the poor weather conditions that would otherwise force them into the low-altitude distribution. For this reason, a relatively small proportion of migrating birds in the fall are subject to the low-altitude distribution compared to migrating birds in the spring. Most of the spring collisions are occurring during poor weather or low-altitude flights, and the spring fatality rate is relatively insensitive to changes in the high-altitude distribution, as this affects a very small number of birds.

By contrast, fatality rates in both seasons were sensitive to variation in the low-altitude flight distribution (Figure 4.7b). This result was expected, as most of the collisions in both seasons occurred while birds were flying in the adverse weather conditions that caused them to hug the water's surface. Conversely, under favorable weather conditions in both seasons, the vast majority of birds migrated at altitudes well above the rotor-swept zone of the turbines, where collision risk was zero. One implication of this sensitivity is that obtaining accurate information

on the migratory flight altitudes of Red Knots under adverse weather conditions is important for generating accurate Red Knot fatality rate predictions at offshore wind energy facilities.

4.3.3 Adjustment of Band Collision Probability at Non-Perpendicular Approach Angles

Our model included an experimental adjustment to the basic geometry of collision risk as incorporated into the Band (2012) model, enabling us to relax the Band model's assumption that the angle of approach is always perpendicular to the rotor. We relaxed this assumption by increasing the odds ratio of collisions for non-perpendicular approach angles, as determined by the orientation of the birds' flight, taken from the migratory flight direction distributions (Figures 3.3, 3.4) and the wind direction, taken from empirical weather data summaries compiled for the Facility region for the migratory seasons of interest (Figure 3.11). The odds ratio is the component of the Band model that drives the likelihood of collision when the defined conditions are met. For each of the alternative odds ratios we explored, we conducted 10 simulations, each consisting of 100,000 iterations of the model. The results of these simulations are presented in Figure 4.8.

a

b
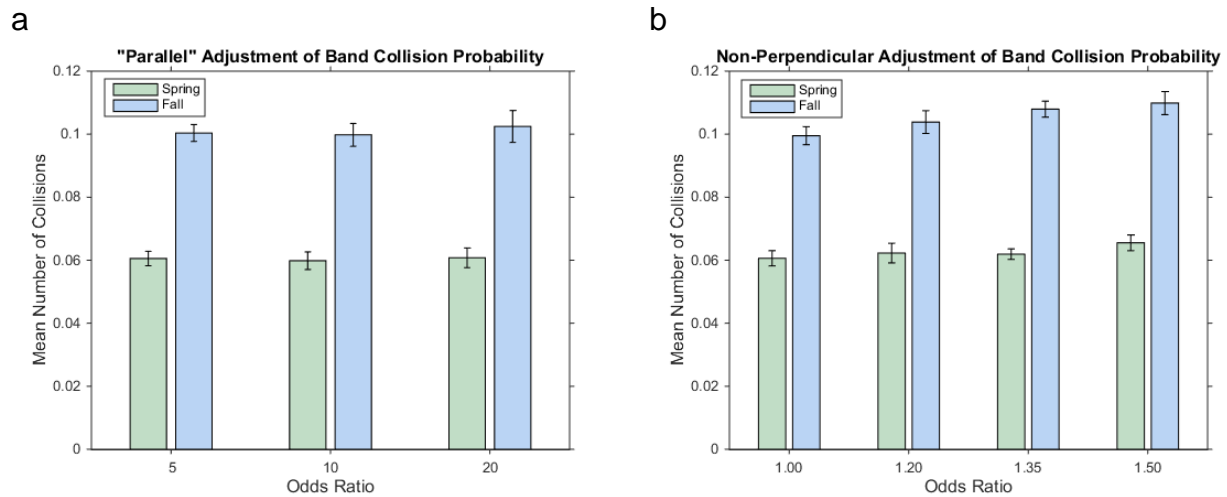
Figure 4.8 Bar plots showing the mean number of Red Knot collisions in spring and fall as a function of adjustments to Band model collision probabilities for approach angles.

Approach angles are (a) less than 25° and (b) 25° − 90°. Baseline conditions were odds ratio = 5 in (a) and odds ratio = 1 in (b). Bar height represents the grand mean of 10 repeated simulations, each with a unique random number seed, and each simulation representing 100,000 iterations. Error bars indicate ± one standard deviation, based on the 10 repetitions. Parallel and non-perpendicular adjustments reflect conditions of near-parallel, and near-perpendicular approach angles, respectively (see text).

We made two separate adjustments to the collision probabilities for active rotors to account for approach angles (between bird flight lines and the rotor plane) other than the perpendicular approach assumed by the Band (2012) model. The first adjustment was for near-parallel approaches, that is all approach angles less than 25°. For such angles, the baseline odds ratio was 5, and we also explored alternative odds ratios of 10 and 20 (Figure 3.23a). This adjustment had negligible effect on mean number of Red Knot collisions (Figure 4.8a). There were very slight increases in number of collisions at higher odds ratios, but these increases were barely

discernible in comparison to simulation variation. This result is likely due to the rarity of rotor encounters at such small approach angles. The probability of encountering a rotor is much reduced as approach angles near the parallel such that even very large increases in the collision risk have very little effect on numbers of collisions. Furthermore, as noted above, most collisions involved the turbine tower rather than the rotor, particularly in the spring.

The second adjustment applied to less shallow angles of approach, that is, all angles greater than 25° including perpendicular approach. Under baseline conditions, no adjustment was applied (odds ratio = 1). We explored alternative odds ratios of 1.20, 1.35, and 1.50 (Figure 3.23b). The mean number of collisions increased with increasing odds ratios (Figure 4.8b) as expected, particularly in the fall. Under an odds ratio of 1.50, the number of collisions was approximately 10% higher than under baseline (0.11 collisions vs. 0.10 collisions in the fall). These results indicate that relaxing the Band (2012) model's assumption of perpendicular approach angles does affect the model's predictions, though this affect is marginal for modeled scenarios where collisions with turbine rotors are very rare (e.g., spring migration).

4.3.4   Headwind Threshold

Our model incorporated two types of behavioral threshold responses of birds to effective headwinds. First, birds switched between high-altitude and low-altitude flight distributions depending on effective headwinds. With effective headwinds underneath the threshold, birds migrated using the high-altitude flight distribution (Figure 3.5). When effective headwinds were over the threshold, birds migrated using the low-altitude flight distribution (Figure 3.6), reflecting their tendency to hug the water's surface under such conditions. The second behavioral threshold related to effective headwind speed reflected Red Knot's tendency to delay migratory flight departures until there are following winds. This threshold was applied in our model only during the fall season, as this was the only season in which birds' crossings of the Facility area occur very soon after their departure from land. We conducted additional simulations to explore the model's sensitivity to variation in these thresholds, performing 10 additional simulations consisting of 100,000 iterations each, for a set of 27 alternative scenarios, consisting of a fully factorial combination of three different threshold values for the altitude switch, three different threshold values for the fall departure delay decision, and three different values for the proportion of flocks that delayed their departure when the threshold was crossed. The results of these simulations are presented in Figure 4.9.

a

b

c
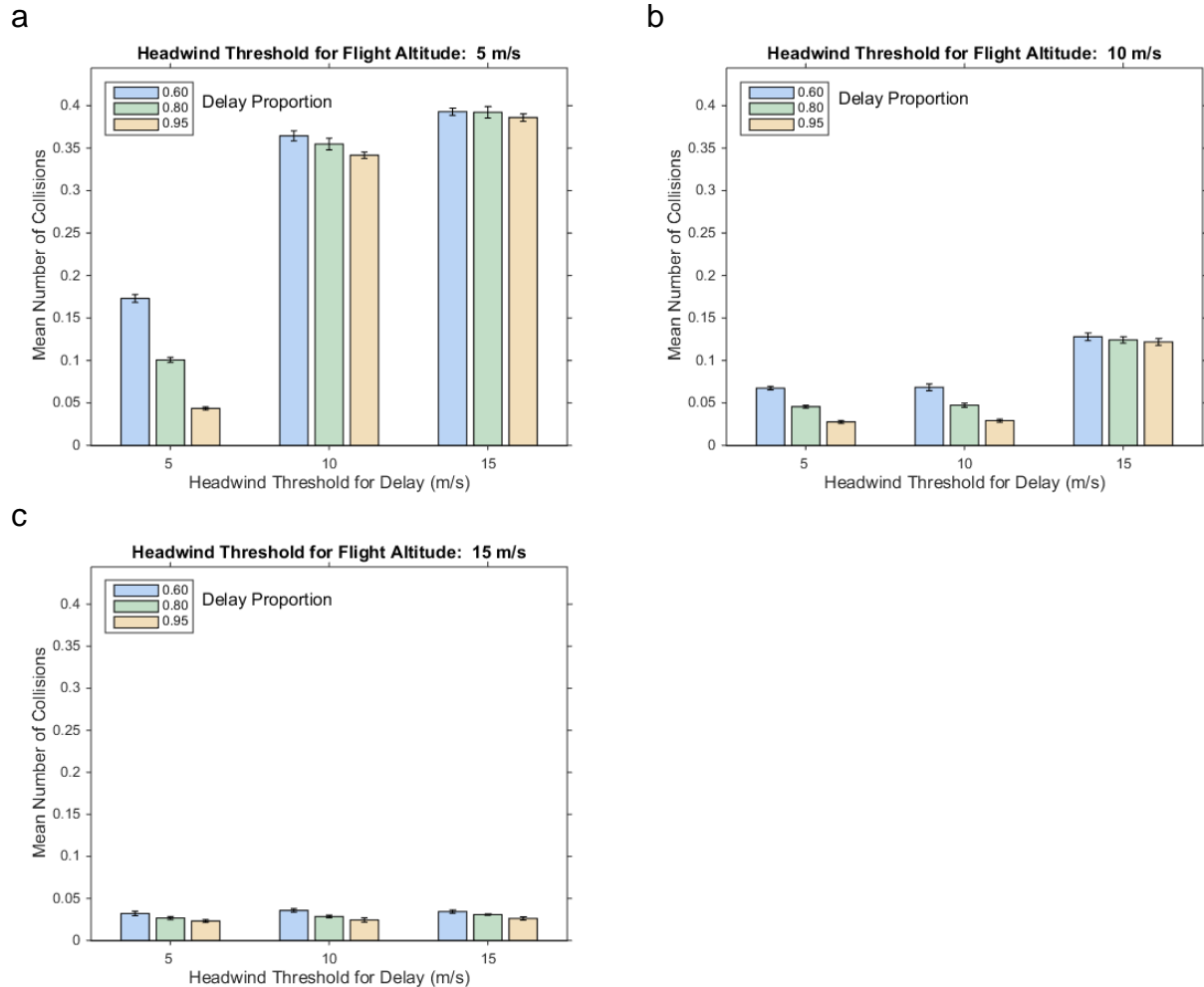
Figure 4.9 Bar plots showing the mean number of Red Knot collisions in fall as a function of the proportion of delay sensitive flocks, the headwind threshold for fall departure delay, and the headwind threshold for flight altitude switches.

The proportion of delay sensitive flocks is 0.60, 0.80, or 0.95; the headwind threshold for fall departure delay is 5.0 m/s, 10 m/s, or 15 m/s; and the headwind threshold for flight altitude switches is 5.0 m/s, 10 m/s, or 15 m/s. Baseline conditions were 5.0 m/s for both headwind thresholds and delay proportion = 0.8. Bar height represents the grand mean of 10 repeated simulations, each with a unique random number seed, and each simulation representing 100,000 iterations. Error bars indicate ± one standard deviation, based on the 10 repetitions.

These simulations illustrate two primary areas of sensitivity. The most pronounced of these is the model's sensitivity to variation in the delay threshold when the delay threshold value was above the altitudinal switch threshold value. This impact is shown in Figure 4.9a, reflected in the large difference in the height of the bars for the 10 m/s and 15 m/s delay thresholds compared to the 5.0 m/s delay threshold when the altitude switch threshold was 5.0 m/s. The most likely underlying explanation for this pattern is that when the delay threshold was the same as, or below the altitude switch threshold, then the birds were only tending to fly under favorable conditions. When the headwinds were strong enough to cause birds to fly low, most birds were staying put. By contrast, if the delay threshold was above the altitude switch threshold, then there was a non-trivial set of headwind conditions under which the birds made the decision to depart,

76

but the headwinds were still strong enough to cause the migrating birds to fly low, bringing them into increased contact with the structures of the Facility. This was the only combination of conditions that caused a large proportion of migrating birds in the fall to fly at lower altitudes, and therefore it resulted in significantly higher fatality rates.

The other primary area of sensitivity reflected in Figure 4.9 was the sensitivity of the model to delay proportion when the departure threshold was less than or equal to the flight altitude switch threshold. Under such conditions, as described above, birds were only tending to fly using their high-altitude distributions, and relatively few birds were exposed to potential conditions. Under these conditions, adjusting the proportion of birds that made the delay decision had a significant impact because that was the only way to cause more birds to depart under the headwind conditions that caused them to fly at lower altitudes.

Finally, we note with respect to effective headwind thresholds, that the frequency of threshold crossing conditions is an important factor driving the sensitivity of modeled fatality rates to these thresholds. Whereas threshold crossing events for heavy precipitation and low visibility were relatively rare events (always affecting below 12% of flocks within turbine height, sometimes below 5%; Figure 3.12), threshold crossing conditions for effective headwinds were not uncommon in both spring and fall seasons (affecting up to 64% of flocks; Figure 4.10). For this reason, adjustments in the effective headwind threshold affected a larger proportion of the flocks in most simulations, and this threshold exerted a more important influence on modeled fatality rates.
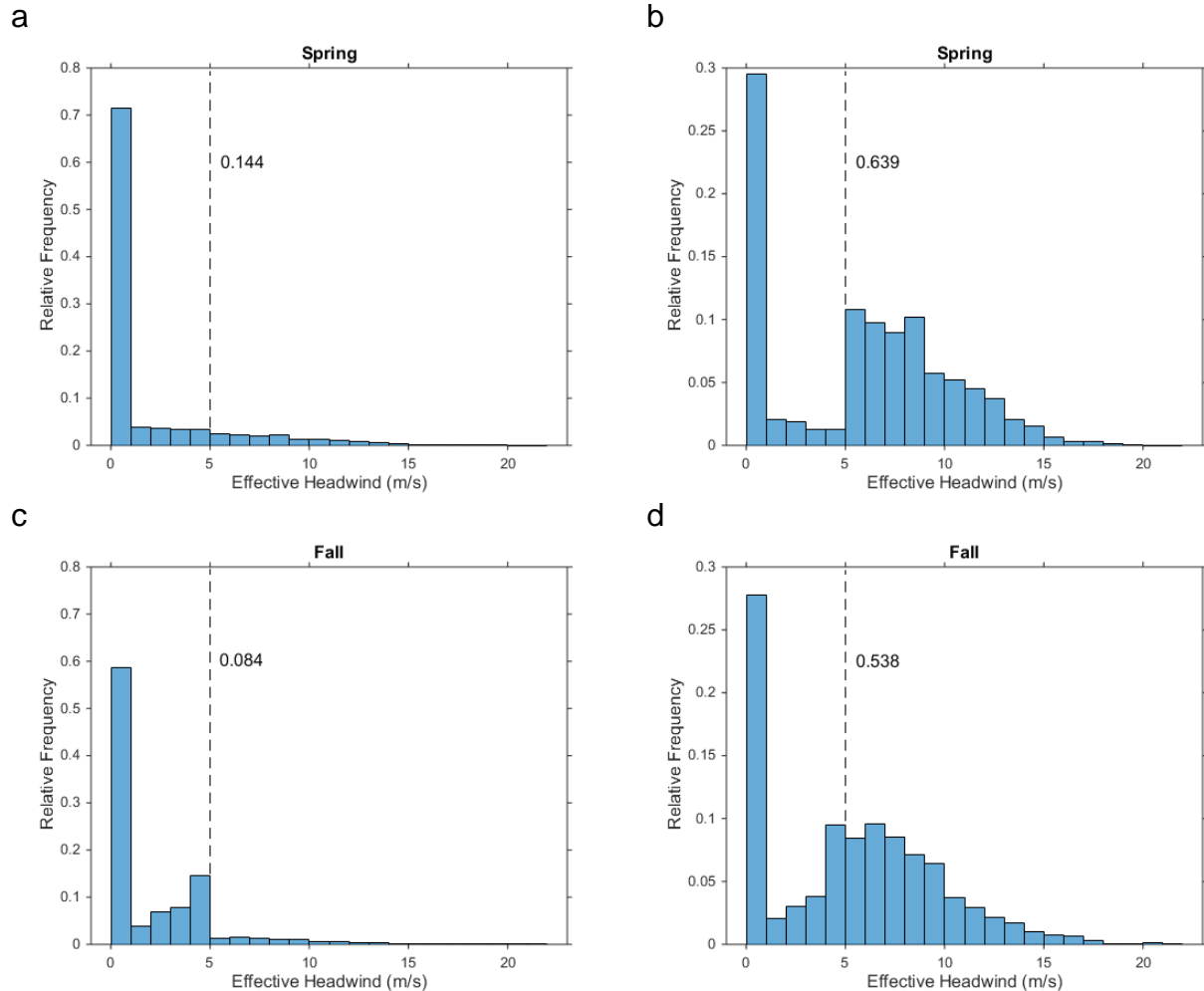
Figure 4.10 Histograms showing relative frequencies of effective headwinds experienced by flocks under baseline conditions.

Relative frequencies shown for flocks (a) in spring for all flocks flying directly above the Facility at all heights, (b) in spring for flocks flying through the Facility within turbine heights, (c) in fall for all flocks flying directly above the Facility at all heights, and (d) in fall for flocks flying through the Facility within turbine heights. Note that Y-axis limits are the same for (a) and (c), and the same for (b) and (d). The dashed vertical lines represent the 5.0 m/s headwind threshold for choice of altitude distribution in both seasons, and the threshold for departure delay in the fall. The value to the right of each vertical line indicates the proportion of observations that exceeded the threshold. Results from the 10 repeated baseline simulations for each season were pooled for histogram calculations; each simulation represented 100,000 iterations.

4.3.5   Population Size

Our sensitivity analysis related to population size was targeted at predicting fatality levels under a "recovered" population scenario, in which the overall population of rufa Red Knots recovers to three times its current level, as envisioned by the USFWS in the listing decision (USFWS 2014a, 2014b). To explore this scenario, we conducted 100 simulations, each consisting of 100,000 iterations, for each of four population scenarios (fall current, fall recovered, spring current, spring recovered). For each simulation, the population size was drawn at random from the corresponding population size distribution (Figure 3.1). For these simulations, we assumed that

78

population recovery was random with respect to individuals' chances of migrating through the Facility area (i.e., recovery was uniform with respect to long-distance and short-distance migratory population segments). Results of these simulations illustrate the simple result that the mean number of collisions scales linearly with population size (Figure 4.11). A tripling of population size led to a tripling of the number of collisions, in both seasons, as expected. Assuming all other model inputs held at baseline values, recovered exposed population sizes of 450 Red Knots in spring and 4,500 in fall lead to predicted fatality rates of 0.18 and 0.3 collisions/season, respectively, or 0.48 total collisions per year.
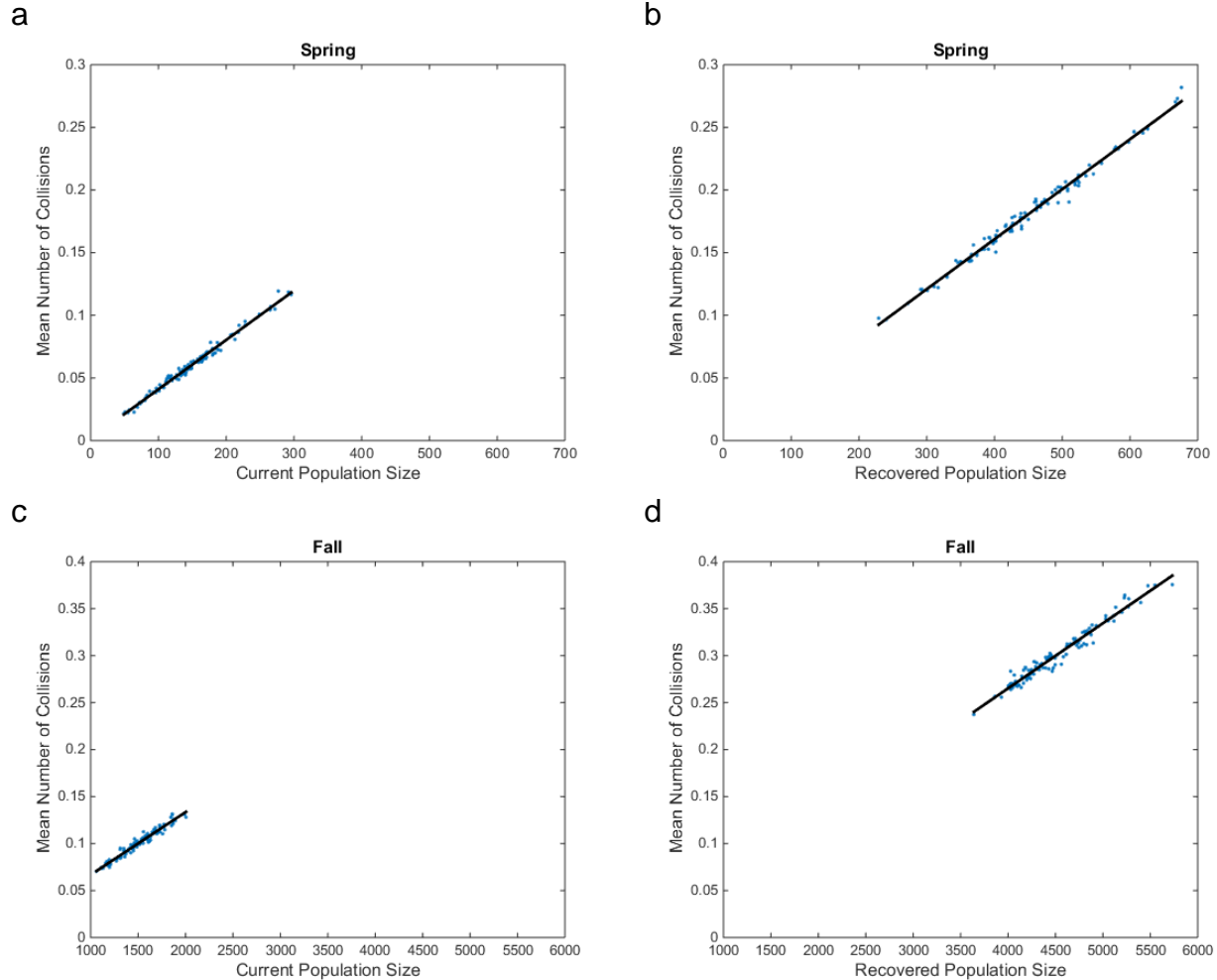
Figure 4.11 Mean number of collisions as a function of population size by season and population status (current or recovered).

Each blue dot represents one simulation consisting of 100,000 iterations, at a population size randomly drawn from the distributions shown in Figure 3.1. In each panel there are 100 blue dots, for 100 simulations each at a random population size generated from the appropriate distribution. Black lines represent ordinary least squares fits: (a) spring, current population size; (b) spring, recovered population size; (c) fall, current population size; (d) fall, recovered population size. Note that axis limits are the same within each row, but different between rows.

4.3.6   Avoidance Probability

Previous studies have indicated that bird collision risk at offshore wind energy facilities is highly sensitive to avoidance probabilities (Chamberlain et al. 2006; Cook et al. 2012, 2014); hence, we incorporated Red Knots' avoidance behaviors within our model with a high degree of biological realism, and we focused significant attention on responses of model outputs to variation in a variety of different avoidance assumptions during our sensitivity analysis.

We assumed that Red Knot avoidance would operate hierarchically, first at the level of the Facility (macro-avoidance) and then at the turbine (or ESP) level (micro-avoidance). The latter was further sub-divided into active rotor and stationary structure avoidance. In each of these three cases, we assumed separate baseline probability values under favorable and unfavorable weather conditions (Table 3.3). To characterize the model's sensitivity to variation in these six baseline avoidance probabilities, we represented them in our model, not as fixed parameter values, but as parameter values selected from distributions (Figure 3.7). For each of these six avoidance parameters, we conducted 100 simulations, each consisting of 100,000 iterations of the model, using a randomly generated parameter value selected from the corresponding distribution (Figure 3.7). Results of these simulations are illustrated in Figures 4.12 (spring) and 4.13 (fall).

Several patterns of note relating to the model's sensitivity to avoidance probabilities are apparent in the results of these simulations. We divide our discussion of these patterns into two subsections, corresponding to the two different types of avoidance represented in the model (macro-avoidance and micro-avoidance).

a

b

c

d

e

f
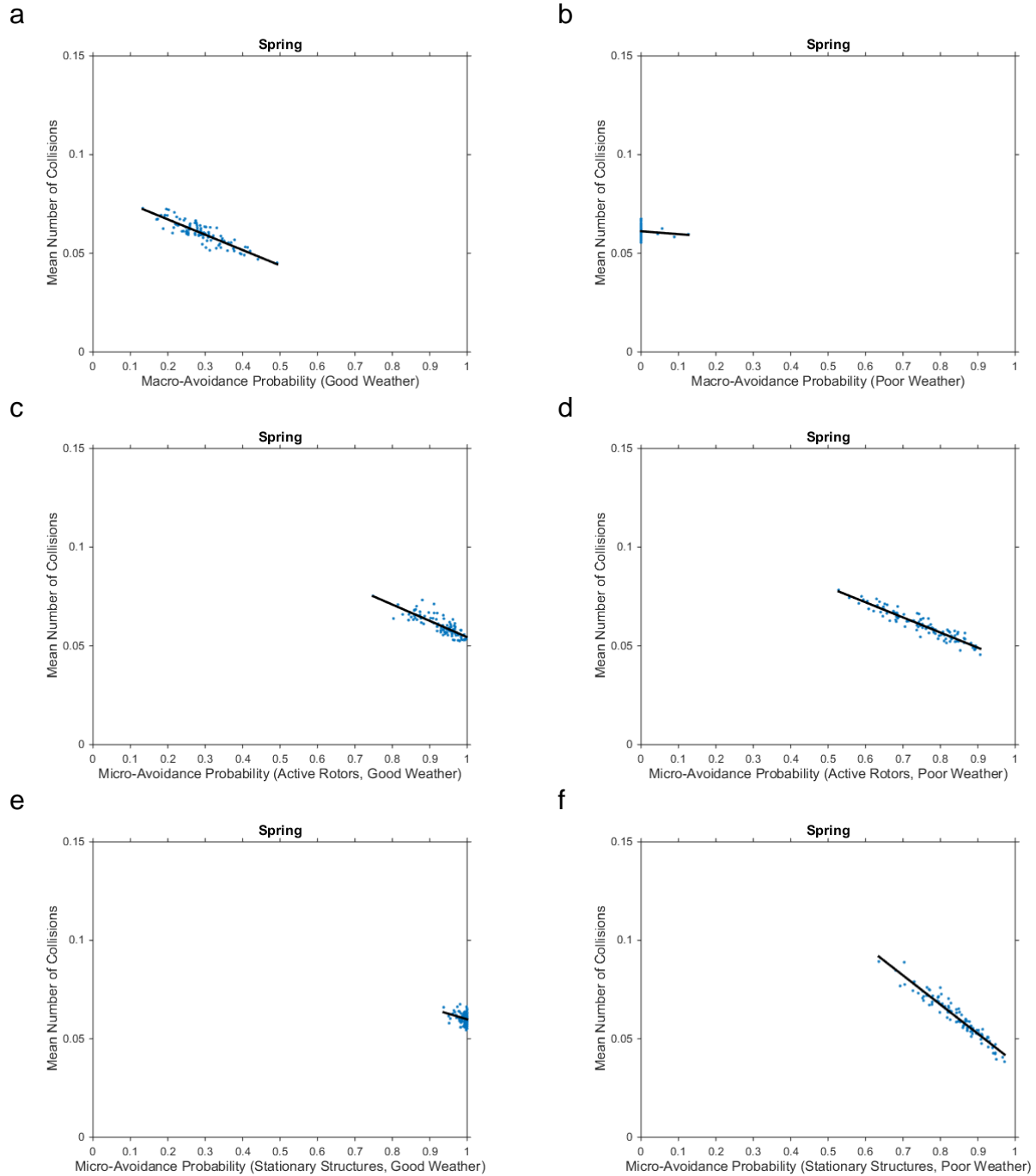
Figure 4.12 Mean number of collisions in the spring as a function of avoidance probability.

Avoidance probabilities shown for (a) the Facility (macro-avoidance) in good weather, (b) the Facility (macro-avoidance) in poor weather, (c) active rotors (micro-avoidance) in good weather, (d) active rotors (micro-avoidance) in poor weather, (e) stationary structures (micro-avoidance) in good weather, and (f) stationary structures (micro-avoidance) in poor weather. Each blue dot represents one simulation consisting of 100,000 iterations, at a randomly generated avoidance probability drawn from the distributions in Figure 3.7. In each panel there are 100 blue dots, for 100 simulations each at a random probability generated from the appropriate distribution in Figure 3.7. Black lines represent ordinary least squares fits.

81
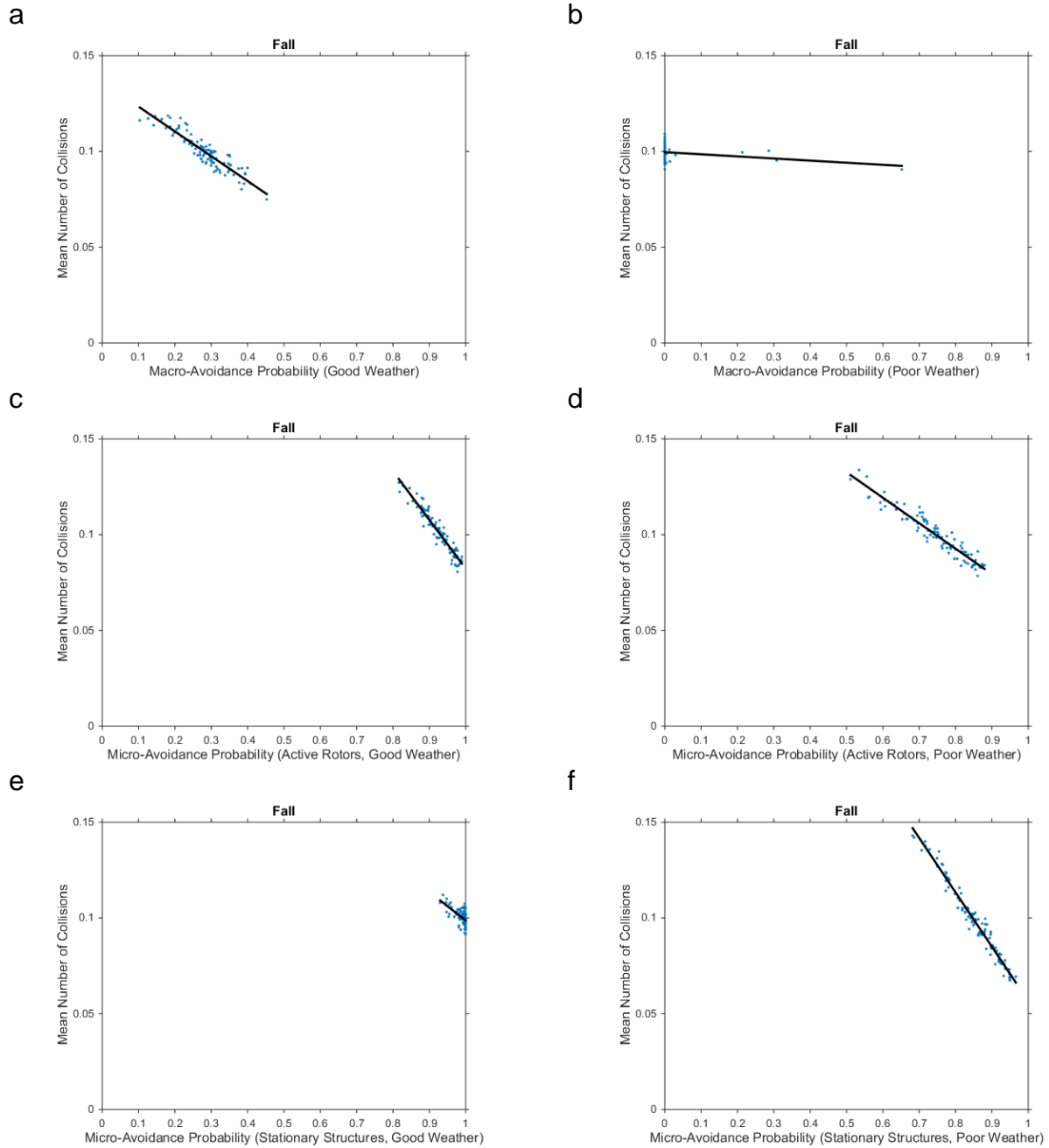
Figure 4.13 Mean number of collisions in the fall as a function of avoidance probability.

Avoidance probability shown for (a) the Facility (macro-avoidance) in good weather, (b) the Facility (macro-avoidance) in poor weather, (c) active rotors (micro-avoidance) in good weather, (d) active rotors (micro-avoidance) in poor weather, (e) stationary structures (micro-avoidance) in good weather, and (f) stationary structures (micro-avoidance) in poor weather. Each blue dot represents one simulation consisting of 100,000 iterations, at a randomly generated avoidance probability. In each panel there are 100 blue dots, for 100 simulations each at a random probability generated from the appropriate distribution in Figure 3.7. Black lines represent ordinary least squares fits.

Sensitivity to Macro-Avoidance

The first pattern of note with respect to macro-avoidance is that the model was relatively insensitive to variation in the macro-avoidance parameter under poor-weather conditions in both seasons (Figures 4.12b, 4.13b). This is a simple function of the fact that macro-avoidance behaviors were negligible under such conditions in both seasons. In poor weather, birds were assumed not to be able to exhibit macro-avoidance behavior. In favorable weather, when birds' ability to perceive and avoid the entire Facility from a distance was assumed to be non-trivial (mean of 0.28 macro-avoidance probability), variation in macro-avoidance probabilities had moderate impact on mean collision rates, particularly in fall (Figures 4.12a, 4.13b). This result is understandable, given that macro-avoidance behaviors result in the complete elimination of collision risk for the birds exhibiting such behaviors, and it underscores the importance of understanding the occurrence of such behaviors in nature.

Sensitivity to Micro-Avoidance

In general, our simulations revealed a moderate to high degree of sensitivity of predicted fatality rates to variation in micro-avoidance parameters, as expected (Figures 4.12, 4.13). This sensitivity was notable under all simulated conditions from which the sampled parameter value distributions contained a reasonable degree of parameter value variation (we note that for micro-avoidance of stationary structures under good weather conditions, the sampled parameter value distributions were very concentrated, representing the assumption that micro-avoidance probabilities under such conditions were relatively invariant and uniformly high). One pattern evident in our results is that the fatality rates were more sensitive to variation in micro-avoidance probabilities for stationary structures than for active rotors in both seasons. The most likely explanation for this result is that the overall fatality patterns were largely driven by collisions with stationary structures, as shown in Figure 4.3 and discussed previously. Another pattern of note in our results is that sensitivity to variation in micro-avoidance parameters was higher in fall than in spring. The most likely explanation for this result is that a higher proportion of fatalities occurred under favorable weather conditions in fall than in spring, owing to the birds' ability to delay migratory departures under poor weather conditions in the fall season only. Under favorable weather conditions, micro-avoidance behaviors were a more important driver of collision rate outcomes, as micro-avoidance probabilities were assumed to be reduced under poor weather conditions. The overall high sensitivity of collision rates to micro-avoidance probabilities indicates that further characterization of birds' micro-avoidance behaviors in nature can potentially yield important improvements to our ability to accurately model and predict birds' collision rates at wind energy facilities.

5.   References

Alerstam, T., G. A. Gudmundsson, P. E. Jonsson, J. Karlsson, and A. Lindstrom. 1990. Orientation, Migration Routes and Flight Behaviour of Knots, Turnstones and Brant Geese Departing from Iceland in Spring. Arctic 43(3): 201-214.

Alerstam, T., M. Rosén, J. Bäckman, P. G. P. Ericson, and O. Hellgren. 2007. Flight Speeds among Bird Species: Allometric and Phylogenetic Effects. PLOS Biology 5: 1656-1662 Protocol S1.

Bailey, B. H., S. L. McDonald, D. W. Bernadett, M. J. Markus, and K. V. Elsholz. 1997. Wind Resource Assessment Handbook: Fundamentals for Conducting a Successful Monitoring Program. Prepared by AWS Scientific, Inc. for National Renewable Energy Laboratory.

Baker, A., P. Gonzalez, R. I. G. Morrison, and B. A. Harrington. 2013. Red Knot (*Calidris canutus*). A. Poole, ed. The Birds of North America Online. Cornell Lab of Ornithology. Ithaca, New York. Retrieved from the Birds of North America Online: http://bna.birds.cornell.edu.bnaproxy.birds.cornell.edu/bna/species/563; doi:10.2173/bna.563

Band, W. 2000. Calculating a Theoretical Collision Risk Assuming No Avoiding Action. Guidance Notes Series. Scottish Natural Heritage.

Band, W. 2012. Using a Collision Risk Model to Assess Bird Collision Risks for Offshore Windfarms. Strategic Ornithological Support Services (SOSS), The Crown Estate, London, United Kingdom. SOSS project: www.bto.org/science/wetland-and-marine/soss/projects; Band report available online at: http://www.bto.org/sites/default/files/u28/downloads/Projects/Final_Report_SOSS02_Band1ModelGuidance.pdf

Band, W., M. Madders, and D. P. Whitfield. 2007. Developing Field and Analytical Methods to Assess Avian Collision Risk at Wind Farms. Pp. 259-275. *In*: M. J. de Lucas, G. F. E. Janss, and M. Ferrer, eds. Birds and Windfarms: Risk Assessment and Mitigation. Quercus, Madrid, Spain.

Barter, M. and D. Tonkinson. 1997. Wader Departures from Chongming Dao (near Shanghai, China) During March/April 1996. The Stilt 31(12): 17.

Bolker, E. D., J. J. Hatch, and C. Zara. 2006. Modeling Bird Passage through a Windfarm. Draft. University of Massachusetts, Boston. Available online at: www.cs.umb.edu/%7Eeb/windfarm

Bolker, E. D., J. J. Hatch, and C. Zara. 2014. Modeling How Wind Farm Geometry Affects Bird Mortality. Cornell University. Available online at: http://arxiv.org/pdf/1408.1580.pdf

Burger, J., C. Gordon, L. Niles, J. Newman, G. Forcey, and L. Vlietstra. 2011. Risk Evaluation for Federally Listed (Roseate Tern, Piping Plover) or Candidate (Red Knot) Bird Species in Offshore Waters: A First Step for Managing the Potential Impacts of Wind Facility Development on the Atlantic Outer Continental Shelf. Renewable Energy 36: 338-351.

Cape Wind Associates. 2011. Construction and Operations Plan, Cape Wind Energy Project, Nantucket Sound, Massachusetts.

Cape Wind Associates. 2014. Construction and Operation Plan (COP) Revision #1. Cape Wind Energy Project, Nantucket Sound, Massachusetts.

Chamberlain, D. E., M. R. Rehfisch, A. D. Fox, M. Desholm, and S. J. Anthony. 2006. The Effect of Avoidance Rates on Bird Mortality Predictions Made by Wind Turbine Collision Risk Models. Ibis 148(S1): 198-202.

Cook, A. S. C. P., E. M. Humphreys, E. A. Masden, and N. H. K. Burton. 2014. The Avoidance Rates of Collisions between Birds and Offshore Turbines. Scottish Marine and Freshwater Science. Marine Scotland Science. Vol. 5, No. 16.

Cook, A. S. C. P., A. Johnston, L. J. Wright, and N. H. K. Burton. 2012. A Review of Flight Heights and Avoidance Rates of Birds in Relation to Offshore Wind Farms. Strategic Ornithological Support Services (SOSS) Project SOSS-02. BTO Research Report Number 618. 59 pp.

Department of Energy & Climate Change. 2012. Record of the Appropriate Assessment Undertaken for Applications under Section 36 of the Electricity Act 1989. Projects: Docking Shoal Offshore Wind Farm (as amended), Race Bank Offshore Wind Farm (as amended), Dudgeon Offshore Wind Farm. December 2011. Updated June 2012. Available online at: https://www.og.decc.gov.uk/EIP/pages/projects/AAGreaterWash.pdf

Desholm, M. and J. Kahlert. 2006. A Stochastic Model Analysis of Avian Collision Risk at Wind Farms. Manuscript in PhD Thesis, M. Desholm: Wind Farm Related Mortality among Avian Migrants - A Remote Sensing Study and Model Analysis. National Environmental Research Institute, Ministry of the Environment, Denmark. Available online at: http://www2.dmu.dk/Pub/phd_mde.pdf

Drewitt, A. L. and R. H. W. Langston. 2006. Assessing the Impacts of Wind Farms on Birds. Ibis 148: 29-42.

eBird. 2014. An Online Database of Bird Distribution and Abundance (Web Application). eBird, Ithaca, New York. Accessed December 2014. Online at: http://ebird.org/content/ebird/

Eichhorn, M., K. Johst, R. Seppelt, and M. Drechsler. 2012. Model-Based Estimation of Collision Risks of Predatory Birds with Wind Turbines. Ecology and Society 17: 1.

Endangered Species Act (ESA). 1973. 16 United States Code §§ 1531-1544, Public Law 93-205, December 28, 1973, as amended, Public Law 100-478 [16 United States Code 1531 *et seq.*]; 50 Code of Federal Regulations 402.

Finn, J., J. Carlsson, T. Kelly, and J. Davenport. 2012. Avoidance of Headwinds or Exploitation of Ground Effect – Why Do Birds Fly Low? Journal of Field Ornithology 83: 192-202.

Gordon, C. E., G. Forcey, J. Newman, I. Baldwin, C. Ribe, W. Warren-Hicks, L. Vlietstra, J. L. Niles, and J. Burger. 2011. New Insights and New Tools Regarding Risk to Roseate Terns, Piping Plovers, and Red Knots from Wind Facility Operations on the Atlantic Outer Continental Shelf. A final report for the US Department of the Interior, Bureau of Ocean Energy Management (BOEM), Regulation and Enforcement, Report No. BOEMRE 048-2011. Contract No. M08PC20060 to Normandeau Associates.

Green, A. and M. Perrow. 2012. Comparison of Two Different Collision Risk Models in the Offshore Environment: Band vs. Folkerts. Poster presentation at Conference on Marine Renewables and Birds British Ornithologists Union. November 26, 2012. Peterborough, United Kingdom.

Green, M. 2004. Flying with the Wind - Spring Migration of Arctic-Breeding Waders and Geese over South Sweden. Ardea 92(2): 145-160.

Gudmundsson, G. A., A. Lindstrom, and T. Alerstam. 1991. Optimal Fat Loads and Long-Distance Flights by Migrating Knots *Calidris canutus*, Sanderlings *C. alba* and Turnstones *Arenaria interpres*. Ibis 133: 140-152.

Gundmundsson, G. A. 1994. Spring Migration of the Knot Calidris C. canutus over Southern Scandinavia, as Recorded by Radar. Journal of Avian Biology 25: 15-26.

Hansen, M. H., A. Hansen, T. J. Larsen, S. Øye, P. Sørensen, and P. Fuglsang. 2005. Control Design for a Pitch-Regulated, Variable Speed Wind Turbine. Risø National Laboratory, Roskilde, Denmark.

Harrington, B. 1996. The Flight of the Red Knot: A Natural History Account of a Small Bird's Annual Migration from the Arctic Circle to the Tip of South America and Back. W.W. Norton & Company, New York, New York.

Harrington, B. A., S. Koch, L. J. Niles, and K. Kalasz. 2010. Red Knots with Different Winter Destinations: Differential Use of an Autumn Stopover Area. Waterbirds 33: 357-363.

Hatch, J. J. and S. Brault. 2007. Collision Mortalities at Horseshoe Shoal of Bird Species of Special Concern. Final Draft. Cape Wind Report No. 5.3.2-1. January 2007.

Holmstrom, L. A., T. E. Hamer, E. M. Colclazier, N. Denis, J. P. Verschuyl, and D. Ruché. 2011. Assessing Avian-Wind Turbine Collision Risk: An Approach Angle Dependent Model. Wind Engineering 25: 289-312.

Hsu, S. A., E. A. Meindl, and D. B. Gilhousen. 1994. Etermining the Power-Law Wind-Profile Exponent under near-Neutral Stability Conditions at Sea. Journal of Applied Meteorology and Climatology 33: 757-765.

Krijgsveld, K. L. 2014. Avoidance Behaviour of Birds around Offshore Wind Farms. Overview of Knowledge Including Effects of Configuration. Report 13-268. Bureau Waardenburg, Culemborg, the Netherlands.

Krijgsveld, K. L., R. C. Fijn, M. Japink, P.W. van Horssen, C. Heunks, M. P. Collier, M. J. M. Poot, D. Beuker, and S. Dirksen. 2011. Effect Studies, Offshore Wind Farm Egmond Aan Zee: Final Report on Fluxes, Flight Altitudes and Behaviour of Flying Birds. Report: OWEZ_R_231_T1_20111114_flux&flight. Wageningen Institute for Marine Resources & Ecosystem Studies (IMARES), Culemborg, the Netherlands. November 14, 2011.

Legland, D. 2014. MatGeom Library for Geometric Computing. Sourceforge.net. Retrieved November 15, 2014.

Martinez, W. L. and A. R. Martinez. 2002. Computational Statistics Handbook with Matlab. Chapman & Hall/CRC, Boca Raton, Florida.

Mateos, M., G. Muñoz Arroyo, and J. Alonso del Rosario. 2011. Modelling Seabird Collision Risk with Off-Shore Windfarms. Oral presentation at the Conference on Wind Energy and Wildlife Impacts, May 4, 2011. Trondheim, Norway.

MathWorks. 2014. MATLAB and Statistics Toolbox, Release 2014b. The MathWorks, Inc., Natick, Massachusetts.

May, R. 2015. A Unifying Framework for the Underlying Mechanisms of Avian Avoidance of Wind Turbines. Biological Conservation 190: 179-187.

May, R., P. L. Hoel, R. Langston, E. L. Dahl, K. Bevanger, O. Reitan, T. Nygård, H. C. Pedersen, E. Røskaft, and B. G. Stokke. 2010. Collision Risk in White-Tailed Eagles. Modelling Collision Risk Using Vantage Point Observations in Smøla Wind-Power Plant. Report 639. NINA, Trondheim, Norway. 25 pp.

National Climatic Data Center (NCDC). 2015a. Global Hourly Data. NCDC, National Oceanic and Atmospheric Administration, Stennis Space Center, Massachusetts. Acessed July 2015. Available online at: http://www.ncdc.noaa.gov/cdo-web/datasets

National Climatic Data Center (NCDC). 2015b. Precipitation Hourly Data. NCDC, National Oceanic and Atmospheric Administration, Stennis Space Center, Massachusetts. Acessed July 2015. Available online at: http://www.ncdc.noaa.gov/cdo-web/datasets

National Data Buoy Center. 2015. Station 44020 (LLNR 13665) - Nantucket Sound. Nantucket Sound Main Channel Lighted Gong Buoy 17. National Data Buoy Center, National Oceanic and Atmospheric Administration, Stennis Space Center, Massachusetts. Updated July 21, 2015. Available online at: http://www.ndbc.noaa.gov/; Station 44020 data available online at: http://www.ndbc.noaa.gov/station_history.php?station=44020

Nations, C. and W. Erickson. 2010. Marbled Murrelet - Wind Turbine Collision Model for the Radar Ridge Wind Resource Area. Western EcoSystems Technology, Inc. (WEST). 56 pp.

Newton, I. 2010. The Ecology of Bird Migration. Academic Press, London, United Kingdom.

Niles, L. J., J. Burger, R. R. Porter, A. D. Dey, S. Koch, B. Harrington, K. Iaquinto, and M. Boarman. 2012. Migration Pathways, Migration Speeds, and Non-Breeding Areas Used by Northern Hemisphere Wintering Red Knots (*Calidris canutus*) of the Subspecies Rufa. Wader Study Group Bulletin 119: 195-203.

Niles, L. J., J. Burger, R. R. Porter, A. D. Dey, C. D. T. Minton, P. M. Gonzalez, A. J. Baker, J. W. Fox, and C. Gordon. 2010. First Results Using Light Level Geolocators to Track Red Knots in the Western Hemisphere Show Rapid and Long Intercontinental Flights and New Details of Migration Pathways. Wader Study Group Bulletin 117: 123-203.

North American Datum (NAD). 1983. NAD83 Geodetic Datum.

National Geographic Society (National Geographic). 2014. World Maps. Digital Topographic Map.

Petersen, I. B., T. K. Christensen, J. Kahlert, M. Desholm, and A. D. Fox. 2006. Final Results of Bird Studies at the Offshore Wind Farms at Nysted and Horns Rev, Denmark. National Environmental Research Institute,Ministry of the Environment, Denmark.

Piersma, T. and J. Jukema. 1990. Budgeting the Flight of a Long-Distance Migrant: Changes in Nutrient Reserve Levels of Bar-Tailed Godwits at Successive Spring Staging Sites. Ardea 78: 315-337.

Podolsky, R. 2005. Application of Risk Assessment Tools: Avian Risk of Collision Model. S. S. Schwartz, ed. Pp. 86-87. *In*: Proceedings Onshore Wildlife Interactions with Wind Developments: Research Meeting V. Lansdowne, Viginia. November 3-4, 2004. Prepared for the Wildlife Subcommittee of the National Wind Coordinating Collaborative (NWCC) by RESOLVE, Inc., Washington D.C.

Podolsky, R. 2008. Method of and Article of Manufacture for Determining Probability of Avian Collision. United States Patent number US 7,315,799 B1.

Robinson Willmott, J., G. Forcey, and A. Kent. 2013. The Relative Vulnerability of Migratory Bird Species to Offshore Wind Energy Projects on the Atlantic Outer Continental Shelf: An Assessment Method and Database. Final report to the U.S. Department of the Interior, Bureau of Ocean Energy Management (BOEM), Office of Renewable Energy Programs. OCS Study BOEM 2013-207. 275 pp. Available online at: www.data.boem.gov/PI/PDFImages/ESPIS/5/5319.pdf

Seiler, P., A. Pant, and J. K. Hedrick. 2003. A Systems Interpretation for Observations of Bird V-Formations. Journal of Theoretical Biology 221: 279-287.

Silverman, B. W. 1986. Density Estimation for Statistics and Data Analysis. Chapman and Hall, London, United Kingdom.

Smales, I., S. Muir, C. Meredith, and R. Baird. 2013. A Description of the Biosis Model to Assess Risk of Bird Collisions with Wind Turbines. Wildlife Society Bulletin 37: 59-65.

Sugimoto, H. and H. Matsuda. 2011. Collision Risk of White-Fronted Geese with Wind Turbines. Ornithological Science 10: 61-71.

Sullivan, B. L., C. L. Wood, M. J. Iliff, R. E. Bonney, D. Fink, and S. Kelling. 2009. eBird: A Citizen-Based Bird Observation Network in the Biological Sciences. Biological Conservation 142: 2282-2292.

Swennen, C. 1992. Observations on the Departure of Knots from the Dutch Wadden Sea in Spring. Wader Study Group Bulletin 64(Suppl.): 87-90.

Troost, T. 2008. Estimating the Frequency of Bird Collisions with Wind Turbines at Sea. Guidelines for using the spreadsheet 'Bird Collisions Deltares v.1-0.xls'. Deltares, Delft, Netherlands.

Tucker, V. A. 1996. A Mathematical Model of Bird Collisions with Wind Turbine Rotors. Transcripts of the ASME Journal of Solar Energy Engineering 118: 253-262.

US Fish and Wildlife Service (USFWS). 2014a. Endangered and Threatened Wildlife and Plants; Threatened Species Status for the Rufa Red Knot; Final Rule. Department of the Interior, Fish and Wildlife Service, 50 CFR Part 17. 79 Federal Register (FR) 238: 73706-73748. December 11, 2014. Available online at: http://www.gpo.gov/fdsys/pkg/FR-2014-12-11/pdf/2014-28338.pdf

US Fish and Wildlife Service (USFWS). 2014b. Rufa Red Knot Background Information and Threats Assessment. *Supplement To*: "Endangered and Threatened Wildlife and Plants; Threatened Species Status for the Rufa Red Knot". Docket No. FWS-R5-ES-2013-0097; RIN AY17. December 11, 2014. Available online at: http://www.gpo.gov/fdsys/pkg/FR-2014-12-11/pdf/2014-28338.pdf

US Naval Observatory. 2015. Nantucket Sound: Rise and Set for the Sun. Astronomical Applications Department, US Naval Observatory, Washington, D.C. Accessed July 2015. Available online at: http://aa.usno.navy.mil/data/docs/RS_OneYear.php

Appendix A Responses to Peer Reviewers' Comments

Introduction

WEST conducted a formal peer review of the interim report as part of the process of completing this report. Four peer reviews were received, and WEST's peer-review director, Steven Courtney, directed the process of evaluating and summarizing the reviewer's comments and incorporating them into a revision of the interim report to produce the final report. As one product of this review, WEST produced a peer review report containing a synthesis of the reviewers' comments, with each of the reviewers' complete comments appended. During the process of synthesizing the peer reviews, Dr. Courtney identified twenty-two "substantive" reviewer comments that required attention and response from the Project's technical team, as well as additional "editorial" comments, many of which were useful to improve the report, but which were not deemed to warrant additional explanation or discussion. In this appendix, we have reproduced each of the 22 substantive reviewer comments and provided a written response to each, as well as a description of what revisions, if any, were made to the body of the final report in response to each comment. These reviewer-directed revisions to the report, and the written responses to the 22 substantive reviewer comments contained within this appendix were prepared by the Project's technical leaders, Caleb Gordon and Chris Nations.

The four technical experts from whom we received peer reviews on the interim report were the following:

- Dr. Mark Desholm, Head of Conservation and Science, Birdlife Denmark.

- Dr. Marc Mangel, Distinguished Research Professor, Center for Stock Assessment Research and Department of Applied Mathematics and Statistics, University of California, Santa Cruz.

- Dr. Barry Noon, Professor, Department of Fish, Wildlife, and Conservation Science, Colorado State University.

- Dr. Michael Runge, Research Ecologist, US Geological Survey, Patuxent Wildlife Research Center.

In the section below, we list each of the 22 substantive reviewer comments, grouped by the reviewer who offered them, along with a written response to each from the Project's technical team.

Substantive Peer Reviewer Comments and Responses from Project Technical Team

From the comments of Mark Desholm

1) I would have liked to see a distinction between birds migrating at daylight and at night time – collisions risk are for sure very different between these two periods.

Response
We agree with the comment that collision risk for Red Knots may vary between day and night. However, during the fall migratory season, when a larger number of individual knots have potential to pass through the Facility area, the diurnal timing of passage is relatively invariant. The reason this timing is relatively invariant in the fall season is that Red Knots are known to initiate their migratory flights near sunset, generally in the few hours preceding sunset but occasionally shortly after sunset. This assertion is based on the extensive, but unpublished personal observations of Project technical team member Dr. Lawrence, J. Niles, who is one of the world's foremost experts on Red Knot biology. Because the Facility area is located fewer than 50 miles from the assumed departure points in the southeastern portion of Cape Cod, Massachusetts, the passage of southbound migrating Red Knots during the fall season is always expected to occur at the same time of day, close to sunset. We have added a reference to Dr. Niles' observations to support the statement of our assumed migratory departure timing in the text of the report. By contrast, during the spring season, our model assumes that migrating Red Knots may pass through the Facility area at any time of day. This is because their departure points are located so far to the south of the Facility area, that the diurnal timing of passage through the Facility area is effectively decoupled from the diurnal timing of departure. Nonetheless, we note that during the spring season, the number of Red Knot individuals that potentially pass through the Facility area is an order of magnitude smaller than it is during the fall season. Furthermore, our model does not explicitly incorporate daylight/nighttime differences in Red Knot behavior; therefore, the only diurnal differences in collision risk during the spring would be due to diurnal differences in weather conditions. The decision of whether or not to include any source of complexity in a biological model is a balance between the marginal benefit of the additional realism versus the marginal cost of the additional model complexity. The model we present in this report is already the most complex and realistic model of collision risk for a bird species at an offshore wind energy facility of which we are aware. For the reasons described above, while we agree that variation in collision risk at different times of day is realistic, we do not believe that the small marginal improvement from incorporating this source of variation would warrant the additional cost of incorporating this additional model complexity.

2) P8: Here it is stated that "this evasive action is generally regarded to be trivial…." – but where does this conclusion comes from? Winkelman have described how birds indeed could person evasive action and towards moving blades. I do not at all find this figure to by any near trivial. Difficult to estimate yes – but not trivial!

Response
We agree with the reviewer's comment that this form of avoidance is not necessarily trivial, and have revised the corresponding section of the text of the report accordingly, incorporating a new discussion of how birds' evasive maneuvers within the rotor-swept plane of turbines can be modeled if the Tucker (1996) model is selected as the basic machinery to represent collision geometry, but not if the Band (2012) model is used. In the case of the present study, the Band model was selected over the Tucker model because of other considerations discussed elsewhere in the report; hence, our incorporation of avoidance behaviors into the model was necessarily constrained to processes occurring outside of the rotor-swept planes, themselves. We note that this constraint, and the assumption that birds cannot take evasive actions to avoid rotors once they are inside the rotor-swept plane, is a conservative assumption with respect to collision risk.

Incorporating this additional form of avoidance could only have the impact of reducing predicted fatality rates below the outcomes presented in the current study.

3) P12: Third paragraph: really nice that the collision risk with static structures like of the turbines and the transformer platform is also included in the model. However, what about the fatalities from birds being harmed by the wake turbulence of the rotating turbine blades as described in the studies by Winkelman. Maybe they could be incorporated or at least referee too in this report?

Response
We agree with the reviewer's suggestion that it is possible for Red Knots to be harmed by interactions with the wind energy Facility other than potential collisions with moving and stationary structures as modeled, for example by being thrown off course from encountering the wake turbulence of rotors as suggested by Winkelman. However, we are not aware of a quantitative basis for incorporating this particular effect into a collision risk model. Furthermore, we do not feel that there is a scientific consensus that wake turbulence effects are likely to be significant enough to warrant their inclusion within collision risk models, evidenced by the observation that no previous collision risk models of which we are aware have incorporated this factor.

4) P17: You assume that fall flights occur near sunset – and base this assumption on the assumption that birds pass over the project area not long after the departure from land – this does not make much sense to me! If you do not have data on the departure time – how big a bias will expect from this lack of data?

Response
This comment parallels the author's previous comment (#1), and we reference our response to that comment here. We further add that the assumption of fall migratory flight departures occurring near sunset, supported by Larry Niles' personal observations of Red Knots at migratory stopover sites in the field, is not surprising or unexpected, as it is consistent with a very general and consistent taxonomic trend of *Calidris* sandpipers and most other migratory shorebirds being nocturnal migrants.

5) P17: Timing for spring migrants are assumed to occur with equal probability of the day – do you not have real field data on timing – e.g. from eBird?

Response
We are not aware of any specific data on the diurnal timing of spring migratory arrivals of Red Knots in the vicinity of the Facility area. We note that individual eBird observations (checklists) commonly span multiple hours, and therefore cannot inform fine-scale (e.g. hourly) temporal analyses. In the absence of specific data, and because the diurnal timing of arrival in Massachusetts is likely to be decoupled from the diurnal timing of departure from remote departure locations in South America and/or the Caribbean, we feel that our assumption of randomizing the time of day of spring arrivals in Massachusetts is the most parsimonious and justifiable.

6) P18: I my humble opinion, it is rather dangerous to estimate flight directions at rather local scales, from data on long distance migration scales (from known breeding areas and/or from geolocaters positions). This because the decision of flight direction at the local Cape Cod scale could be influenced by e.g. in spring by the presence of the two larger island to the south or the future wind farm it selves – simply because the birds could chose to navigate towards these physical structures when flying over water using them as navigational cues. The local wind conditions is also very likely to influence the local migration directions, even thought they might not influence the overall long distance goal of their journey. You simply do not know whether your resulting migration paths are realistic or not – they might be but they might also by very wrong with a resulting bias in collisions risk estimates. In spring I would argue that the migration directions of the knots flying over the approved wind farm area would be influence more by the presence of nice staging areas on the shore than on the direction towards the breeding grounds. Again – and sorry to say it, but you don't know where your knots are flying – in my humble opinion! You make assumptions - but you do not know! I would also have liked to see a discussion of the potential difference in migration directions between daylight and night time hours of the day – we know this have a huge impact on flight altitudes.

Response
We agree with the reviewer's comment that at small spatial scales, the flight directions and trajectories of migrating Red Knots is likely to be responsive to small scale spatial factors, such as the configuration of coastlines, land forms, and also wind directions. However, we are not aware of any data or other quantitative basis for representing this fine-scale directional variation within the migratory flight trajectories of our model. We note that our model represents a significant advancement and incorporates significant biological realism in migratory flight trajectories of birds relative to all other bird collision risk models of which we are aware, in that we used large telemetry and resighting datasets on Red Knots migrating along the east coast of the United States to create an empirically-derived, spatially-explicit representation of Red Knots' migratory flight trajectories in the Facility region. Although it is true that these trajectories were derived from large-scale point-to-point trajectories that do not incorporate fine scale precision on flight paths, we feel that relying on these empirical data, including drawing most parsimonious straight line trajectories between successive location points, is the most biologically realistic and appropriate basis for modeling Red Knot migratory flight trajectories in the current study, given the limits of available data.

7) P20: High-altitude distributions: I find it very unlikely that the knots distribute themselves equally vertical-wise during migration. Why should this be the case? My own observations of knots is the opposite. On days when they generally fly high – no flocks pass low over water! I would suggest not to use an equal distribution. Try and find data on flight altitudes on migrating shorebirds and find a more appropriate distribution.

Response

We agree with the reviewer's observation that on days when migrating Red Knots fly high, they exhibit a strongly skewed altitudinal distribution with most, if not all birds flying at high altitudes. The Project's technical team had a lengthy set of discussions of this issue, and we contemplating using a fair weather altitudinal distribution that was even more strongly skewed toward high altitudes, as we also had a consensus on the technical team that this was more realistic. However, in the end, we decided to use the uniform distribution, in order to err on the side of conservatism. When we experimented with alternative distributions, it was virtually impossible to apply any type of simple geometric distribution with overall high altitude flights, as suggested by best available evidence, without making Red Knots completely avoid rotor-swept altitudes altogether during fair weather, effectively dropping that part of the system out of the collision model. Even though the technical team recognized that Red Knots are most likely to have a strong tendency to fly at high altitudes, in the vicinity of 1,000-2,000 m (3,281-6,562 ft) elevation above the water's surface, during favorable weather conditions, we also recognized that certain conditions that fell within our "fair weather" definition might bring some Red Knots lower, such as variation in time of day, wind speed and direction, different wind directions in different altitudinal strata, or limited precipitation. For this reason, we thought it best to make the conservative assumption that as many as 5% of birds may fly at rotor-swept altitudes or lower even during fair weather conditions. When we tried to apply different types of distributions with this constraint, we found that applying a uniform flight altitude distribution was one of the only ways, and certainly the simplest way to achieve this, and still maintain a high mean flight altitude (1,000 m) , as determined by best available evidence. If we applied virtually any other type of distribution, we would either have to remove more Red Knots from rotor-swept altitudes, lowering collision risk, deviate from best available evidence with respect to mean flight altitude under favorable weather conditions, or apply a more complex, irregular altitudinal distribution that would result in significant additional model complexity for unclear gain.

8) P23 second last paragraph: But we know that birds can take last second evasive action when trying to fly through the rotor sweep area – so why not try to include it in the model?

Response

This comment parallels the reviewer's earlier comment (#2) about the potential for birds to take evasive actions even as they pass through the rotor-swept plane, and we reference our response to comment #2, and the associated revisions that we have incorporated into the final report in response to this point. We further suggest that generating an alternative model that uses the Tucker (1996) mechanism rather than the Band (2012) mechanism for representing rotor-bird collision geometry inside the rotor-swept plane would be a reasonable approach for further research, but is beyond the scope of the current study. In the case of the present study, the Band model was chosen for a variety of other reasons, thereby incorporating the conservative assumption that birds cannot take evasive actions of rotors once they have entered the rotor-swept plane. We note that creating and evaluating a different model based on the Tucker model in order to be able to relax this assumption would only further reduce the collision rates below those predicted with the current model.

9) P28: Does Niles not have the data from where you got your 10-200 range flock sizes, then you use a real distribution and not just a subjectively chosen distribution? Come on – flock sizes of migrating red knots must be available from somewhere!

Response
We are not aware of a source of data on flock sizes of migrating Red Knots for the Facility region. We also note that flock sizes are likely to be linked with population sizes. For that reason, data on Red Knot flock sizes from other regions (e.g. the Old World), or even earlier times in the US, when the overall population of "*rufa*" Red Knots was substantially different, would not necessarily be representative of the likely flock sizes of Red Knots passing through the Facility area under the modeled scenarios that were based on estimated current and recovered population sizes along the east coast of the U.S. The mean flock size and flock size distribution we used were based on best available science, largely from recent personal observations of Dr. L. J. Niles, one of the world's foremost experts on the biology of "*rufa*" Red Knots, and are therefore appropriate and reasonable.

10) P54: Last paragraph: The authors assume a factor five when approach angles are less than 25 degrees. The devils advocate could argue – why incorporate this factor if you don't have input data? Alternative odds ratios are use also to "account" for the lack of data. However, it makes perfectly sense to me to add this factor to your model, if you plan to collect data for your model after this project. I would like to add here – if you chose to add this correction factor on collision probability then you should also add a correction factor on avoidance for birds approaching at angles less than 90 degrees. For sure birds approaching at a small angle will perceive the blades as a higher threat compared to a 90 degree approach angle.

Response
We agree with the reviewer's suggestion that when birds approach rotors at angles other than 90 degrees, they may exhibit increased micro-avoidance probabilities as the rotors may be easier for the birds to perceive (increased visibility) and avoid (decreased silhouette area), further reducing collision risk below that predicted by our model. However, we are not aware of any other collision risk model that has incorporated this variation in avoidance rate with approach angle, nor any other quantitative treatment of this issue. For this reason, we feel that the conservative assumption of keeping micro-avoidance rate constant for all approach angles is the most reasonable and appropriate choice.

11) P66: Please take into account or at least discuss the fact that a flock of red knots do not fly in one long line perpendicular to the flight direction. They often fly in Vs, and hence, birds colliding in front will likely warn the followers during a collision event. So I find your way of treating the flock structure in relation to collisions rather primitive. Well I know that we do not have data on these flock behaviors, but pleas discus it at least.

Response

We agree with the reviewer's assertion that migrating Red Knots often fly in V formations, and we note that we did, indeed, incorporate chevron-shaped flock configurations into our model. The reviewer's comment about the significance of flock shape is suggestive of an additional type of avoidance behavior: avoidance of rotors by birds after they have perceived collisions or evasive maneuvers occurring in individual birds that are physically located in front of them within flocks, and we did not incorporate this form of avoidance behavior into our model. We believe that the occurrence of this hypothesized additional avoidance behavior is plausible. However, we note that incorporating such behavior into the model could only have the effect of further reducing collision probabilities below those predicted by our model, hence we are comfortable retaining the conservative assumption of no such avoidance behavior, in the absence of specific evidence to the contrary.

12) P71: As stated earlier, I do not think that the uniform distributions is what knots do for real. In my 15 year long career as an radar ornithologist, I have never seen uniform distribution of avian migrants in the airspace altitude-wise. There are always one or mores layers where the concentration of birds are higher. And at night time a general trend exist – namely that birds fly higher. I think that it is extremely rare that avian migrants fly close to the water surface during the dark hours.

Response

This comment parallels the reviewer's earlier comments #7 regarding uniform flight altitude distributions, and #1 regarding variation with time of day, and we reference our earlier responses to these comments. We further note that the assumption of uniform flight altitude distribution during favorable weather conditions is not intended to be a realistic representation of birds' distributions at any individual moment (we agree that at any one time, they are likely to have a clumped distribution), but rather an aggregate of all momentary distributions across the entire spectrum of times and conditions that are included within our "favorable weather" parameter space.

13) P79: Yes you have payed attention on variation in avoidance assumptions – but you don't know how realistic your input values are. As also stated earlier – there are several avoidance issues that I disagree about. I think you should be more prudent – yes you guys have produced a well designed model and yes you have incorporated a lot of variation – but that do not counteract the lack of knowledge that you guys have. The model lack a lot of real biological data – you have used a lot of assumptions in the lack of data. That is ok – but please do not indicate that you now have all the answers to red knot collision risk. You have a brilliant model – but you desperately needs real data to use as input parameters.

Response

We agree with the reviewer's observation that the accuracy of model's inputs, assumptions, and therefore predictions, is constrained by the limits of available data, and that efforts to fill existing data gaps could result in significant improvements to the accuracy of collision models and their predictions. We have added a brief caveat paragraphs to the overview subsection of the Results and Discussion section (Chapter 4) to this effect.

14) Lines 603: You are clearly treating the avoidance as a probability (see below about the conceptual issue). Indeed this equation makes no sense otherwise since a rate has units of time^{-1} and the right hand side then involves non-commensurate quantities.

Response

We agree with the reviewer's comment that we have treated avoidance as a probability rather than as a rate. Accordingly, we have changed the terminology from "avoidance rate" to "avoidance probability" throughout the report. We have also substituted a more accurate annotation for the composite macro- micro avoidance probability, to which the reviewer referred in this comment.

15) Figure 3.11ab: It seems to me that extreme events are going to be the ones that really endanger the birds. Have you done any explorations with changing the tails of those distributions? This would become particularly important for your explanation in lines 2164-2166 about the insensitivity of output to variation in visibility and precipitation thresholds.

Response

We agree with the reviewer's observation that rare weather events, present in the tails of the weather data distributions, may be important for driving fatality events and predicted fatality rates in the model. However, we feel that the reviewer may have misunderstood the nature of the distributions shown in Figures 3.11a and b. These are empirical distributions of actual weather data obtained from the Facility region, not theoretically generated distributions. Therefore, we do not feel that it would be appropriate to explore changing the tails of the distributions as the reviewer suggests. The actual frequencies of rare, and potentially hazardous weather events are already included in those empirical distributions, hence they have already been incorporated into the model in the most realistic way possible under the limits of existing data.

16) As described above, the equation on line 603 only makes sense if the right hand side deals with probabilities. A bird only needs to micro-avoid if it did not macro-avoid. Hence

Pr{bird does not avoid}=Pr{did not avoid the facility and did not avoid all turbines in the facility} (1)

Using the definition of conditional probability (Hilborn and Mangel 1997, Mangel 2006) we have

Pr{bird does not avoid }=Pr{did not avoid all turbines in the facility given that it did not avoid the facility}•Pr{did not avoid the facility} (2)

If we introduce the symbols p_{Macro} and $p_{Micro|Macro}$ for the probability that a bird avoids the facility and the probability that it avoids all turbines given that it did not avoid the facility then Eqn 2 becomes:

$$\Pr\{\text{bird does not avoid }\}=(1-p_{Macro})(1-p_{Micro|Macro}) \tag{3}$$

And the equation on line 603 follows directly from:

$$\Pr\{\text{bird avoids all turbines}\}=1-\Pr\{\text{bird does not avoid }\}=$$
$$1-(1-p_{Macro})(1-p_{Micro|Macro}) \tag{4}$$

Thus, the equation in line 603 and subsequent analysis are fine, but the use of rate is confusing, even if others use it in the literature.

Response
This comment parallels the reviewer's earlier comment #14, and we reference our earlier response to that comment, as well as the associated revisions that have been made to the composite avoidance probability equation and the text of the report. We also agree with the reviewer's observation that this is a confusing issue in technical literature, as parameters most accurately referred to as "probabilities" have sometimes been referred to as "rates."

From the comments of Barry Noon

17) One aspect of this model that may need further evaluation is the assumption that collisions of individual birds within a flock are appropriately modeled as independent events. By definition a flock is a dense spatial aggregation of individuals that collectively compose the flock. As a result, it may be that the probability of collision with the wind tower infrastructure is more appropriately modeled as a set of conditionally dependent events—that is, given that a bird collides with the tower complex, the neighboring birds within the same flock may have an increased probability of collision resulting from spatial adjacency to the mortality source.

Response
We agree with the reviewer's comment that collisions of individual birds within flocks with wind Facility structures are not independent, in the sense that if one bird in the flock is close to a structure, then the other flock members are likely to be close to that structure as well. Our response to this comment is 2-parted, as this issue is effectively very different for representing birds' collisions with stationary Facility structures compared with moving Facility structures (e.g. spinning rotors).

With respect to birds' collisions with stationary structures, including the ESP, the turbine towers and nacelles, and the rotors under low wind speed conditions when the rotors are not spinning, we note that the conditional probability to which the reviewer refers is already built into the model as a function of the spatially explicit representation of the physical structures of the Facility and the flocks of birds flying within it in the simulations. This is fundamental reason why the most frequent number of collisions that occur when any occur at all is seven or eight (see text and Figure 4.2), which is the typical result when a flock of knots encounters a turbine tower, as a function of the width of the tower and the spacing of Red Knots in flocks (see Figure 3.20).

With respect to birds' collisions with spinning rotors, it is true that our model does not incorporate the conditional probability of adjacent birds being struck by the same moving blade within individual simulations; indeed, the last paragraph of Section 3.4 in the text addresses this issue. However, we note that the changing the assumption that birds' collision probabilities are independent of one another in this way is not possible within the Band (2012) model, and would therefore entail the development of a fundamentally different modeling approach, potentially eliminating the other advantages of the Band model. Furthermore, we hypothesize that changing this assumption would not yield substantial gains in prediction accuracy, as we suspect that the overall likelihood of birds' collisions with moving rotors is not likely to be biased one way or another by the inclusion of this assumption.

18) On those occasions when weather conditions result in flight altitudes that require Red Knots to avoid wind tower infrastructure, either at the macro or micro scale, is there any possibility that this results in important behavioral disruption to the flock? For example, could one consequence be a significant increase in energy expenditure during flight?

Response

We agree with the reviewer's suggestion that Red Knots may experience effects other than collision fatality as they pass through an offshore wind energy facility, including the expenditure of additional energy during flight. We note that the modeling of effects other than collision fatality is beyond the scope of the present study, and therefore not appropriate for incorporation within our model. Nonetheless, we also point out that the specific effect of additional energy expenditure from the additional flight mileage associated with migratory routes that circumvent offshore wind energy facilities is unlikely to be significant in this case. This phenomenon was modeled by Masden et al. (2009) for Common Eiders (*Somateria mollissima*) migrating along the eastern Atlantic Ocean, who reached the conclusion that the additional energetic expenditure of taking a longer trajectory to avoid flying through an offshore wind energy facility on a long-distance migratory route was negligible in that case. This result is likely to be applicable to Red Knots in the western Atlantic as well, as the additional mileage entailed in avoiding an offshore wind facility is similarly small in relation to the length of the overall migratory journey.

19) The flight altitude distribution for Red Knots during migration suggests that only a small percentage of birds would be exposed to wind tower infrastructure. However, as pointed out by Burger et al. (2012), during ascent and descent from long-distance flights Red Knot exposure to wind towers may be much higher. This potential behavioral subtlety may not have been adequately modeled.

Response

We agree with the reviewer's suggestion that ascent and descent may be the times when wind turbine collisions are most likely for systems such as the current one, in which flight altitudes are likely to be concentrated above rotor-swept altitudes under most circumstances. However, the exclusion of ascent and descent from the current model was a conscious choice by the Project team, made on the basis of a comprehensive review of best available evidence that suggested that Red Knots were unlikely to be engaged in flight ascent or descent in the vicinity of the approved wind energy Facility. The basic elements of this rationale are as follows:

- The Red Knot is strictly terrestrial (including coastal) with respect to all non-flying behaviors.

- All of the above water structures of the approved wind energy Facility are located over four miles from the nearest land.

- The distance required for Red Knots to fully ascend to, or descend from migratory flight altitudes is not well-known, but it is believed to be substantially less than four miles (L. Niles, personal observations).

20) Finally, I believe it is important to emphasize that the mortality projections from this model be viewed as preliminary—that is, as an hypothesis conditional on subsequent model validation. This is not a weakness of the model discussed in this report—the need for model validation is a requirement for all projection models. Validation will obviously be difficult in oceanic conditions because finding carcasses would be quite difficult and subjection to low probabilities of detection (Smallwood 2007, 2013). This may require some real-time monitoring during periods of peak migration.

Response
We agree with the reviewer's suggestion that the predictions of this model would be strengthened with validation. This parallel's Mark Desholm's comment (#13) regarding overall uncertainty levels, and the prospect of model improvement through future data gathering efforts, and we reference our response to that comment, as well as the additional caveat we have added to the overview of the "Results and Discussion" section (Chapter 4) of the report in response. We also agree with the reviewer's observation that obtaining the data necessary for validation of the current model would be difficult, given the marine location of the Facility, and we note that it is beyond the scope of the present report to make recommendations or suggestions for post-construction monitoring efforts associated with the approved Facility.

From the comments of Michael Runge

21) Although the authors have taken the issue of uncertainty (especially parametric uncertainty) seriously, the structure of the simulations does not appropriately incorporate or analyze that uncertainty. At issue is the distinction between process uncertainty and parametric uncertainty and how they should be handled differently in a simulation (see McGowan et al. 2011 for a treatment of this issue). The process uncertainty (e.g., the weather conditions) is not reducible, representing aspects that we can neither control nor gain more detailed information about. The parametric uncertainty (e.g., thresholds for departure delay, avoidance probabilities) is epistemic uncertainty, that is, it represents our limiting knowledge, and it is potentially reducible. Another way to think about the distinction is that if we had perfect knowledge, we'd know all the parameters (so wouldn't have to sample over them), but would still have to sample over the process uncertainty. In this kind of forecasting model, parametric uncertainty is of great concern. In this report, the distinction between process and parametric uncertainty is not clearly made, parametric uncertainty is not expressed for all parameters, the baseline scenario does not fully incorporate parametric uncertainty,

and the process of taking the grand mean and standard error hides the importance of parametric uncertainty. Fig. 4.1 may or may not be biased, but it is extremely overconfident; the precision of these results is nowhere near as good as the SE on this graph indicates.

Addressing this concern will not require re-structuring the model itself, but will require restructuring and re-running all the simulations. It will affect all the results, especially in the depiction of uncertainty. Further, addressing this concern will affect many places in the report. In what follows, I've tried to break down the suggestion into manageable steps; these need to be understood together—they are not independent suggestions that can be accepted or rejected separately.

(a) Beginning in Section 3.3.1 and continuing throughout, the distinction between process and parametric uncertainty needs to be more tightly drawn. It would be helpful to clearly categorize which sources of uncertainty are considered in each type.

(b) Parametric uncertainty should be expressed for all parameters, and included in the baseline scenario. I don't think there's much value in running a baseline that has fixed values for many of the parameters, because the results will be misleadingly precise. Rather, sample from the full parametric uncertainty for each parameter so that that baseline results express a full accounting of uncertainty.

(c) For many of the parameters in Table 3.1, this means moving the "Alternative" probability distribution into the "Baseline" column.

(d) For a number of parameters, parametric uncertainty is expressed as a few discrete values (e.g., the headwind threshold for fall departure delay is expressed as 5, 10, or 15 m/s). Can these be treated as continuous distributions instead? Or at least as a discrete random variable that is sampled from?

(e) In the baseline scenario, distinguish two levels of replication: a higher level of replication, in which samples are drawn from the parametric distributions; and a lower level of replication, in which samples are drawn from the process distributions, while holding the parameters constant. I don't think you really need much replication at the lower level (in fact, you might just have only 1 process replicate for each parametric replicate); the emphasis is on replication across the possible parameter values.

(f) The distribution that comes out of the baseline scenario will fully express uncertainty in the possible outcomes, and can be read as a probability distribution (e.g., you could make such conclusions as, "the probability the collision rate will be greater than 2 birds/season is…"). The mean is of some interest, but the standard error is of no interest at all. The prediction intervals are probably of most value (e.g., the range expressed between the 10th and 90th quantiles provides an 80% credible interval for the seasonal mortalities).

(g) The baseline results will then actually contain all the information you need for sensitivity analysis. You can regress the results against any of the parameter values to see how much of an effect that parameter is having. (This will require saving the parameter values for each replicate).

Response

We agree with the reviewer's suggestion that additional study of "parametric uncertainty" would add value, but we disagree with the suggestion that it has been treated insufficiently in the present study. We agree that our running of multiple simulations and inclusion of means and other statistics to describe the variation in predicted fatality outcomes for fixed model parameter values represents a type of uncertainty analysis that is distinct from exploring variation in outcomes under different parameter values ("process uncertainty" rather than "parametric uncertainty", as defined by the reviewer). However, we have analyzed both types of uncertainty in the present study, and we maintain that both types of uncertainty are important to explore. In the case of process uncertainty, we typically ran 10 trials of 100,000 iterations each for each simulated set of parameter values. Our presentation of summary statistics from those simulations sheds important light on the dynamics of the system, particularly as many of the model inputs took the form of distributions rather than fixed values, meaning that outcomes were likely to, and in fact did vary substantially across iterations within a single set of modeled conditions, for example as different micro- and macro-avoidance probabilities were drawn from their distributions.

In the case of parametric uncertainty, we analyzed variation in headwind thresholds for migratory flight delays, proportion of birds sensitive to delay threshold, good weather flight altitude distribution, bad weather flight altitude distribution, headwind threshold for altitude switching, precipitation threshold for altitude switching, macro-avoidance under different visibility and precipitation conditions, micro-avoidance probability under different wind and precipitation conditions, and micro-avoidance probability in relation to structure motion (moving vs. stationary). Our exploration of parametric uncertainty was based on extensive discussions and input with field-leading experts to develop *a priori* hypotheses regarding which areas of the potentially infinite parameter space were most important to explore. We maintain that the reviewer's suggestions to sample "the full parametric uncertainty for each parameter" and to study continuous variation of parameters rather than selected, discrete values would be a virtually limitless task. At a minimum, it is well beyond the scope of the current study. We also note that this comment is purely theoretical. The reviewer did not suggest any specific parameter space that was not adequately explored based on any biological or phenomenological need or justification.

22) I have several questions about the micro-avoidance stage, the Band sub-model for active rotors, and their use in combination. I'm basing these questions on my experience with eagles at terrestrial wind facilities. We took a very different, less mechanistic approach to estimating collision risk (New et al. 2015). Our collision risk parameter (the probability of a fatal collision given presence in the hazardous volume around the tower), based on several empirical studies, was around 0.5%. That includes both micro-avoidance and the luck of geometry that the Band model calculates. What's the equivalent effective rate in the red knot model? (It would be helpful to calculate this, to allow comparison to other models). In good conditions, you have a micro-avoidance probability of 0.93, and the Band calculation can also produce a high miss rate. In combination, the risk can be quite low. Is it possible there's double-counting going on? Does the estimate of 0.93 already include the probability of flying through the rotor swept area but not getting hit? Even if there's not double-counting, I've always worried that the Band geometric calculation only considers the geometric risk of a physical collision, and not other ways in which a close encounter with an active rotor could be fatal (e.g., barotrauma, or diversion from the flight path into another structure or the sea). Breaking this down into more specific suggestions:

(a) Please calculate the conditional risk of collision, given macro-avoidance fails and there's a path through the wind turbine bounding polygon. Compare this to other published or unpublished estimates, especially from empirical studies.

(b) Discuss in more detail whether the parameters estimated by Peterson et al. (2006) and Cook et al. (2012) are exactly analogous to the micro-avoidance parameter as expressed in this model, or whether they might have been measuring a combination of micro-avoidance and geometric miss.

(c) Make explicit (and perhaps reconsider) your assumptions that in the final stage, it's only the geometry of the rotor and the bird that is considered in the probability of collision. Justify why other mechanisms of harm from a near-miss are not included.

Response
As modeled, the phenomena of macro-avoidance (bird flocks deciding to fly through, or avoid the wind energy Facility altogether), micro-avoidance (bird flocks either making, or not making evasive maneuvers to avoid flying into a stationary structure or the rotor-swept plane of a moving rotor they are approaching), and Band collision geometry (the probability of an individual bird striking a moving rotor if it flies through the rotor-swept plane) are completely distinct and non-overlapping, hence there is no "double-counting" as the reviewer speculates might be the case. We note that the reviewer's uncertainty regarding this, and other points regarding the types of avoidance and collision probabilities that have been modeled in this, and previous studies is understandable, as different authors have modeled different types of collision probabilities in different ways that partly overlap one another, sometimes using aggregate avoidance probabilities that integrate multiple different types of avoidance, sometimes separating out different avoidance phenomena into different parameters, and sometimes avoiding avoidance altogether. That said, Peterson et al. (2006) and Cook et al. (2012) are clear on this matter: micro-avoidance (i.e., active avoidance involving evasive maneuvers around a wind turbine) and geometric near-miss (i.e., passively avoiding collision when flying through a rotor) are not

confounded. Our report contains in-depth discussions of model precedents and a detailed justification of our selected approach. We hope that we have provided enough specific information for a diligent reader to parse out what we have done, and how it relates to previous approaches, but we note that this subject matter is inevitably murky.

Regarding the conditional risk of collision, given that both macro-avoidance *and* micro-avoidance have failed, we have not conducted additional analyses of our simulation results. However, we do note that Figure 3.22 addresses this risk in the sense defined by Band (2012), i.e., the conditional risk of collision for a Red Knot passing through a rotor similar to that approved for the Cape Wind Offshore Wind Facility, when flight direction is perpendicular to the plane of the rotor, for both downwind and upwind flight. The probabilities of collision depicted in Figure 3.22 should give the reader a sense of the "luck of geometry".

With regard to the reviewer's suggestion to include non-collision effects such as barotrauma or other possible adverse effects caused by near misses, we note that this partly parallels one of Mark Desholm's comments (#3) and we reference our response to that comment. Furthermore, we are not aware of any suggestion or evidence that barotrauma is likely to be a significant adverse effect experienced by birds as a result of near misses with wind turbine rotors, hence we do not feel that incorporating this phenomenon into the model is justified.

References

Masden E. A., D. T. Haydon, A. D. Fox, R. W. Furness, R. Bullman, and M. Desholm. 2009. Barriers to Movement: Impacts of Wind Farms on Migrating Birds. ICES Journal of Marine Science 66: 746-753.

The Department of the Interior Mission

As the Nation's principal conservation agency, the Department of the Interior has responsibility for most of our nationally owned public lands and natural resources. This includes fostering sound use of our land and water resources; protecting our fish, wildlife, and biological diversity; preserving the environmental and cultural values of our national parks and historical places; and providing for the enjoyment of life through outdoor recreation. The Department assesses our energy and mineral resources and works to ensure that their development is in the best interests of all our people by encouraging stewardship and citizen participation in their care. The Department also has a major responsibility for American Indian reservation communities and for people who live in island territories under US administration.

The Bureau of Ocean Energy Management

As a bureau of the Department of the Interior, the Bureau of Ocean Energy (BOEM) primary responsibilities are to manage the mineral resources located on the Nation's Outer Continental Shelf (OCS) in an environmentally sound and safe manner.